DISSERTATION

submitted to the
Combined Faculties for the Natural Sciences and for Mathematics
of the Ruperto-Carola University of Heidelberg, Germany
for the degree of
Doctor of Natural Sciences

put forward by

Mgr. Diana Morozová
born in Český Brod, Czech Rep.

Oral examination: 15. 12. 2010

Mesoscopic simulations of membrane-mediated protein-protein interactions

Referees: **Prof. Dr. Michael Hausmann**
Prof. Dr. Matthias Weiss

Zusammenfassung

In dieser Arbeit werden mesoskopische Computersimulationen zur Erforschung des dynamischen Verhaltens von Transmembranproteinen und membranasoziierten Proteinen benutzt. Zunaechst untersuchen wir die sogenannte Acylierung, eine in eukaryotischen Zellen haeufig vorkommende chemische Modifikation. Diese besteht in der Anbindung einer Acylkette an das Protein, welche loeslichen Proteinen als Membrananker dient. Bei Transmembranproteinen weisen Experimente darauf hin, dass Acylierung den Proteinverkehr beeinflussen koennte. Unsere Resultate nun zeigen, dass die Acylierung in signifikanter Weise den Neigungswinkel von Transmembranproteinen zur Membransenkrechten erhoeht. Dadurch bewirkt sie eine Aenderung der Clusterbildung und Proteinaufteilung. Unsere Ergebnisse deuten hiermit eine Regulierung des Transmembranproteinverkehrs durch Acylierung an. Im zweiten Teil der Arbeit studieren wir monotopische Proteine, die nur in eine Membraneinzelschicht eingebettet sind. Wir untersuchen, wie diese in Abhaengigkeit von Radius und hydrophober Laenge ihre Membranumgebung stoeren und als Folge hiervon Cluster bilden. Die Staerke der membranvermittelten Anziehung zwischen Proteinen haengt von deren Geometrie ab, und entsprechend von den entropischen Kosten der proteinverursachten Membranstoerung. Wir beobachten die Bildung einer Vielzahl von Strukturen hoeherer Ordnung, z. B. von Transmembrandimeren. Diese koennten eine Rolle in der intrazellulaeren Signalausbreitung spielen und damit eine Alternative zu Transmembranfaktoren darstellen.

Abstract

In this work we use coarse-grained simulations to study the dynamical behaviour of transmembrane and membrane-associated proteins. First, we address acylation, a chemical modification ubiquitous in eukaryotic cells. This modification (attaching an acyl chain to a protein), serves as a membrane anchor for soluble proteins. The role of acylation for transmembrane proteins is less clear. We follow up on recent experimental indications that acylation influences trafficking of transmembrane proteins. We find that acylation significantly enhances the tilting of transmembrane proteins with respect to the bilayer normal. Also hydrophobic mismatch-driven clustering and partitioning behavior is altered. Our results highlight a possible mechanism of how acylation regulates the trafficking of transmembrane proteins. Second, we study monotopic membrane proteins embedded in only one membrane leaflet. We inspect how they perturb the surrounding lipid bilayer in dependence on their radius and hydrophobic length. When two or more proteins are present in the bilayer, they may colocalize. The strength of the membrane-mediated attraction between proteins depends on their geometry and thus the entropic cost of the membrane perturbation they induce. We observed the formation of a multitude of higher-order structures, e.g. a cross-leaflet dimerization. We propose that the cross-leaflet dimerization may play a role in intracellular signal transduction, offering an alternative to transmembrane factors.

Contents

Chapter 1

Introduction

All living organisms are defined by a boundary that separates their interior from the external world. Such a barrier is necessary to maintain the non-equilibrium character of life. It is also useful to confine discrete functional units where specific chemical reactions take place. In the cellular context these compartments are called organelles. Such an arrangement on one hand enhances biochemical efficiency, on the other hand the reaction products of a variety of chemical compositions are safely enclosed within the compartment's interior. At the same time, the passage of nutrients and waste through the barrier needs to be allowed. Also, the boundary is required to be very flexible, to be able to form organelles with complicated shapes and to grow and divide with the cell. For this purpose Nature developed a beautiful structure - the biological membrane.

1.1 Hydrophobic effect

The building blocks of membranes are lipids. Although there is a great diversity of lipid species with a variety of molecular structures, they all share a common arrangement: a hydrophilic part denoted as headgroup connected with (usually two) hydrophobic tails [1]. Lipid heads and tails differ from each other in their interactions with the universal solvent in living matter: Water. Head groups of lipids are polar, similarly to water, and they are able to strongly interact with it, e.g. by forming hydrogen bonds. Hydrophobic tails on the contrary are nonpolar and interact only weakly with water. Note that besides these amphiphilic[1] molecules,

[1] from Greek, "loving both" - hydrophilic parts associate with water and hydrophobic (nonpolar) parts with oil

there is a great number of entirely hydrophobic substances, generally referred to as fats or oils. For membrane lipids, the amphiphilic organization is crucial as it allows for the formation of a thin film consisting of two layers of molecules. Lipids are oriented tail-to-tail, so that the hydrophobic heads are exposed to the water environment whereas the hydrophobic tails are protected from it. In the biological context the impact of the hydrophobic effect is not limited to membrane formation – it is an important driving force in many biophysical processes including protein folding, insertion of membrane proteins to the membrane or interactions of proteins with small non-polymeric molecules.

Entropic origin of the hydrophobic effect The hydrophobic effect is defined as the tendency of water to exclude nonpolar molecules, for example pure hydrocarbon structures. While there is, to a certain degree, an attraction between all molecules involved in the hydrophobic effect, the interaction of polar water molecules with each other is (due to the presence of hydrogen bonds) much stronger than the attraction between hydrophobic molecules and the water-hydrophobic interaction. A nonpolar molecule cannot take part in the highly dynamic hydrogen-bond network between water molecules. Loosely speaking, a nonpolar molecule in aqueous solvent disrupts the hydrogen bonding which is then partially reconstructed by building a "cage" around the hydrophobic molecule. This arrangement, however, strongly restricts the mobility of water molecules. In this way, the hydrophobic effect is based on the decrease of entropy associated with the ordering of water molecules around hydrophobic molecules. In order to minimize this energetically unfavorable effect, hydrophobic molecules are pushed together to form a bulk with a smaller overall surface area meaning a smaller number of affected water molecules. Hence, hydrophobic molecules have a passive role in this segregation and it is rather water that is "lipophobic". Note that hydrophobic substances may be soluble in many non-polar solvents, but only weakly soluble in water as opposed to substances with a generally low solubility because of formation of solids with strong intermolecular cohesion [2].

Macroscopically, hydrophobicity is often traced by the contact angle of a water droplet on the hydrophobic surface. On the molecular scale, the origin of the hydrophobic effect is still under debate although it has been studied since the early experiments by B. Franklin (1773) and Lord Rayleigh (1890). The first quantitative measurements on the oil/water interactions were done by Agnes Pockels [3] and Irvin Langmuir [4] at the beginning of the 20th century. The difficulty with developing a theory for the hydrophobic effect is related to its unusual thermo-

dynamical properties, temperature, and solute molecular size dependence. The complex structure of water as the prime mover of the hydrophobic interaction is also not yet fully understood.

Microscopic models There are several concepts that try to explain the underlying molecular origins of the hydrophobic effect. In the following only some of them are discussed. The "iceberg" model by Frank and Evans [5] predicts a highly ordered structure around the hydrophobic moieties: "the water forms frozen patches or microscopic icebergs around such solute molecule, the extent of the iceberg increasing with the size of the solute molecule". Nonpolar solutes are here surrounded by so-called clathrate water cages. As temperature increases, water molecules in the solvation shell broaden their orientational distribution thus increasing entropy but also increasing the enthalpy due to breaking of water-water hydrogen bonds. The analogy with the crystalline structure is, however, only illustrative, and the degree of ordering in a clathrate is supposed to be much lower than in ice. This is indirectly indicated by experimental observations, e.g. freezing increases the molar volume of water whereas insertion of a nonpolar solvent decreases it [6]. Also, the unfavorable free energy associated with dissolving a hydrocarbon chain in water differs strongly from the estimates summing up the data for a single dissolved hydrocarbon molecule [7].

Another view, the so called scaled-particle theory, was proposed by M. Lucas and B. K. Lee [8]. The free energy costs of inserting a nonpolar solute into water is explained by the difficulty to find an appropriate cavity in water. The argument is based on an approximation of water as a Lennard-Jones fluid with molecules of a rather small size that does not allow for the formation of big unoccupied regions that would accommodate the solute. A follower of this approach is the "information theory approximation" developed at Los Alamos [9]: Pratt and Pohorille [10] argue that the most probable cavities which occur in liquid water are not smaller than those which form in n-hexane. However, the cavities which form in liquid water constitute a narrower distribution than those in n-hexane or in a random medium of the same density.

A different approach is used in "MB" [11] model where each water molecule is treated as a two-dimensional circular disc interacting with other molecules via a Lennard-Jones potential and three hydrogen-bonding arms arranged as a Mercedes-Benz logo [12]. This model (studied with Monte Carlo simulations) predicts an entropy cost for small solutes (ordering of neighboring waters) whereas large solutes break the hydrogen bonds and so the enthalpy cost prevails. However,

all of these models have some limitations and are only partially able to reproduce experimental data.

Thermodynamic considerations The signature of the hydrophobic effect is the unusual thermodynamics of mixing oil and water. Let us consider a system of two phases, e.g. water and oil, where the particles of both phases can cross the oil-water interface in both directions. At constant temperature T and constant pressure P, the Gibbs free energy can be written as $G = N\mu$, where μ is the chemical potential and N is the number of particles. For a weak solvent with concentration $c_i \ll 1$, we can express the chemical potential as

$$\mu_i = \mu_i^0 + k_B T \ln c_i, \tag{1.1}$$

where i stands for the oil (1) or water (2) phase. The chemical potential is hence given by a concentrational contribution saying that the higher is the concentration, the more difficult it is to add a new particle into the solution. There is also a concentration-independent term μ^0, which will be denoted here as the solute chemical affinity for the oil or water phase [13]. If the partitioning between the two phases reaches equilibrium, the chemical potential difference $\Delta\mu = \mu_1 - \mu_2$ must be zero. The difference in chemical affinities $\mu_1^0 - \mu_2^0 = \Delta\mu^0$ is now counterbalanced by the difference in concentrations: $\Delta\mu^0 = -k_B T \ln(c_2/c_1)$. In case that the ratio of equilibrium concentrations depends on temperature, we can express

$$\Delta\mu^0(T) = \Delta h^0 - T\Delta s^0 \tag{1.2}$$

in terms of molar transfer (associated with the transfer of one molecule from one phase to the other) entropy and enthalpy, Δs^0 and Δh^0, respectively. The quantity Δs^0 represents entropies not included in the translational entropy term, for example the solvent reorganization contribution.

The difference between a hydrophobic and a regular solute is illustrated in Fig. 1.1. Here, the thermodynamics of a small hydrophobic molecule, neopentane, coming from its own phase to water is shown in contrast to the transfer of neopentane from gas to the neopentane phase. For the latter case (the regular system), the dominant contribution to the negative free energy $\Delta\mu^0$ comes from enthalpy, and both the entropy and enthalpy terms are rather independent of temperature as can be seen in Fig. 1.1B. On the contrary, the free energy of a transfer

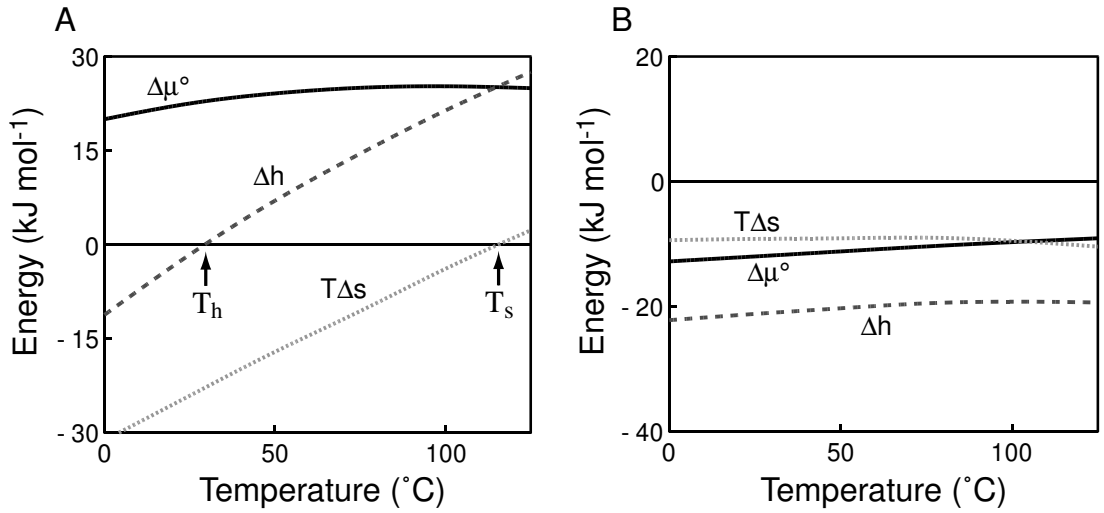

Figure 1.1: *Thermodynamics of the hydrophobic effect: (A) a hydrophobic solute - transfer of neopentane from its own phase into water, (B) a regular solute - transfer of neopentane from gas into neopentane phase. T_h indicates the temperature with zero transfer enthalpy ($\approx 25°$C for small molecules like neopentane), at temperature T_s there is a zero transfer entropy ($\approx 113°$C). Courtesy of N. T. Southall [13] (combined experimental and computational data, adapted from [8]).*

of a non-polar molecule from the oil phase into water (Fig. 1.1A) is large and positive ($\Delta\mu^0 \gg 0$), thus the process is unfavorable. At room temperature the hydrophobic effect is entropy-driven and the enthalpic contribution is vanishing but at high temperatures (near to the boiling point of water) the opposite is true. The solubility of oil in water is proportional to $\Delta\mu^0/k_BT$ and it is maximal at the temperature T_h (where the enthalpy component is zero). It is worth noting, however, that the maximum free energy $\Delta\mu^0$, where the oil-water interaction is least favorable, occurs at a different temperature, T_s (entropy component vanishing). Over the full range of temperatures for liquid water, there is a large positive heat capacity change ΔC_p upon transfer of a hydrophobic solute into water[2].

$$\Delta C_p = \frac{d\Delta h^0}{dT}. \tag{1.3}$$

ΔC_p is incorporated in the plot Fig. 1.1 as the slope of the molar transfer enthalpy dependence on temperature.

[2]The heat capacity C_p is the amount of heat needed to change the temperature by one degree at constant pressure.

1.2 Membrane biochemistry

Lipids The most common lipid type in eukaryotic membranes, **phospholipids**, are based on phosphate that serves as a linker between the hydrophilic head and hydrophobic tails. In case of phosphoglycerides the phosphate is accompanied by glycerol, a molecule with three carbon and hydroxyl groups [1]. While one of these hydroxyl groups is used for a bond with the headgroup, the two remaining usually form an ester bond with the tails (see Fig. 1.2). Owing to this modular construction, the same basic enzymatic machinery can be used to assemble different lipids. The hydrophobic tails typically consist of a sequence of 12-18 hydrocarbon units, some of them connected by a double bond that induces a kink in the chain. The hydrophilic head on the phosphate may be a sugar or an amino acid. A similar organization around a central phosphate can be found also in **sphingolipids**. Here only one lipid tail is added since sphingosine, the basis of sphingolipids, already possesses one long hydrocarbon chain. In **glycolipids**, found in particular in animal nervous system tissues, the hydrophobic moiety is linked directly to one or more monosaccharides via a glycosidic linkage. Completely different is the structure of **cholesterol** with its rigid planar array of four rings and a tiny hydrophilic head consisting only of the hydroxyl OH-group (Fig. 1.2). Due to its special shape, cholesterol aligns tightly to phospho- and sphingolipids and thus increases the membrane rigidity and thickness. Cholesterol is crucial for the regulation of membrane fluidity in the range of physiological temperatures, and it reduces the permeability of the membrane for small ions. Cellular membranes contain different fractions of these lipid types, and in this way a variety of different physical properties can be achieved. Although all lipids share the common amphipathic organization, there are thousands of different lipid species in a membrane and approximately 5% of the eukaryotic genomes encode proteins for lipid synthesis.

In contrast to eukaryotes, bacterial cells contain no cholesterol but those with a double membrane envelope (Gram negative bacteria) are decorated by lipopolysaccharides, large molecules formed by sugars and complex hydrocarbon chains. Lipopolysaccharides are the major antigen for the human immune system to recognize bacterial enemies. An interesting and quite different lipid species called bolalipids is typical for Archea, the third branch of the phylogenetic tree. Here, the hydrophobic part is twice as long as in phospholipids and it is enclosed on both sides with a hydrophilic head. In contrast to a bilayer of phospholipids, a membrane formed from bolalipids has only one layer, hence assuring a higher stability on the expense of a less dynamic and heterogeneious envelope [14]. Such properties

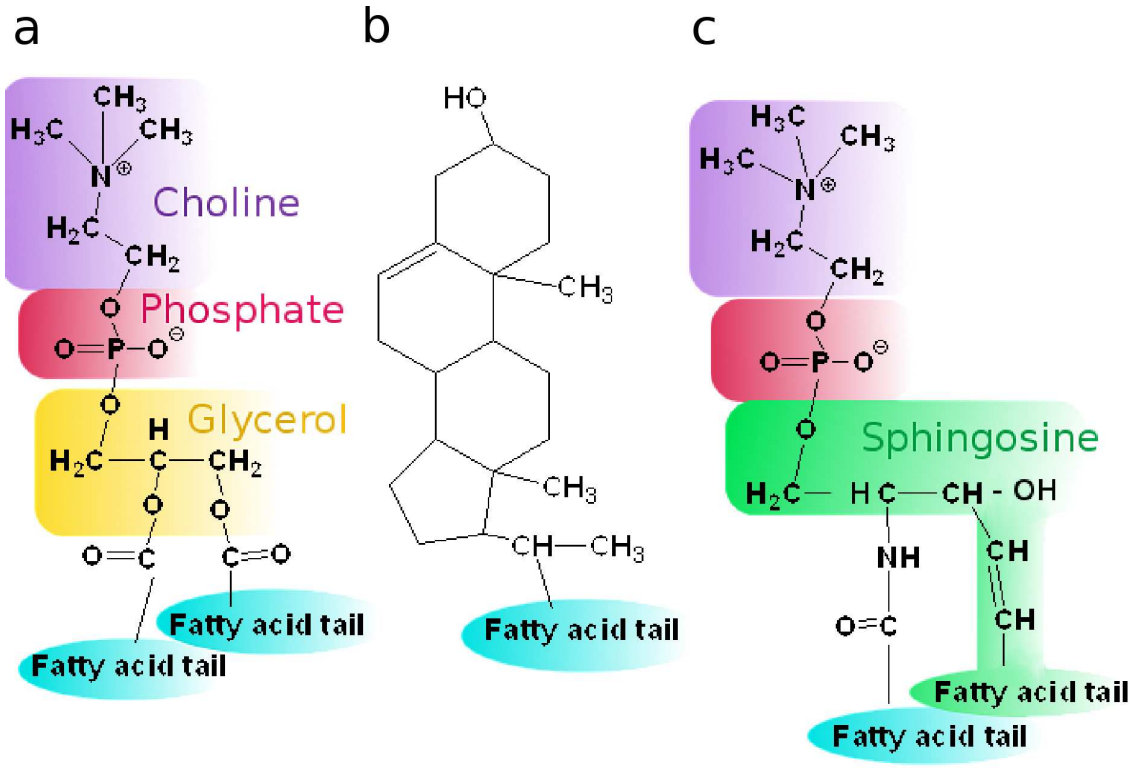

Figure 1.2: *Three representatives of membrane lipids: (a) phosphatidylcholine, (b) cholesterol and (c) sphingomyelin.*

can be particularly useful especially for creatures exposed to severe conditions like high temperatures and high salt.

The geometrical shape of lipids has a strong influence on lipid packing. As illustrated in Fig. 1.3, lipids distributed in water will self-assemble to form planar bilayers with the headgroups facing the water solvent and the tails hidden inside if the overall geometrical shape of a lipid molecule is cylindrical. The number and degree of saturation[3] of tails and the size of the heads can induce a strong anisotropy of lipids leading to a spontaneous curvature of the membrane. In this case, other spatial arrangements can be favorable like micelles, inverted hexagonal or cubic phases as opposed to the lamellar phase of a planar bilayer. When several lipid types with different geometries coexist in the same membrane, they may segregate into microdomains. This spontaneous segregation can (under certain

[3]Fatty acids with no double bonds are called saturated which refers to their saturation with hydrogens attached to carbons.

conditions) induce complex vesicle geometries with regions of different intrinsic curvatures.

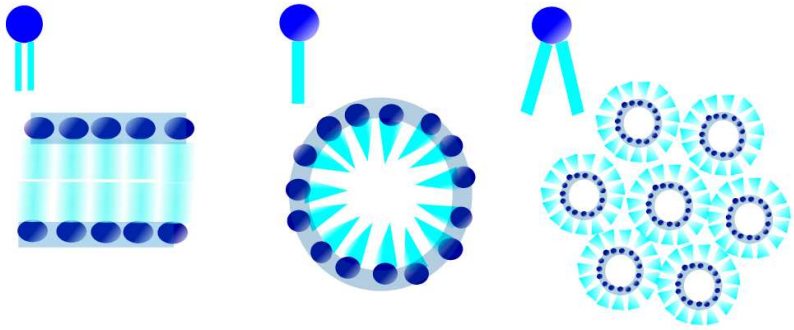

Figure 1.3: *Different membrane shapes resulting from the lipids' geometry: lamellar phase, micelle, inverted hexagonal phase*

Membrane proteins Among the various functions of membranes there is not only the passive spatial confinement of cells and organelles. Membranes are also involved in information and material flow. To be able to fulfill this function, a large fraction of the membrane mass is made up from membrane proteins. Their importance is highlighted by the fact that membrane proteins constitute about one third of the eukaryotic genome [15]. Indeed, more than a half of all proteins in a cell interact with membranes. The protein to lipid mass ratio in membrane differs widely for different membranes: It was estimated to be 2.4 for endoplasmic reticulum, 2.0 for the cytoplasmic membranes of *E. coli* and 1.8 in Golgi membranes [16]. In case of mitochondrial membranes, proteins are estimated to be responsible for roughly 70% of the total membrane mass. These data comprise all parts of proteins including those covering the surface area or extended beyond the membrane. However, also the actual area occupied by proteins within the membrane can be high: in the midplane of the plasma membrane of a human red blood cell the area occupied by transmembrane protein domains was measured to be at least 23% [17].

Membrane proteins associate with the lipid bilayers in different ways[4]:

- **Integral transmembrane proteins** usually have a transmembrane segment which is hydrophobic. It can be formed by β-barrels or α-helices.

[4]The classification of membrane proteins is not very settled, e.g. the "monotopic" proteins are also often referred to as "peripheral" in the literature.

- **Integral monotopic proteins** are attached to the membrane only from one side. Both types of integral proteins are permanently attached to the membrane.

- On the contrary, **peripheral proteins** are attached only temporarily to the bilayer or to integral proteins via non-covalent interactions. Post-translational modifications with fatty acids, prenyl chains or GPI[5] can serve to anchor both, integral and peripheral proteins to the bilayer. The membrane surface is populated asymmetrically with proteins with the majority of them residing on the cytoplasmic side of the membrane.

- Finally, some of the polypeptide toxins and proteins involved in apoptosis can aggregate and associate irreversibly with membranes even though they are water-soluble. For example, the water soluble monomer of Staphylococcus aureus alpha-toxin contains no extended stretch of hydrophobic acids. This protein was proposed [18] to associate with specific membrane receptors and at high concentrations it binds to lipid bilayers via nonspecific (maybe electrostatic) interactions. At the membrane surface the monomers form a ring-structured hexamer and upon aggregation a membrane-penetrating pore is formed.

1.3 Historical concepts of lipid bilayer

The historical view on membranes (Fig. 1.4) developed from the simplest model of a lipid bilayer by Gorter and Grendel [19] in 1925. Using the Langmuir's method for controlling the spreading of oil on a water surface, they estimated the area occupied by lipids extracted from erythrocytes. They proposed that cells are covered by a layer of fatty substances that is two molecules thick. The first widely accepted model came ten years later from Danielli and Davson [20]. Here the lipid bilayer was additionally covered with proteins on both sides. Thanks to electron microscopy the idea arose that all cellular membranes might have a common basic structure. However, the relevance of the bilayer concept was still discussed and alternative possibilities for membrane architecture were considered, e.g. membranes composed of discrete globular subunits [21]. It lasted until 1972 when the bilayer concept was consolidated in the "fluid mosaic" model proposed by the biochemists

[5]GPI anchor - glycosylphosphatidylinositol - is a glycolipid that can be attached to the C-terminus of a protein during post-translational modification.

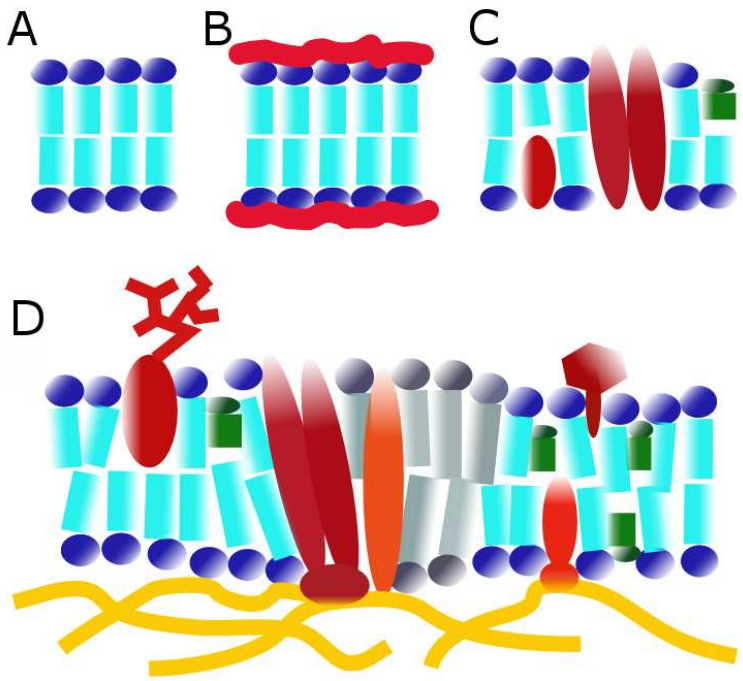

Figure 1.4: *The development of membrane models. (A) Gorter and Grendel observed that the layer covering cells is two molecules thick. (B) Danielli and Davson's model with proteins on the surface. (C) The fluid mosaic model - a dynamic structure with an isotropic diffusion of membrane components. (D) The current view: a complex crowded environment with heterogeneities, functional platforms and association with cytoskeleton. Proteins in red, cholesterol in green, other membrane lipids in blue and cyan or gray, cytosckeleton in yellow.*

S. J. Singer and G. L. Nicolson [22]. The proteins in this model have a globular shape, with a sharp distinction between peripheral and integral membrane proteins. They are randomly distributed in the membrane at a fairly low concentration, and they float within the bilayer like ships in the sea. Also the lipid molecules move freely within the bilayer. Lipids surrounding a protein can affect its function which might explain the high diversity of lipid molecules present in membranes. The model worked very well in allowing for molecular interactions and capturing the complexity of a membrane. On the other hand, it neglected the possible non-random distribution of lipids and the local order corresponding to specific biological functions of a membrane.

The current view on membranes is more complex as it takes into consideration the experimental evidence for inhomogeneities [6], self-separation and asymmetry of

[6]The first experiments used mixtures of gel and fluid lipid phases, later they were performed

inner and outer leaflet as well as peripheral membrane proteins attached to microfilaments in the cytoskeleton [24]. A rather "patchy" architecture is proposed with segregated regions of different compositions as biologically functional units. The self-organized micro- and nanodomains vary in lifetimes, thickness and fluidity. It has been found that a membrane is a fairly crowded environment in which membrane proteins suffer from many restrictions (ectodomain collisions, transbilayer interactions, adhesion sites and cytoskeletal structure) that hinder their movements [25]. Despite extensive research still secrets remain in the field of biological membranes. Current areas of active reasearch are especially trafficking events, e.g. vesicle transport and the dynamics of membrane components on different scales (studied with single particle tracking methods).

1.4 Biophysical description of membranes

Many biological functions of membranes depend critically on encounters and interactions of membrane constituents. Therefore it is important that even the fairly crowded and heterogeneous membrane environment allows for a diffusive movement of lipids and other membrane compounds of the bilayer. A lipid in a membrane is surrounded by elements of comparable size, and it is allowed to change its position only if a sufficiently large free cavity appears in its vicinity. The diffusion is thus characterized by a discrete lattice movement and the diffusion coefficient can be expressed as $D \sim \exp(-a_c/a_f)$ where a_c is the minimal free area that has to exist so that transport occurs and a_f is the average free area per molecule [26]. Measurements on lipids in a bilayer yield diffusion coefficients in the order of micrometers squared per second [27] resulting in the estimate that the membrane is roughly a hundred times more viscous than water.[7] Considering a larger inclusion that floats in the membrane, e.g. a transmembrane protein, we can regard the lipids as a continuous solvent. The formula for the two-dimensional diffusion coefficient for this case was derived analogously to the Einstein-Stokes

with immiscible fluid lipids and also on whole cells, e.g. in case of the fibroblast surface membrane where protein-rich domains of micrometer diameter were found with photobleaching [23].

[7] Sometimes the viscosity of membrane is compared to the viscosity of crocodile fat on a warm summer day [24].

equation[8] by Saffman and Delbruck [28]

$$D = \frac{k_B T}{4\pi\eta_m t}\left[\log\left(\frac{\eta_m t}{\eta_f R}\right) - \gamma\right], \tag{1.4}$$

where t is the membrane thickness, η_m the membrane viscosity, η_f the viscosity of the external fluid in which the membrane is immersed, and γ is Euler's constant. Note that Eq. (1.4) gives an unphysical, negative diffusion coefficient for large inclusion radii R as it was derived via perturbation theory for small radii. An extended theory can be found in [29].

In contrast to the fast lateral diffusion of lipids, a spontaneous switching of a lipid from one layer to the other (transverse diffusion, flip-flop) is an extremely rare process. Its waiting time is 6-20 hours as the hydrophilic head of the lipid has to cross the hydrophobic core of the membrane. Despite that, many cellular membranes show a considerable asymmetry of lipid composition between the two leaflets (first described in [30]), which is the result of a special kind of enzymes, lipid flippases [31]. Energy independent flippases serve to rapidly equilibrate common phospholipids between the two leaflets, whereas ATP[9]-dependent flippases assure the membrane asymmetry by transferring specific phospholipids to one of the leaflets.

Membranes as elastic sheets When we are interested in the curvature or deformations of membranes it is useful to zoom out from the individual bilayer components and consider a continuous elastic sheet [14]. In our description we will also exploit the small aspect ratio - the very tiny thickness of membrane as compared to its, typically orders of magnitude larger, latitude. We can use this feature to reduce the dimensionality of our system and consider only a two-dimensional surface.

To describe a membrane conformation we will be mainly interested in understanding how the Gibbs free energy[10] depends on the membrane shape. An elastic

[8] The Einstein-Stokes equation gives the diffusion coefficient for a three-dimensional diffusion of a spherical particle in liquid with a low Reynolds number: $D = k_B T/(6\pi\eta r)$. The equation is an example of a fluctuation-dissipation theorem, relating thermal fluctuations and viscosity η.

[9] ATP - adenosine triphosphate - is a coenzyme used as the main energy storage and transfer molecule in the cells.

[10] The Gibbs free energy G is a natural thermodynamical potential for systems at constant pressure as those mostly occurring in experiments. The Helmholtz free energy F with volume as the natural argument is more often used in theoretical considerations. The two free energies are related by a Legendre transform [32].

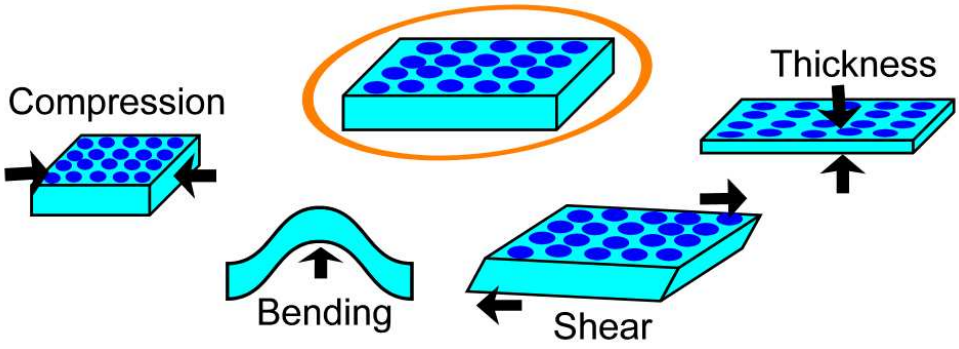

Figure 1.5: *Basic types of membrane deformations*

sheet can be deformed in several basic ways (Fig. 1.5):

- **membrane stretching and compression** - at vanishing and low surface tension there are thermal fluctuations which present a temporary supply of surface area. Therefore upon slight stretching only a flattening of the membrane occurs, and only an increased surface tension (e.g. by micropipette aspiration) makes a non-negligible contribution to the free energy.

- **bending** - its energy is the most important contribution that has to be taken into account when considering biological processes. The bending geometry (without overlaps) can be described using a height function $h(x_1, x_2)$ which measures the distance of the membrane surface from the underlying plane at a point (x_1, x_2), as depicted in Fig. 1.6. This way of describing the conformation of the surface, i.e. the parametrization of the surface with a position vector $\vec{r} = (x_1, x_2)$ in the projection plane and the corresponding $h(\vec{r}) = x_3$, is referred to as the Monge gauge. The height function in the neighborhood of a point (x_1^0, x_2^0) can be approximated by the Taylor expansion in the following way

$$\begin{aligned} h(x_1, x_2) &= h(x_1^0, x_2^0) + \frac{\partial h}{\partial x}\Delta x + \frac{\partial h}{\partial y}\Delta y + \\ &+ \frac{1}{2}\left(\frac{\partial^2 h}{\partial x^2}\Delta x^2 + 2\frac{\partial^2 h}{\partial x \partial y}\Delta x \Delta y + \frac{\partial^2 h}{\partial y^2}\Delta y^2\right) \end{aligned} \tag{1.5}$$

  where the derivatives are evaluated at the point (x_1^0, x_2^0). We can understand the formula as a mapping of a small patch of the size $\Delta x \times \Delta y$ to the membrane surface around the point $h(x_1^0, x_2^0)$. The constant term shifts the patch

in height and the first order terms give the tilting of the patch to make it tangent to the membrane surface. Finally, the second derivatives correspond to the bending and thus they are directly related to curvature. At every point of a curve, the curvature can be defined as the inverse radius of a circle that fits best into the landscape (osculating circle, Fig. 1.6). For a description of a two-dimensional object we can use a plane cutting through the surface to obtain a curve. However, there are infinite ways how to orient the plane giving different curvature values. To capture the bending of a surface we need to find two so called principal curvatures (from Euler's theorem [33]), i.e. we are looking for two special orthogonal planes that intersect the membrane resulting in two extreme values of curvature, the lowest and the highest one. Considering the quadratic part of the function $h(x_1, x_2) = \sum_{i,j=1}^{2} \kappa_{ij} x_i x_j$ where $\kappa_{ij} = \frac{1}{2}\frac{\partial^2 h}{\partial x_i \partial x_j}$, we can calculate the two principal curvatures as the eigenvalues of the matrix

$$\kappa = \begin{pmatrix} \kappa_{11} & \kappa_{12} \\ \kappa_{21} & \kappa_{22} \end{pmatrix}. \tag{1.6}$$

The diagonalization of the matrix κ corresponds to the search for such orthogonal planes that give the principal curvatures.

- **shear deformations** - these do not play an important role for fluid membranes (as opposed to the gel state with a higher ordering of lipids and a very restricted diffusion) since lipids can move freely and individually.
- **the thickness variation of the membrane** - it can be changed e.g. as a result of the presence of a membrane protein - note that this deformation goes beyond the realm of the two-dimensional approximation.

Free energy of deformation The various deformations are associated with a free energy cost. For changing the area of a lipid bilayer we can write the free energy

$$G_{stretch} = \frac{K_A}{2} \int \left(\frac{\Delta a}{a} \right)^2 dA, \tag{1.7}$$

where Δa is the change in area and a is a reference area, and we sum up over all elements of area dA. The stretching/compression of the average area per molecule is analogous to a sound wave. The area stretch modulus K_A typically has values 55-70 $k_B T/nm^2$.

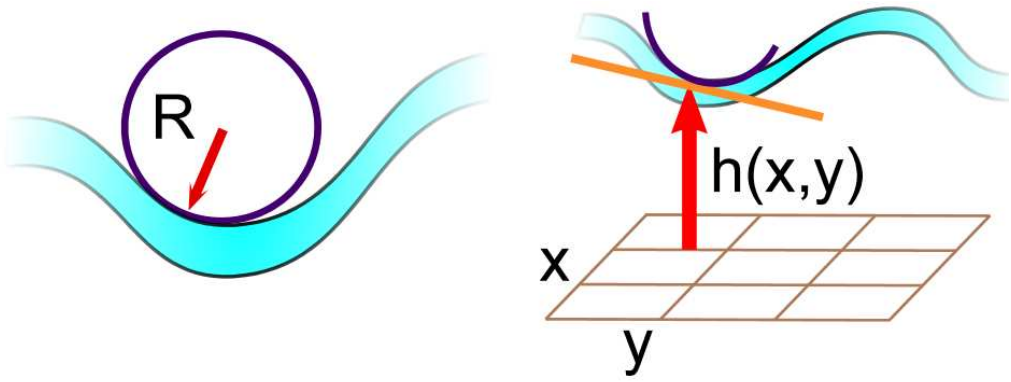

Figure 1.6: *Definition of membrane curvature and the height function geometry*

The bending of a lipid bilayer that is not associated with a spontaneous curvature also costs energy, which can be described as

$$G_{bend} = \frac{K_b}{2} \int [\kappa_1(x_1, x_2) + \kappa_2(x_1, x_2)]^2 dA, \tag{1.8}$$

This term is often referred to as Helfrich-Canham-Evans free energy. The principal curvatures κ_1 and κ_2 are the eigenvalues of the matrix κ in Eq. (1.6). The energy cost is determined by the square of mean curvature, $(\kappa_1 + \kappa_2)/2$, which means that the direction of bending does not influence the free energy. The bending energy K_b is usually not very high, reaching 10-20 k_BT, i.e. the membrane is not very resistant against this type of deformation. If we consider the product of the two principal curvatures instead of the sum, we obtain an additional energy term, the Gaussian curvature energy. The Gaussian curvature is an intrinsic value because it can be determined from measurements of length on the surface itself, independent on the ambient space (Theorema Egregium [34]). An interesting property of the Gaussian curvature is that it changes only when the topology of the surface is changed (Gauss-Bonnet theorem). Therefore it may be significant when membrane holes, tubes or vesicles are formed. The bending modulus of the Gaussian curvature can be positive or negative and the sign is related to the preferred shape the membrane will adopt (locally convex/locally saddle).

A similar equation can be written for the contribution of a thickness variation $t(x_1, x_2) - t_0$

$$G_{thick} = \frac{K_t}{2} \int \left(\frac{t(x_1, x_2) - t_0}{t_0} \right)^2 dA, \tag{1.9}$$

Here, t_0 is the equilibrium thickness. The parameter K_t has the value of cca. $60k_BT/nm^2$ and it expresses how much effort we need to change the equilibrium thickness of the membrane, e.g. in the presence of a transmembrane protein with a hydrophobic mismatch with the bilayer.

Fluctuating membranes Fluid membranes are highly flexible and exhibit thermally induced shape fluctuations in the absence of an external force [35]. To discuss the behavior of an elastic membrane with small local curvatures in a phenomenological way, we will consider the Helfrich Hamiltonian [36, 37]

$$\mathcal{H} = \int_A ds \left[\sigma^0 + \frac{1}{2}K_b^0(\kappa_1 + \kappa_2 - 2c^0)^2 + K_G^0\kappa_1\kappa_2\right] \tag{1.10}$$

where the first term denotes the surface tension coefficient σ^0, in the second term the total curvature with the bending modulus K_b^0 and the spontaneous curvature c^0 appear and the third term stands for the Gaussian curvature with the saddle-splay modulus K_G^0. In the ensemble of conformations which the surface can attain, the Hamiltonian determines the probability p_i of a conformation i

$$p_i = \frac{\mathrm{e}^{-\mathcal{H}_i/k_BT}}{Z}. \tag{1.11}$$

The partition function $Z = \sum_i \mathrm{e}^{-\mathcal{H}_i/k_BT}$, T denotes the temperature and k_B the Boltzmann constant. The Helmholtz free energy F is related to the Hamiltonian via the partition function $F = -k_BT \log Z$. For a planar bilayer with zero spontaneous and Gaussian curvatures the free energy of a surface with bending and stretching can be written in the form of the Helfrich free energy

$$F(h) = F|_{h=0} + \sigma(A(h) - A_p) + \frac{1}{2}K_bJ^2(h) + \mathcal{O}(h^4) \tag{1.12}$$

The coefficients σ and K_b are also usually called surface tension and bending modulus, but they are not equivalent to σ^0, K_b^0, c^0 and K_G^0 appearing in the Hamiltonian (Eg. 1.10). Whereas the Hamiltonian-related parameters represent material properties of the membrane, the surface tension and bending modulus in the free energy context are thermodynamical quantities that may depend on temperature and the size of the system. Again we use here the Monge gauge with $h(x_1, x_2) = x_3$, $A(h)$ is the total area of the membrane surface, A_p is the projected area to the plane (x_1, x_2) and $J^2(h)$ is the integrated total curvature $J^2(h) = \int_{A_p}[\kappa_1(h)+\kappa_2(h)]^2 dx_1dx_2$. Tak-

ing into account the geometrical meaning of A and J^2, where stretching can be written as a derivative, and bending is associated with the second derivative of the height h, we obtain the energy change per unit projected area

$$\Delta f(h(x_1, x_2)) = \frac{1}{2}\sigma| \bigtriangledown h(x_1, x_2)|^2 + \frac{1}{2}K_b| \bigtriangledown^2 h(x_1, x_2)|^2 \tag{1.13}$$

In Fourier space the derivatives $\partial_x f$ simplify to a multiplication, $-iq\, f$, and we get

$$\Delta f(h(q)) = \frac{1}{2}\left(\sigma q^2 + K_b q^4\right) h(q)^2 \tag{1.14}$$

which leads to the spectrum of fluctuations

$$< h^2(q) >= \frac{k_B T}{A}\,\frac{1}{\sigma q^2 + K_b q^4} \tag{1.15}$$

where σ denotes the surface tension and K_b the bending rigidity.

The thermal motion of a lipid bilayer is a combination of different processes on different scales [38]. At intermolecular distances, single or collective protrusions of lipids in each monolayer prevail. The spectral intensity $< h^2(q) >$ in this region is governed by a q^{-2} dependence and characterized by an effective surface tension. At length-scales larger than the membrane thickness it becomes possible to model the layers as continuous surfaces. An undulatory and peristaltic motion can be observed, i.e. fluctuations of the membrane as a whole and fluctuations of the membrane thickness due to anticorrelated motions of the two monolayers. These relaxations are given by bending energy and the spectral intensity is proportional to q^{-4}. The peristaltic motion at large wavelengths is limited by the equilibrium membrane thickness, so that it asymptotically tends to a constant value for modes involving ~ 400 lipids and more. Therefore, zooming out even more, the peristaltic motion is overridden by undulatory modes and the bilayer resembles a single-layer surface.

It should be noted that even if the thin interface elastic model of membranes is a good approximation of some biological membranes, it neglects the association of cellular membranes with cytoskeleton or their coupling to adjacent membrane complexes, the presence and activity of membrane proteins, and also the heterogeneous composition of membranes with regions of diverse chemical and physical properties.

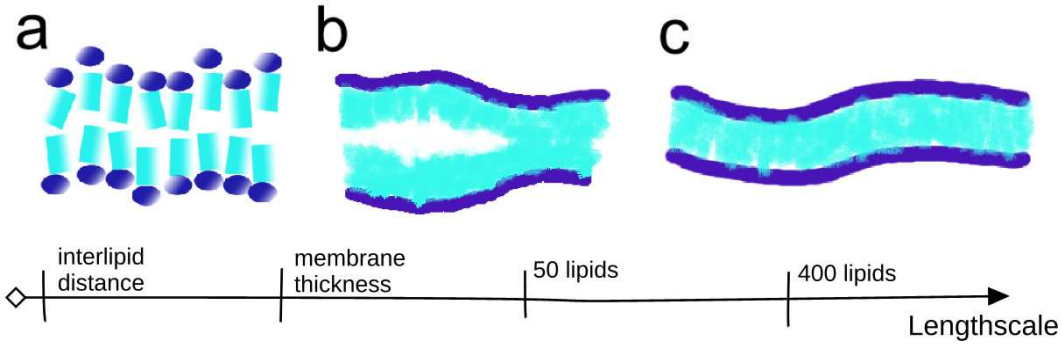

Figure 1.7: *Membrane fluctuations on different scales: (A) single and collective lipid protrusions, (B) membrane thickness fluctuations in peristaltic motion, (C) long-range membrane undulations.*

1.5 Transmembrane proteins and the concept of hydrophobic mismatching

For transmembrane proteins in a lipid bilayer the central concept is the so-called hydrophobic mismatch. A difference in the length of the hydrophobic transmembrane domain of an integral membrane protein and the width of the hydrophobic core of the membrane leads to a deformation of the surrounding lipid bilayer (Fig. 1.7). The reason is the high cost of exposure of a hydrophobic region to the water environment which is energetically unfavorable (about 100 J/Å), so that a 5Å mismatch in the hydrophobic length between a protein and the membrane of 5Å results in a cost of $\approx$ 0.5 kJ/mol [25]. In case of a negative mismatch, i.e. when the transmembrane hydrophobic domain of a protein (TMD) is shorter than the membrane thickness, a local compression of the membrane emerges. In case of a positive mismatch (TMD longer than the membrane thickness) a stretching of neighboring lipids is induced. If the height difference is too big to be compensated by stretching, the protein tilts relative to the bilayer normal (Fig. 1.8). The thickness profile of a membrane perturbed by a mismatching protein can be described by the theoretically derived [39, 15] expression

$$t(r) = t_0 + \Delta t \, \mathrm{e}^{-\frac{r}{\lambda}} \tag{1.16}$$

The membrane thickness directly at the rim of the protein Δt is most affected by the presence of the inclusion and the perturbation decays exponentially as a function of the radial distance r with a characteristic decay length λ towards the

unperturbed thickness, t_0. While shielding the hydrophobic domain is desirable, the accompanying membrane deformation comes at an energetic cost. If possible, the inclusions preferentially choose a lipid environment that does not enforce any mismatch-related membrane deformation. A simple estimate for the free energy of a system with hydrophobic mismatch derived from an elastic distortion of a bilayer can be written [15] as

$$G = G_0 + k\left(\frac{r_P}{\pi\lambda} + 1\right)|\Delta t|^2. \tag{1.17}$$

The constant k is related to the bilayer area compressibility modulus and r_P is the radius of the inclusion. This expression does not account for the local thickness of the membrane so it is not suitable for deriving the membrane profile Eq. (1.16), but it can be used to describe the equilibrium thermodynamics of the lipid-protein system. The constraints of the lipid configuration near to the protein may result in an entropy-driven clustering of proteins in order to minimize the amount of affected lipids. In the presence of lipid microdomains of different thicknesses this leads to a demixing of proteins of different transmembrane domain lengths [40].

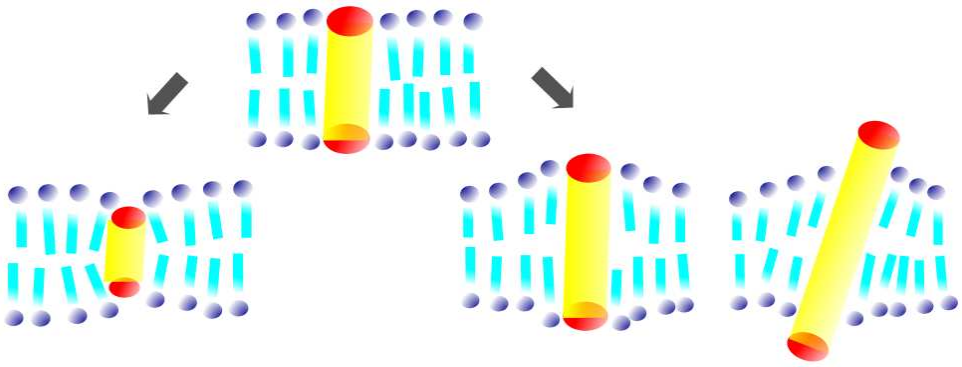

Figure 1.8: *Membrane deformations due to the presence of a protein with a negative (left) and positive (right) hydrophobic mismatch. A strong positive mismatch induces a tilting of the protein with respect to the bilayer normal.*

The concept of hydrophobic mismatching was first proposed in a theoretical work in 1976 [41]. A mean-field theoretical approach was used to derive the perturbation profile and bilayer energy change with embedding an inclusion [39], and the 'mattress model' [42] was applied to describe the phase behavior of membrane inclusions with hydrophobic mismatch. The dynamics of lipids and inclusions in various systems with a hydrophobic mismatch was examined in several *in-silico*

studies [43, 44, 45].

Hydrophobic mismatch in nature Direct measurements of a hydrophobic mismatch and its consequences like oligomerization and tilt of transmembrane segments have been performed in systems with synthetic amphiphilic polypeptides [46]. Synthetic α-helical transmembrane proteins with a simple sequence (e.g. WALP peptides) can be designed to span the bilayer with the desired mismatch and thus represent a useful model. For natural transmembrane proteins the presence and action of a hydrophobic mismatch has not yet been described in molecular detail. The relevance of this concept is, however, supported by a manifold of experimental observations: mismatch-driven oligomerization was observed for instance in case of gramicidin A [47], a channel for small molecules. The functional form of this protein is a dimer of two monomers joined back to back. It was shown that the dimerization occurs most efficiently if there is no hydrophobic mismatch between the resulting cross-leaflet dimer and the membrane.

Hydrophobic mismatching was also proposed to be a tool for self-organized protein sorting. During the travel of a newborn protein towards its destination in the cell the protein has to visit several discrete membrane-bound organelles. As a means of transport vesicles bud from the initial organelle and fuse specifically with the target membrane. The first stop of the proteins is the endoplasmic reticulum (ER) where folding, assembly and basic covalent modifications occur. Next, proteins are transported (via COPII vesicles) to the Golgi apparatus where the proteins acquire extensive modifications, e.g. glycosylation. Sorting of proteins and packing for exocytosis takes place here. The Golgi apparatus is a complex dynamical structure formed from several compartments (stacks of cisternea). Cargo proteins and resident proteins are sorted differentially into the different cisternea via COPI vesicles, leading to a non-uniform stationary distribution across the organelle. The mechanism of protein progress through this organelle and its correct localization are not yet fully understood. Nonetheless, Golgi resident proteins have been shown to have transmembrane domains on average five residues shorter than plasma membrane residents. Also, membranes in different organelles throughout the secretory pathway (from ER to Golgi to plasma membrane) are getting thicker due to an increasing content of cholesterol and sphingomyelin [16]. There is a strong evidence that the localization of transmembrane proteins in the Golgi is influenced by their TMD length [48, 49]. Similar observations of a length dependent non-specific partitioning were published also concerning the endoplasmic reticulum and the ER/Golgi boundary [50]. Also the lateral organization of proteins within

a membrane might be driven by a matching condition with different membrane microdomains [40].

Lateral pressure profile Besides the thickness change of the surrounding membrane, the hydrophobic mismatch could exert its influence on proteins also by means of the change of lateral pressure. In the absence of an external force, a membrane reaches a minimum free energy state with an optimal area per molecule and a zero total force in the plane of the bilayer. Nevertheless, there are non-zero forces present locally on the membrane cross-section originating from the bilayer anisotropy (see Fig. 1.9). At the head-tail interface there is a tension (negative pressure) because of the hydrophobic interaction between the two phases. Acting alone, this contribution would drive a formation of a highly packed bilayer with aligned lipid chains and a small area per molecule. This effect is, however, counterbalanced by the competition of lipid heads for water molecules to increase their hydration. Also, the pressure arising from the chain conformational entropy increases the pressure in the core of the membrane. The conformational entropy namely is higher if there is sufficient space and thus more conformational freedom for the lipid molecules. Subsequently, a relatively smaller pressure can be detected in the midplane of the bilayer. In case of a tensionless membrane, the total pressure must be zero giving $\int_z \Pi dz = 0$. Distortions of the bilayer are expected to influence the conformation of a (a non-cylindrical) protein [51] and modulate the protein function as it was observed for mechanosensitive channels [52]. Also the function of several ion pumps and sugar transporters was found to be suppressed or enhanced by alterations of the lateral pressure profile [15].

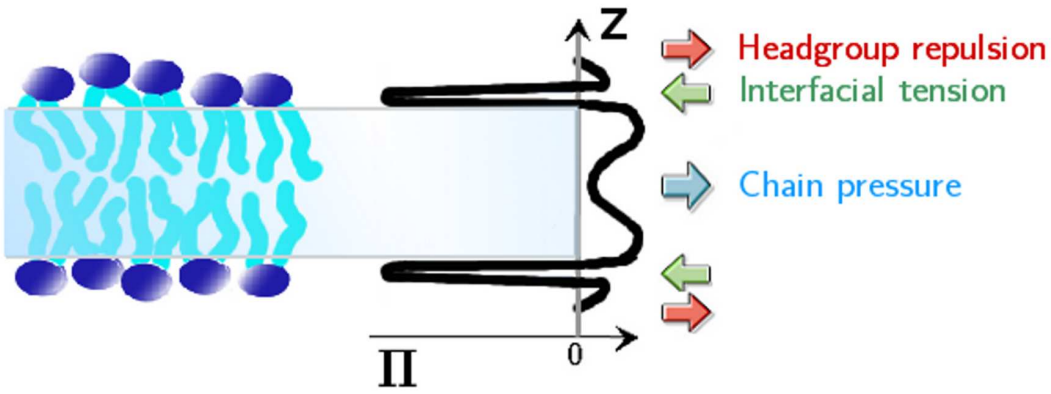

Figure 1.9: *Typical lateral pressure profile. The pressure is anisotropic on the membrane cross-section: Lipid headgroup repulsion gives a positive pressure* Π *(red arrows). At the head-tail interface there is a tension due to hydrophobic interactions (green arrows). In the membrane core the pressure is positive again due to the competition of lipid chains for sufficient space (blue arrow).*

Chapter 2

Mesoscopic simulations

The subject of our studies are processes that involve tens of transmembrane or membrane-associated proteins embedded in a correspondingly large membrane patch. We are interested in collective phenomena like membrane-mediated protein-protein interactions or protein-induced changes of membrane shape which are based on interactions of a large amount of lipid molecules. The time-scale is given by the requirement to allow for a free diffusion to all parts of the system within microseconds. Additionally, we have to consider also the solvent that is responsible for some characteristic properties of our system, influencing e.g. the fluctuation dynamics of the membrane [53].

In order to gain a microscopic understanding of such processes, the straightforward way would be to include all atoms and calculate the interactions between them. Such an approach is realized in all-atom molecular dynamics simulations (MD). This well-established simulation technique proved to be a powerful tool, e.g. in studies of proteins' conformational changes in the field of drug design. Usually MD is implemented taking into account a variety of geometrical (bonds, angles) and physical (electrostatics, Van der Waals) interactions. All atoms are modeled as rigid bodies with a finite size. The use of the hard-core potential nonetheless enforces a short integration step in order to prevent the particles from overlapping within one iteration. Also, the long-range interactions used here are computationally very expensive. As a result, MD simulations typically are limited to scales of maximally tens on nanometers and tens of nanoseconds. Still, full atomistic simulations of membrane systems or membrane proteins have been used to study e.g. water passage through a membrane pore [54] or formation of a small vesicle [55].

On the other hand, much larger length and time scales can be addressed by

continuum methods as presented in the introductory chapter. Here, the physics of the membrane is modeled by sets of partial differential equations. However, for continuum methods it is difficult to handle individual molecules or a complex spatial structure. Also, the membrane-mediated interactions of membrane inclusions involve processes on a variety of time and length scales.

The systems we are interested in are best characterized at scales between the molecular dimension of lipids and the micron size of the cell, hence being best treated with a mesoscopic technique. Here, the number of degrees of freedom of the system is reduced with respect to an MD system by coarse-graining. Only those properties that are expected to influence the collective behavior of interest, e.g. the amphiphilic nature of lipids, are taken into account. An example of such a method is the coarse-grained MD (e.g. [56]) where several molecules are treated as a single particle with a given hydrophobicity, so that a lipid molecule consisting of more than 100 atoms can be represented with only 10 particles of two types, hydrophilic heads and hydrophobic tails. Still, the particles interact via a hard-core potential that prevents their overlap but requires a small time step when integrating the equations of motion.

2.1 Dissipative particle dynamics

The method used in this work is another explicit solvent coarse-grained simulation technique called dissipative particle dynamics (DPD)[57]. In DPD also several atoms are combined to larger beads. Here, however, the beads represent a small bulk of material as illustrated in Fig. 2.1. To account for the friction due to internal (hidden) degrees of freedom a dissipative force is introduced. The positions of single atoms in a bead are smeared out and thus a soft-core potential allowing for an overlap of beads can be used here. In this way, we can achieve a substantially larger temporal range than in case of the above mentioned methods.

DPD was first introduced by Hoogerbrugge and Koelman in 1992 [58] for simulations of hydrodynamic phenomena. The method was further developed to the currently used formalism by Español and Warren [59] who implemented the fluctuation-dissipation theorem into the original algorithm. In this way, the statistical mechanics of the beads becomes consistent with the Gibbs canonical ensemble, and it yields the correct thermodynamics at sufficiently long time and length scales.

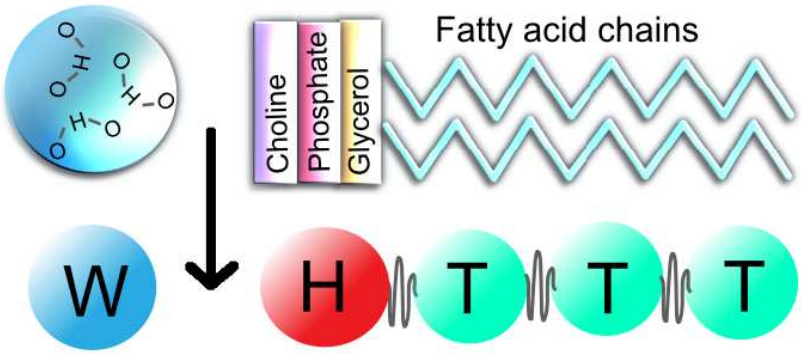

Figure 2.1: *A scheme of the DPD coarse-graining. One water bead (W) represents three water molecules, DPD lipids are formed from a hydrophilic head bead (H) and a chain of hydrophobic tails (T) connected with a spring.*

The motion of the i-th DPD bead is governed by Newton's equations of motion

$$\frac{d\boldsymbol{r}_i}{dt} = \boldsymbol{v}_i, \tag{2.1}$$

$$m\frac{d\boldsymbol{v}_i}{dt} = \boldsymbol{F}_i^T, \tag{2.2}$$

where $\boldsymbol{r}_i$ is the position of the center of mass, $\boldsymbol{v}_i$ the velocity and $\boldsymbol{F}_i^T$ the total force acting on the bead. Considering non-geometrical interactions, the total force $\boldsymbol{F}_i^T$ exerted on a bead is given by three contributions: the dissipative force $\boldsymbol{F}_i^D$, the random force $\boldsymbol{F}_i^R$ and a conservative linear repulsive force $\boldsymbol{F}_i^C$

$$\boldsymbol{F}_i^T = \sum_{i \neq j}^{N} (\boldsymbol{F}_{ij}^C + \boldsymbol{F}_{ij}^D + \boldsymbol{F}_{ij}^R), \tag{2.3}$$

where N is the number of all beads. The potential in DPD is short-ranged, i.e. all forces are non-zero only if the distance between two beads i, j is $r_{ij} = |\boldsymbol{r}_i - \boldsymbol{r}_j| \leq r_0$. The cutoff radius r_0 therefore defines the effective bead size; typically $r_0 = 1$ is used for simplicity.

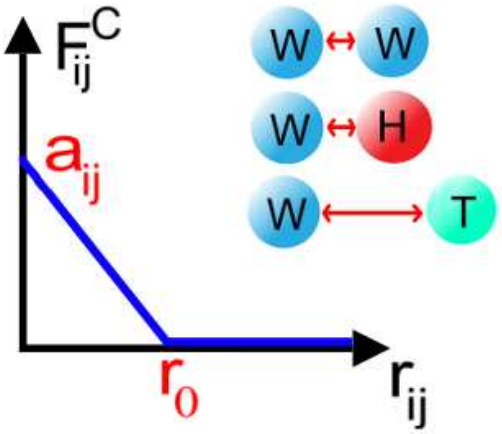

Figure 2.2: *Two beads i, j are repelled by the conservative force F^C which is linear and vanishes at the cutoff distance r_0. The strength of the repulsion is determined by the two bead types via the repulsion parameter a_{ij}.*

2.2 Forces in DPD

Character of beads The repulsive conservative force that mimics excluded volume interactions (Fig. 2.2) is given by

$$\boldsymbol{F}_{ij}^C = a_{ij}(1 - r/r_0)\boldsymbol{e}_{ij}. \tag{2.4}$$

Here $\boldsymbol{e}_{ij} = \boldsymbol{r}_{ij}/r_{ij}$ is the unit vector pointing from particle j to i. The repulsion parameter a_{ij} depends on the combination of the two interacting particles. In this way, it defines the different bead types. In our simulations the system consists of three DPD bead types only: hydrophobic tails (T), hydrophilic heads (H) and water (W) beads. The values of the repulsion constant depend on the system. In our case we used a modification of the lipid model by Laradji [60] which was derived from the model by Shillcock [61]. The interaction constants are

$$a_{ij} = \frac{k_B T}{r_0} \begin{pmatrix} & W & H & T \\ W & 25 & 25 & 200 \\ H & 25 & 25 & 200 \\ T & 200 & 200 & 25 \end{pmatrix} \tag{2.5}$$

Thermostat The dissipative force $\boldsymbol{F}^D$ represents the viscous force a bead feels when it moves near to a neighbor. The random force $\boldsymbol{F}^R$ stands for the thermal

motion of the particles preventing the system from freezing

$$\boldsymbol{F}_{ij}^{D} = -\gamma\omega^{D}(\boldsymbol{r}_{ij})(\boldsymbol{e}_{ij}\cdot\boldsymbol{v}_{ij})\boldsymbol{e}_{ij} \quad (2.6)$$

$$\boldsymbol{F}_{ij}^{R} = -\sigma\omega^{R}(\boldsymbol{r}_{ij})\boldsymbol{e}_{ij}\xi_{ij}. \quad (2.7)$$

The weight function $\omega^{D}(r) = (1 - r/r_0)^2$ is non-zero only for $r \in [0, r_0]$ and the Gaussian white-noise term ξ_{ij} is a random variable with zero mean and unit variance, uncorrelated for different pairs of particles at different times. The random and dissipative force act as a heat source and sink and hence they are often referred to as the DPD thermostat. These two forces are coupled via the fluctuation-dissipation theorem. Therefore, the parameters σ and γ which represent the friction coefficient and the amplitude of the noise are related. Español and Warren [59] proved that the following coupling of the noise and friction terms ensures a correct NVT ensemble

$$\sigma = \sqrt{2k_B T\gamma}, \quad (2.8)$$

while also the weight functions are connected $\omega^{D}(r) = [\omega^{R}(r)]^2$. In our simulations we use the commonly chosen parameters $\sigma = 3$, giving $\gamma = 4.5$ [62].

As already mentioned, different bead types are distinguished only via the conservative force $\boldsymbol{F}_C$. Owing to the pairwise character of all forces ($\boldsymbol{F}_{ij} = -\boldsymbol{F}_{ji}$) the overall conservation of (angular) momentum is secured. This is an important feature of the dissipative particle dynamics approach [63]. As not only conservative but also the thermostat forces are pairwise, all particles obey Newton's third law of action and reaction. For this reason the sum of all forces in the whole system vanishes. Moreover, all forces between all particles enclosed in a subset of the system vanish, too. The total acceleration of any such volume of liquid is then given only by the sum of forces that cross its boundary, which is the starting point condition for the derivation of the Navier-Stokes equation. The intrinsic hydrodynamics is an advantage of DPD as compared to other simulation techniques. In the Brownian motion approach, for example, the random force is not pairwise, but is related to a fixed background so that the momentum is no longer conserved.

Alternative methods of temperature control Besides the DPD thermostat, there are several other methods to control the simulation temperature. The Nosé-Hoover thermostat [64, 65] is widely used in molecular dynamics. Here a heat bath is introduced as an integral part of the Hamiltonian by adding an extra term

- an artificial variable with an artificial mass. The disadvantage of the Nosé-Hoover thermostat is that it does not satisfy Galilean invariance, i.e. a preferential inertial reference frame is singled out by the implementation of the thermostat. Hence, the motion of the center of mass of the system has to be explicitly corrected for, otherwise temperature increases. This is in particular problematic for nonequilibrium simulations. Furthermore, the Nosé-Hoover thermostat is a global algorithm with a uniform, unrealistic dissipation of energy in the system. Hence, it does not allow for a local temperature control. Another approach often used in MD simulations is the Berendsen thermostat [66] which very efficiently reaches a target temperature. However, it suppresses fluctuations of the kinetic energy and hence does not reproduce the canonical ensemble, especially for small systems. Usually it is used in combination with the Nosé-Hoover thermostat for an initial equilibration.

The temperature control method used in this work is the DPD thermostat (described in previous paragraph). This technique was worked out as a modification of the Langevin thermostat [67]. In both methods a random force and a constant friction is applied to all particles. The two forces are related via a fluctuation-dissipation theorem. Similarly to the DPD thermostat, the Langevin thermostat is a stochastic, local method where the energy dissipation in the system is spatially localized. As opposed to the DPD implementation, each particle has its own heat bath independent of all other particles. Another stochastic realization is Andersen's scheme [68] which consists in a velocity rescaling. The velocity of a particle is periodically exchanged for that of a bath particle. This procedure mimics collisions with bath particles at a specified temperature T. The strength of the coupling to the heat bath is given by a collision frequency Γ. The drawback of the Andersen and Langevin thermostats consists in the absence of momentum conservation and thus hydrodynamics. In both these stochastic thermostats, propagation of momentum is disturbed due to uncorrelated random forces so that a reliable reproduction of viscosity is problematic. In case that transport properties play a role in the system of interest, the DPD thermostat is the method of choice.

A variation of the DPD technique based on the Andersen thermostat was introduced by Lowe [69, 70]. In the spirit of Andersen's thermostat, with an exchange frequency Γ new particle velocities are taken from a Maxwell distribution. This stochastic velocity is, nevertheless, imposed on pairs of neighboring particles in such a way as to conserve the overall momentum. This method was developed to combine the advantage of the DPD thermostat (locality, Galilean invariance, conservation of momenta) while satisfying the detailed balance condition[1] like the

[1]The principle of detailed balance describes the relation of transition probabilities P between

Andersen's method. The viscosity of the fluid in this method is proportional to the exchange frequency Γ which in turn determines the thermostat efficiency. Therefore, when aiming at a good thermostat sampling a low viscosity regime cannot be accessed.

Within this context, an important characteristics of the system is the Schmidt number, Sc. This dimensionless quantity is defined as the ratio of kinematic viscosity ν and the diffusion coefficient D. In a fluid, the momentum is transported rapidly via interparticle forces. A different time scale is given by the mass transport, i.e. the displacement of particles, which is slow in comparison to the momentum transport. This results in a rather high Schmidt number for fluids, $Sc_{fluid} \sim 10^3$. In DPD, the soft-core potential does not allow for such an efficient momentum transport. In a DPD fluid the intrinsic viscosity is of the same order as the diffusion coefficient and the Schmidt number takes low gas-like values, $Sc_{DPD} \sim 1$. In this way, when the viscous time scale is matched, the diffusion rate of the DPD fluid is overestimated. Using the Lowe-Andersen method one can achieve a much higher viscosity than with DPD, which can be crucial when the correct representation of viscous flow is essential. On the other hand, in some cases a simulation technique with fast diffusion is useful. For molecular processes that are diffusion controlled, DPD allows to observe the phenomena of interest within a shorter simulation time [71].

2.3 Connecting particles to larger structures

Larger entities like lipids and proteins are constructed by connecting individual beads i, j via a harmonic potential

$$U_{harm}(r_{i,i+1}) = \frac{1}{2} k_{harm}(r_{i,i+1} - l_0)^2. \tag{2.9}$$

In bead-spring polymer models, an anharmonic potential is sometimes used to model the bonds. The finite extensible nonlinear elastic (FENE) potential is given by $U_{FENE} \sim r_0^2 \ln[1-(r/r_0)^2]$ for the interparticle distance $r \leq r_0$ and it is infinite for $r > r_0$. The force derived from the FENE potential is approximately linear at small and intermediate distances. However, it grows dramatically when the two particles get far apart, not allowing for a too large separation between them. In our

two states A, B for a system in equilibrium: $N_A P(A \to B) = N_B P(B \to A)$, where $N_{A,B}$ denote the number of particles in each state. The transition processes must be reversible, which in the DPD thermostat is violated by the dissipative force.

simulations no drag force is applied at the lipids and proteins and the connecting springs oscillate around an equilibrium length only due to thermal motion. The harmonic potential is sufficient to maintain the integrity of the structures.

The rigidity of a hydrocarbon chain model is assured by a three point bending potential assigned to three consecutive beads

$$U_{bend}(r_{i,i+1}, r_{i+1,i+2}) = k_{bend}(1 - \cos(\theta - \theta_0)), \tag{2.10}$$

where $\cos(\theta) = \boldsymbol{e}_{i,i+1} \cdot \boldsymbol{e}_{i+1,i+2}$. For a straight linear arrangement the angle $\theta_0 = 0$ was used. A non-zero preferred angle was also used in some of the simulations, and here the force acting on a bead i as derived from Eq. (2.9) has the form

$$\boldsymbol{F} = \frac{k_{bend} \sin(\theta - \theta_0) \left[\boldsymbol{e}_{jk} - \boldsymbol{e}_{ij}(\boldsymbol{e}_{ij} \cdot \boldsymbol{e}_{jk})\right]}{r_{ij} \left|\sin\theta\right|}. \tag{2.11}$$

2.4 Parameters

The above described interactions are sufficient for manufacturing a model of a membrane in an explicit water solvent. Due to the amphiphilic nature of the lipids, a membrane forms spontaneously from a random distribution of lipids and water in the simulation box [72]. Membrane properties of the DPD model can be linked to experimental values and give comparable results, e.g. for the lateral stress profile, area compression modulus, or the bending rigidity.

The parameters in our simulations have the following values: the spring stiffness $k_{harm} = 100 k_B T / r_0$, the equilibrium bond length $l_0 = 0.45 r_0$ and the bending rigidity $k_{bend} = 10 k_B T / r_0$. In our simulations the lipid model is typically formed by one hydrophilic head bead and three hydrophobic tail beads; the general case of a hydrophobic length n is denoted by L_n. The mass of all beads as well as the temperature is set to unity in our simulations. The bead density of the whole system is $\rho = 3/r_0^3$, the initial lipid area density in the membrane is $\rho = 2.8/r_0^2$. The distribution of particle velocities is well captured by a Maxwell-Boltzmann distribution. According to Ref. [73] it is safe to use time-steps <0.05 in order to avoid errors of temperature over 2%. Our choice of time-step is $\Delta t = 0.01$.

2.5 Barostat

Natural membranes are considered to have a zero surface tension, and there are several strategies to achieve this in simulations. A commonly used technique is combining DPD with a Monte Carlo algorithm to update the box size at random time points. Another method to find the lipid density for a tensionless membrane within a box of fixed dimensions is a trial and error approach. By adding single lipids and evaluating the resulting tension the system size can be fine-tuned.

In this work we used a real-time relaxation method - the barostat algorithm presented by Jakobsen [74]. This method is an analogy of the Langevin piston barostat used in molecular dynamics simulations [75]. Here the simulation box is allowed to shrink and expand due to a virtual piston, so that in every step all the positions of particles are rescaled according to the breathing of the simulation box. The size of the simulation box changes upon the action of a piston force $\boldsymbol{F}_\beta$ described by the Langevin equation. The force $\boldsymbol{F}_\beta$ depends on several contributions: the pressure difference between the actual and the target pressure $(P - P_0)$, DPD bead momenta $\boldsymbol{p}_i$, a dissipative force proportional to the piston force $\boldsymbol{v}_\beta$ and a random force dependent on a random variable ξ_β

$$F_\beta = [\Delta V(P - P_0) + \frac{d}{N_f}\sum_i \frac{\boldsymbol{p}_i^2}{m} - \frac{\gamma_\beta \boldsymbol{v}_\beta}{M_\beta} + \frac{\sigma_\beta \xi_\beta}{2M_\beta\sqrt{\Delta t}}] \tag{2.12}$$

Except for the degrees of freedom N_f of N beads in $d = 3$ dimensions ($N_f = dN - d$), there are three additional degrees of freedom that represent the three edge lengths of an orthorhombic box, $\boldsymbol{\beta}$. In our simulations, the two edges parallel to the membrane bilayer are coupled to assure a square membrane patch, so that there are actually only two free parameters. The mass of the piston M_β is given by $M_\beta = (N_f + d)k_B T\tau^2$, where τ is the characteristic barostat time which is set to $\tau = 2$ in our implementation. Since there are in general different fluid phases in the system, the pressure P is a tensor

$$P^{xy} = \frac{1}{V}\left(\sum_i \frac{v_i^x v_i^y}{m} + \sum_i F_i^{Cx} r_i^y\right) \tag{2.13}$$

where x, y stands for any pair of the three space coordinates. The target pressure P_0 in our simulations has the value of $P_0 = 23.649 k_B T/r_0^3$. The dissipation of piston σ_β and the coefficient for the random force γ_β are again related via the

dissipation-fluctuation theorem

$$\sigma_\beta^2 = 2\gamma_\beta M_\beta k_B T \tag{2.14}$$

Here, the parameters are $\gamma_\beta = 10/\tau = 5$.

Thus, when using the barostat the volume V of the simulation box is slightly fluctuating around the initial value. The Langevin framework, however, does not lead to unphysical oscillations of the simulation box as observed in case of some other barostat implementations. The barostat algorithm introduced in [74] also requires a shorter equilibration time and is characterized by shorter correlation times of various system parameters as compared to other methods. For the practical use, it is important that the coupling of the pressure to the system does not enforce the use of smaller time steps Δt than the simple DPD algorithm, thus allowing for efficient simulations.

2.6 Calculating the trajectories

Knowing the initial conditions and the forces acting on each bead, we are interested in how the system will evolve in time. There are various numerical methods for integrating the equations of motion. The most intuitive one, the Euler method, is based on an approximation to the first derivative. While the Euler method offers the most straightforward way to calculate the trajectories, it is inaccurate and numerically unstable especially for larger timesteps Δt. Velocity-Verlet (VV) falls into the class of second order methods of numerical integration similarly to the basic Verlet or the Leapfrog algorithms. These methods use an approximation to the second derivative. Even more precise higher order algorithms like Runge-Kutta can be used but their accuracy is paid by the fact that they are computationally more demanding.

The basic Verlet algorithm is derived by writing two Taylor expansions of the position vector in times $(t - \Delta t)$ and $(t + \Delta t)$

$$\boldsymbol{x}(t + \Delta t) = \boldsymbol{x}(t) + \boldsymbol{v}(t)\Delta t + \frac{\boldsymbol{a}(t)\Delta t^2}{2} + \frac{\boldsymbol{b}(t)\Delta t^3}{6} + \mathcal{O}(\Delta t^4), \tag{2.15}$$

$$\boldsymbol{x}(t - \Delta t) = \boldsymbol{x}(t) - \boldsymbol{v}(t)\Delta t + \frac{\boldsymbol{a}(t)\Delta t^2}{2} - \frac{\boldsymbol{b}(t)\Delta t^3}{6} + \mathcal{O}(\Delta t^4). \tag{2.16}$$

where $\boldsymbol{a}(t)$ is the acceleration and $\boldsymbol{b}(t)$ is the jerk, i.e. the time derivative of

acceleration, of the particle. Summing up the two equations we obtain

$$\boldsymbol{x}(t+\Delta t) = 2\boldsymbol{x}(t) - \boldsymbol{x}(t-\Delta t) + \boldsymbol{a}(t)\Delta t^2 + \mathcal{O}(\Delta t^4). \tag{2.17}$$

As can be seen from Eq. (2.17), evolving a trajectory requires the knowledge about the positions in the current step and also in one preceding step. For the first iteration, an approximative way of estimating the position shift is used. The absence of explicit terms for the velocity can present a technical challenge in the calculation of many physical variables.

The Velocity Verlet uses a similar approach but includes the velocity explicitly. It is calculated at the same time point as the positions (as opposed to the Leapfrog method)

$$\boldsymbol{x}(t+\Delta t) = \boldsymbol{x}(t) + \boldsymbol{v}(t)\Delta t + \frac{1}{2}\boldsymbol{a}(t)\Delta t^2 \tag{2.18}$$

$$\boldsymbol{v}(t+\Delta t) = \boldsymbol{v}(t) + \frac{\boldsymbol{a}(t) + \boldsymbol{a}(t+\Delta t)}{2}\Delta t \tag{2.19}$$

Velocity-Verlet is usually used to calculate trajectories in molecular dynamics simulations. Among the advantages of VV against the Euler method is, besides the numerical stability, also the possibility to implement constraints more easily on motion, e.g. when connecting particles by springs. It also offers other useful properties like time-reversibility.

The standard algorithm for numerically integrating the equations of motion for dissipative particle dynamics is a modified Velocity-Verlet algorithm (DPD-VV). The VV algorithm assumes the acceleration of a particle to depend on its positions only and not on velocity. This is not fulfilled for non-conservative systems. In dissipative particle dynamics the dissipative force is velocity dependent and the velocities in turn are governed by the dissipative forces. In DPD-VV it is accounted for that in an approximate manner by updating the dissipative forces additionally at the end of every iteration step.

2.7 Integration schemes

The simulation codes for the projects described in this work were written in Fortran90. In case of the NVT ensemble where a fixed simulation box is used, the integration was performed according to [62]. The calculation of the dynamics of the system is performed for N_{steps} iterations where the positions and velocities of all particles are updated. In every step a new velocity is calculated for each

bead according to the total force acting on it. Subsequently, the new positions are calculated from the velocities and the forces are re-evaluated in accordance with the new conformation. At the end the velocities are updated and the dissipative force accordingly changed.

Thus, every iteration according to the DPD-VV integration scheme involves the following steps:

1. Calculate velocities $\boldsymbol{v}_i \leftarrow \boldsymbol{v}_i + \frac{1}{2m}(\boldsymbol{F}_i^C \Delta t + \boldsymbol{F}_i^D \Delta t + \boldsymbol{F}_i^R \sqrt{\Delta t})$
2. Update positions $\boldsymbol{x}_i \leftarrow \boldsymbol{x}_i + \boldsymbol{v}_i \Delta t$
3. Calculate all the forces $\boldsymbol{F}_i^T = \sum_{i \neq j}^{N} \left(\boldsymbol{F}_{ij}^C + \boldsymbol{F}_{ij}^D + \boldsymbol{F}_{ij}^R\right)$
4. Calculate velocities
   (a) $\boldsymbol{v}_i^0 \leftarrow \boldsymbol{v}_i + \frac{1}{2m}(\boldsymbol{F}_i^C \Delta t + \boldsymbol{F}_i^R \sqrt{\Delta t})$
   (b) $\boldsymbol{v}_i \leftarrow \boldsymbol{v}_i^0 + \frac{1}{2m}(\boldsymbol{F}_i^D \Delta t)$
5. Update the dissipative force $\boldsymbol{F}_i^D$
6. Calculate physical quantities of interest

In the self-consistent version of the integrator the loop over steps (4b) and (5) is repeated until the instantaneous temperature has reached its limiting value. Here a more efficient scheme was used that only includes these steps once, as it was shown to give a sufficiently good performance [62]. The random variable ξ_{ij} is supposed to exhibit a Gaussian distribution, the production of which is however computationally very expansive. Here a more efficient way with ξ_{ij} coming from a uniform distribution was used instead. No statistical difference was found between simulations using the two types of random variables [59]. Note that the contribution of the random force is scaled as $\sqrt{\Delta t}$. It results from underlying stochastic equations [63, 59] based on the Wiener process as a simple approach to model Brownian motion.

For the constant normal pressure and constant surface tension ensemble, a more complicated procedure had to be implemented. The DPD-VV algorithm is extended to include the piston motion and the velocities of the particles are now influenced by the piston coordinates and vice versa. The variables not specified up to now are introduced only for the sake of code optimization.

1. Store old piston velocities and box dimensions $\boldsymbol{v}_{\boldsymbol{\beta}}'' \leftarrow \boldsymbol{v}_{\boldsymbol{\beta}}'$, $\boldsymbol{v}_{\boldsymbol{\beta}}' \leftarrow \boldsymbol{v}_{\boldsymbol{\beta}}$, $\boldsymbol{\beta}' \leftarrow \boldsymbol{\beta}$

2. Calculate new bead velocities $\boldsymbol{v}_i \leftarrow \boldsymbol{v}_i + \frac{1}{2m}(\boldsymbol{F}_i^C\Delta t + \boldsymbol{F}_i^D\Delta t + \boldsymbol{F}_i^R\sqrt{\Delta t} - 2\boldsymbol{v}_\beta\boldsymbol{v}_i\Delta t)$

3. Calculate new piston velocity and piston shift
   $\boldsymbol{v}_\beta \leftarrow \boldsymbol{v}_\beta + \frac{\boldsymbol{F}_\beta}{2W}\Delta t, \quad \boldsymbol{\beta} \leftarrow \boldsymbol{\beta} + \boldsymbol{v}_\beta\Delta t$

4. Calculate bead positions $\boldsymbol{x}_i \leftarrow (\boldsymbol{x}_i + \boldsymbol{v}_i\Delta t)\exp(\boldsymbol{\beta} - \boldsymbol{\beta}')$

5. Update volume V

6. Calculate forces $\boldsymbol{F}^C$, $\boldsymbol{F}^D$ and $\boldsymbol{F}^R$

7. Calculate pressure $P = \frac{1}{dV}(\sum_i \boldsymbol{p}_i^2/m + \sum_i \boldsymbol{F}_i^C \cdot \boldsymbol{x}_i)$

8. Store velocities $\tilde{\boldsymbol{v}}_i \leftarrow \boldsymbol{v}_i, \quad \tilde{\boldsymbol{v}}_\beta \leftarrow \boldsymbol{v}_\beta$

9. First guess for piston velocity $\boldsymbol{v}_\beta : \boldsymbol{v}_\beta \leftarrow \boldsymbol{v}_\beta'' + 2\frac{\boldsymbol{F}_\beta}{W}\Delta t$

10. Iterations to find barostat values
    (a) $\boldsymbol{v}_i \leftarrow \frac{1}{1+\boldsymbol{v}_\beta\Delta t}\left[\tilde{\boldsymbol{v}}_i\exp(\beta - \beta') + \frac{1}{2m}(\boldsymbol{F}_i^C\Delta t + \boldsymbol{F}_i^D\Delta t + \boldsymbol{F}_i^R\sqrt{\Delta t})\right]$
    (b) Compute $\boldsymbol{F}_\beta$
    (c) $\boldsymbol{v}_\beta \leftarrow \tilde{\boldsymbol{v}}_\beta + \frac{\boldsymbol{F}_\beta}{2W}\Delta t$

11. Update dissipative force $\boldsymbol{F}^D$

To account for the interplay of particle velocities and the barostat motion a multiple iteration of the steps (10)-(12) takes place. In our code this loop is repeated five times as this allows for the convergence of the iterations. Comparing the two schemes, the algorithm which includes barostat is computationally more expensive and therefore it is typically used only in the initial phase of the simulation. After the system achieves equilibrium, the basic DPD algorithm with fixed box dimensions is used.

2.8 Initial and boundary conditions

For the simulations an orthorhombic simulation box was used with periodic boundaries, i.e. a particle that escapes the box at one boundary appears on the opposite side of the box with the same velocity. The bilayer is spread in a horizontal plane parallel to the base of the box and it virtually continues in all the images of the simulation box forming an "infinite" membrane. The box size has to be chosen

sufficiently large in order to prevent finite size-effects, especially interaction of the bilayer with its own images in neighboring boxes in the vertical direction. For some applications, one also has to consider the influence of the box on bilayer fluctuations taking into account that the periodic boundaries impose a planar non-curved arrangement of the membrane.

If a proper concentration of lipids and water beads is randomly distributed in the box, a membrane will spontaneously self-assemble after a sufficient time. For speeding up the equilibration part of the simulation, we usually used a predefined membrane setting where concrete starting positions in the midplane of the box are assigned for the lipid beads. The initialization also includes assigning velocities to all the beads. The values for initial velocities are generated randomly with the condition of the Maxwell-Boltzmann distribution and an overall temperature set as a parameter. For the integration of equations of motion we use the DPD Velocity-Verlet (DPD-VV) algorithm as described in the previous chapter.

Unless stated otherwise, simulations were performed for $N_{steps} = 10^6$ timesteps of duration $\Delta t = 0.01$ with box dimensions of $10 - 30 r_0^3$. At the beginning of each simulation an equilibration of the system with a barostat was done for $2 \cdot 10^5$ time-steps.

2.9 Physical properties of the simulated system

To prove the correct functionality of the program, several physical quantities were measured.

Temperature During the whole simulation, the temperature has to be constant and equal to the value set in the parameter definition. The temperature of a system with N particles of mass m is given as the kinetic temperature by

$$\langle k_B T \rangle = \frac{m}{3N} \sum \boldsymbol{v}_i^2 \tag{2.20}$$

Due to the operation of the DPD thermostat the temperature fluctuates only slightly around the temperature set up in the initialization part of the simulation. In our implementation it is set to unity, $k_B T = 1$. The plot (Fig. 2.3) shows the kinetic temperature as a function of the simulation time. After a very short period of equilibration, the temperature becomes constant with small fluctuations. The peak in the first steps of the simulation is caused by the random initial positioning of water beads, which can occasionally overlap and thus causes extremely strong

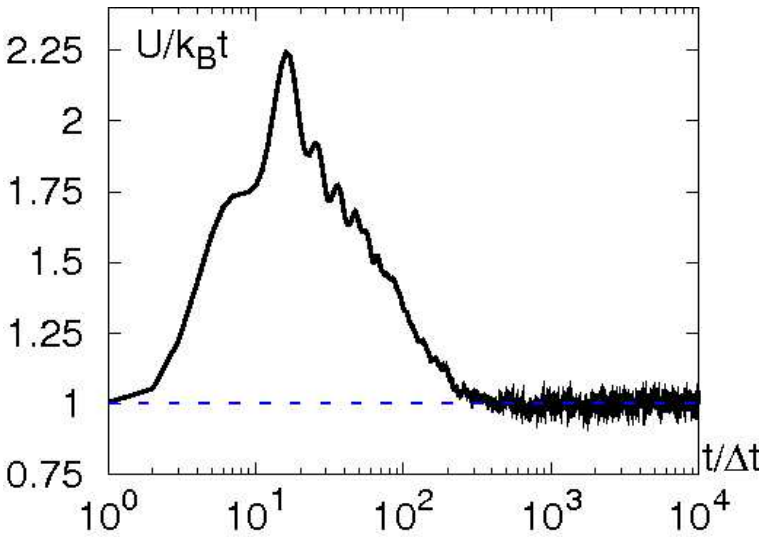

Figure 2.3: *The temperature fluctuates around unity as requested by the parameter settings. The x-axis is plotted logarithmically to show the initial relaxation in more detail.*

repulsions from each other. Owing to the choice of a sufficiently small time-step, this does not occur any more after the initial equilibration.

Bead velocity The average velocity of all beads

$$\langle \boldsymbol{v} \rangle = \frac{1}{N} \sum_{i=1}^{N} \boldsymbol{v}_i \tag{2.21}$$

was measured to be zero throughout the simulations. The velocity distribution (see Fig. 2.4) of the absolute velocities $v = \sqrt{v_x^2 + v_y^2 + v_z^2}$ must have the form of the Maxwell-Boltzmann distribution

$$p(v) = \sqrt{2/\pi} \left(\frac{m}{k_B T} \right)^{3/2} v^2 \exp\left(\frac{-mv^2}{2k_B T} \right), \tag{2.22}$$

which indeed was the case for all timesteps.

Density profiles If not only water beads, but also lipids (which form a membrane) are included in the system, the density of different bead types is not uniform. We therefore measured the average density of beads in $0.25 r_0$ thick slides

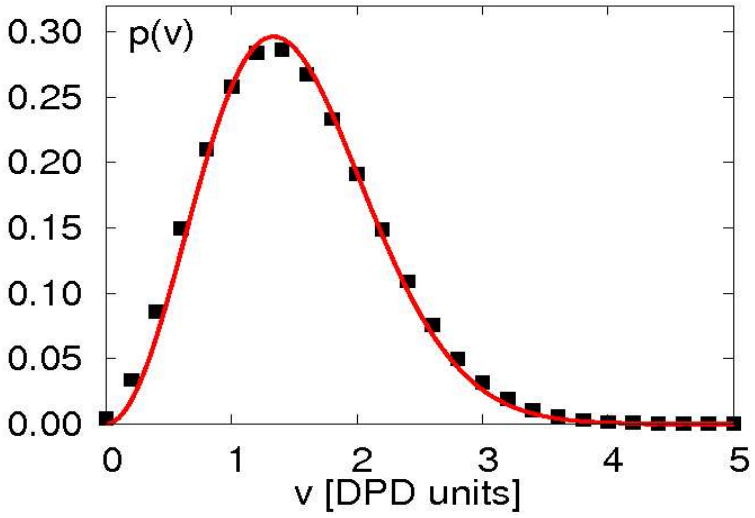

Figure 2.4: *The Maxwell-Boltzmann distribution (red line) characterizes the distribution of absolute velocities of beads (filled squares).*

of the simulation box parallel to the membrane plane. As can be seen in Fig. 2.5, below and above the membrane there is a water layer of a homogeneous density $\rho = 3r_0^3$. The lipid heads are indicated with peaks at the solvent-membrane interface. Whereas there are water beads surrounding the lipid heads, the water density is zero in the hydrophobic core of the membrane due to the strong hydrophobic interaction between water and hydrophobic tail beads. The lipid tails are slightly compressed and the membrane core is filled up with an almost homogeneous density. Thus, the lipid chains are disordered in a way that is characteristic for the fluid phase of a lipid bilayer. There is a visible dip in the bead density in the middle of the bilayer indicating that all lipid tails terminate near to the bilayer midplane. Yet, this dip is not very deep as the lipids of opposite layers are slightly interdigitated. From Fig. 2.5 we can also infer the membrane thickness. The distance between centers of mass of the head beads in opposite leaflets was measured to be $\sim 3.8r_0$.

Barostat We can test the barostat algorithm by calculating the dimensionless compressibility of water

$$\kappa^{-1} = \frac{V}{\langle dV^2 \rangle \rho} \tag{2.23}$$

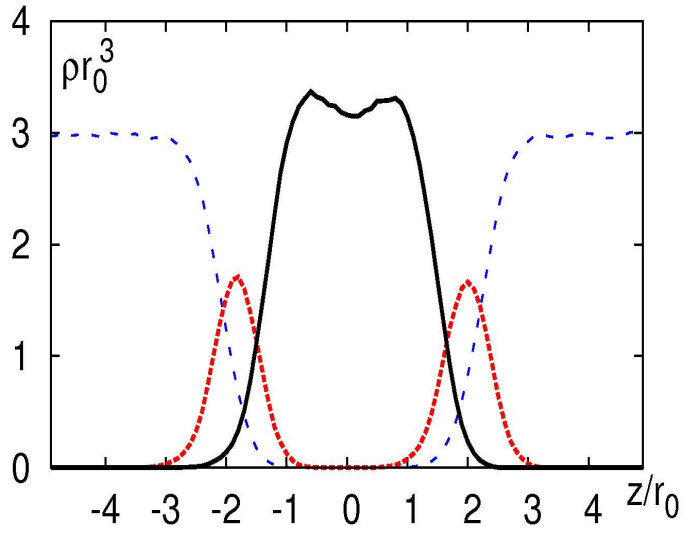

Figure 2.5: *The density profile of the simulation box in the direction normal to the membrane plane. Hydrophobic tails are depicted with a straight black line, hydrophobic heads with red dotted line and waters with blue dashed line.*

in a DPD system consisting of only one bead type with repulsion parameter $a_{ij} = 25k_BT$ and the density $\rho = 3/r_0^3$. A system with these parameters is supposed to reproduce correctly the compressibility of water [73]. We measured the fluctuations of the box volume dV in a simulation box of $(15r_0)^3$ for 10^6 time-steps. The measurement gave the value $\kappa^{-1} = 15.95$ which is in a good agreement with [73] where $\kappa^{-1} = 15.98$ was found.

The fluctuations of the box edges caused by the barostat piston force can be seen in Fig. 2.6. Here, the barostat was used for the whole simulation (10^6). The membrane is placed in the xy-plane. The initial planar density of lipids was too low and so the box xy-dimension had to decrease. This is compensated by an expansion of the z-edge, so that the volume and thus the overall bead density are conserved. We can see that approximately after 2×10^5 time-steps the system already fluctuates only slightly around the final values indicating that this is a sufficient time period for equilibration. The center of gravity of the entire system is placed in the center of the simulation box reacting on the piston movement appropriately.

The effect of the piston on membrane surface tension is shown in the last plot of Fig. 2.6. Surface tension can be computed [76] from the pressure tensor as

$$\sigma = L_z(P_{norm} - \langle P_{lat} \rangle), \tag{2.24}$$

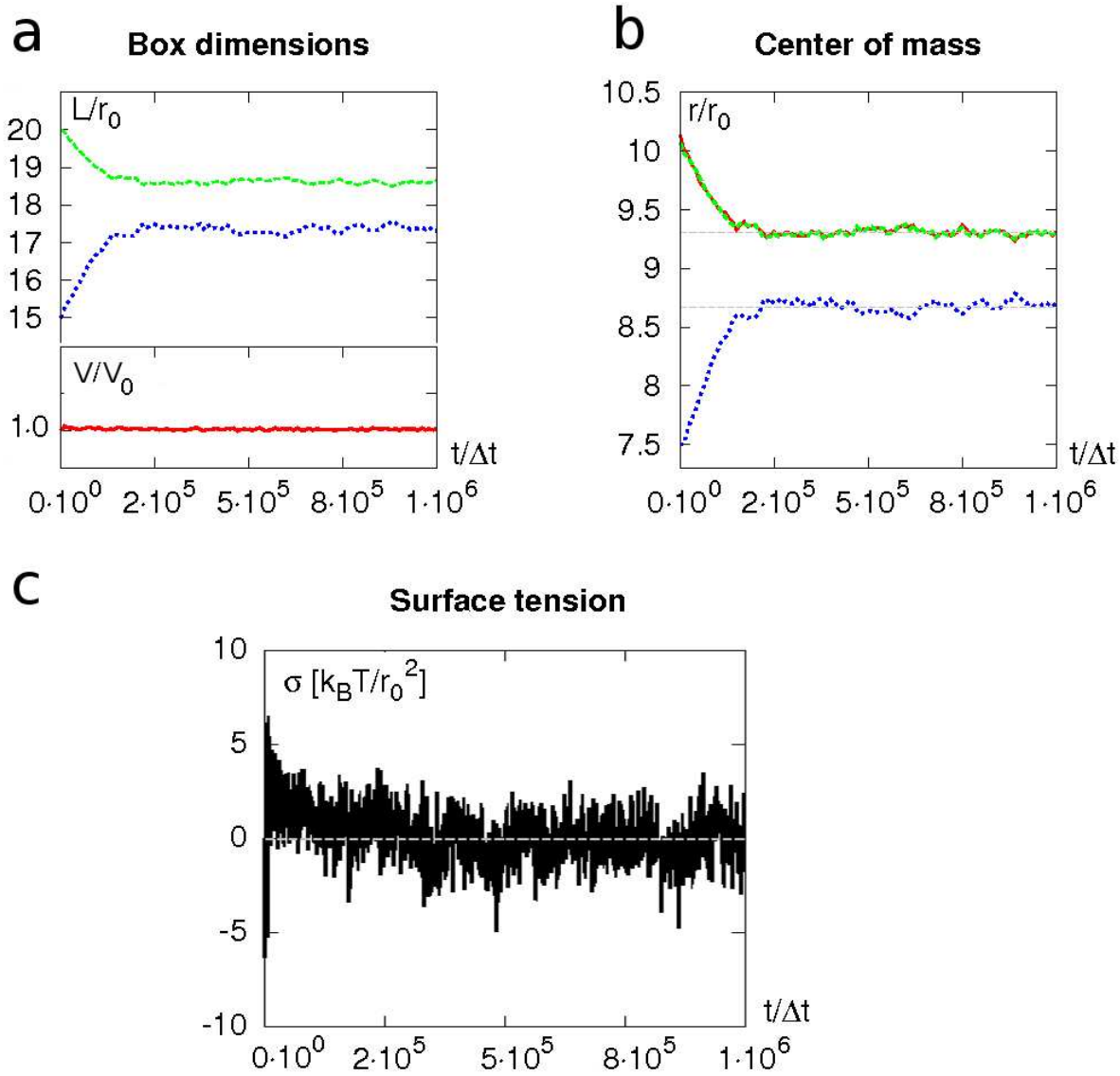

Figure 2.6: *Fluctuations of the box dimensions with barostat. (a) While the coupled x- and y-edges (green) are shrinking, the z-edge (blue) is expanding to keep the volume V (red) constant. (b) The center of mass stays in the middle of the simulation box (x, y, z - red, green, blue). (c) The surface tension of the membrane fluctuates around zero. Data for all the three graphs come from the same simulation run.*

where P_{norm} is the component of pressure in the direction normal to the bilayer plane (here the z-direction) and $\langle P_{lat} \rangle$ is the average of tangential components, P_{xx} and P_{yy}. Although there are fluctuations, after the equilibration the mean surface tension is zero.

2.10 Conversion to SI units

Simulation units are defined by the simulation time $\Delta t = 0.01$ and the cutoff radius for interaction between two beads, $r_0 = 1$. For a conversion to SI units we will take into account that one water bead represents $N_w = 3$ water molecules [77] and the volume occupied by a single water molecule is $V_w = 30\text{Å}^3$ [78]. The overall density of beads set up in our simulations is $\rho = 3r_0^{-3}$. In a simulation box containing only water, a unit volume $1r_0^3$ contains 3 water beads, meaning 9 water molecules of 30Å^3 each. In this way the r_0 can be found as

$$r_0 = \sqrt[3]{\rho N_w V_w} = 6.43\text{Å} \tag{2.25}$$

In case of a heterogeneous composition of the system, where beads of different types form structures, the density varies throughout the simulation box. The effective volume (how much space can be occupied by one bead) depends on the local density of the given bead type and it is influenced by the interactions with the surrounding. Knowing the number of lipids in the bilayer of a given equilibrated area we obtain a surface area of $\sim 65\text{Å}^2$ per lipid which corresponds to the value for lipids in a biological membrane [79]. One hydrophobic tail bead then corresponds to roughly 3.8 hydrocarbon groups.

To match the time unit, we can similarly compare the diffusion coefficient of a single lipid with the experimental value. In our system, a single time-step $\Delta t = 0.01$ corresponds to ~ 90ps [43].

Chapter 3

On the role of acylation of transmembrane proteins

In this chapter, we will study the influence of a protein modification named acylation on transmembrane proteins. We show that acylation influences the tilting of transmembrane proteins and thus their effective hydrophobic mismatch. This leads to a change in clustering behaviour in one and two-species membranes and alters protein sorting into membrane domains.

3.1 Acylation *in vivo*

Acylation is a posttranslational chemical modification that consists of a covalent linking of a fatty acid to a protein. A common type of a posttranslational acylation is palmitoylation (sometimes referred to as S-acylation) where palmitate, a 16-carbon saturated acyl chain (Fig. 3.1), is attached to a Cys-residue of a protein. This type of acylation is particularly useful due to its reversible character. The function of proteins can be modulated via palmitoylation in cycles, switching between activation and deactivation. Other types of acylation involve myristyl and farnesyl groups.

Proteins that undergo acylation are ubiquitous in many eukaryotic cell types (yeast, insect, and vertebrate cells), as well as in viruses that replicate within these cells [81]. Acylation triggers the membrane association of intrinsically hydrophilic proteins. Especially many signaling molecules are anchored by long fatty acid chains to the cytoplasmic face of the plasma membrane [82]. Here, acylation can be used to control the distribution of proteins between membrane and cytoplasm.

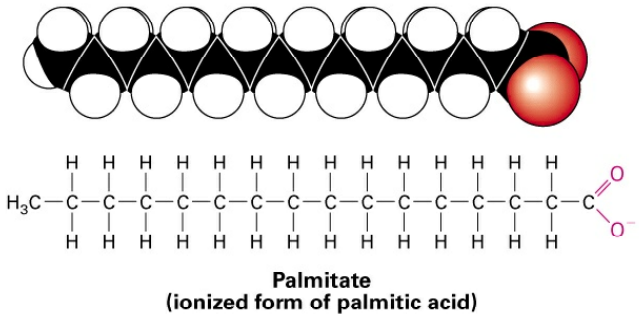

Figure 3.1: *Fatty acid chain that is attached to a protein during palmitoylation [80]*

A single palmitate is considered to be sufficient for membrane association of a short peptide, whereas for larger proteins multiple acylations may be necessary. In this case, the additional lipid modifications are often found at nearby sites. Enzymes involved in signaling like the G protein Gsα [83] or the endothelial nitric oxide synthase (eNOS) [84] undergo palmitoylation cycles. Another example of the regulation of protein transport by palmitoylation is related to signaling pathways in nerve terminals [85]. When the protein PSD-95 (postsynaptic density protein) is palmitoylated, it becomes restricted to the postsynaptic membrane where it can bind ion channels and induce their clustering.

Acylation is often linked to trafficking of peripheral membrane proteins. One of such examples is the palmitoylation of oncogenic Ras proteins [86] where the presence of a palmitate modulates the subcellular localization of the protein. A continuous cycle of de- and reacylation accounts for specific localizations of Ras isoforms to the plasma membrane and the Golgi apparatus, and thus drives a rapid exchange of both protein pools. Acylation also was suggested to promote targeting of proteins to membrane microdomains enriched in glycosphingolipids and cholesterol as it was shown for acylated chimeric green fluorescent reporter proteins, GFPs [87]. In human T-cell lymphoma cell lines, dual acylation of Src-family kinase Hck is required for its targeting to membrane rafts and thereupon for its role in chemotaxis [88]. Lipid modifications also affect protein-protein interactions, e.g. by leading the proteins to the membrane surface, hence increasing their local concentration and the probability of encounter [89].

Besides peripheral membrane proteins, also many transmembrane (TM) proteins are subject to lipid modifications, even though anchoring to a membrane is

already ensured by the transmembrane domain (TMD) of the proteins (Fig. 3.2). The role of acylation of integral proteins is not well understood, but in many cases acylation is here associated with protein segregation and clustering. One of the proposed functions for acylation of transmembrane proteins is also protection from the quality control machinery. [90]

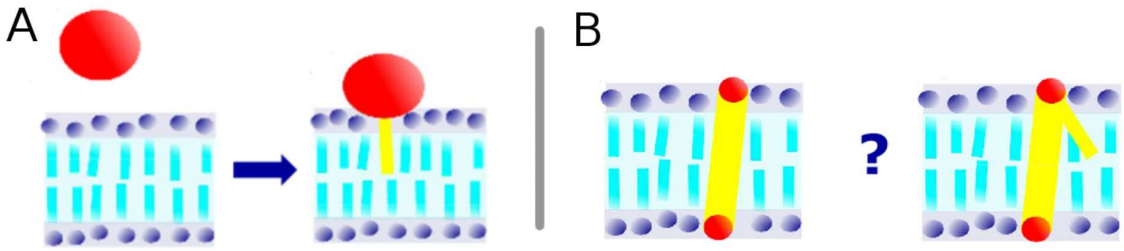

Figure 3.2: *The fatty acid chain acquired via acylation serves to soluble proteins as an anchor for binding at the membrane surface (A). In case of transmembrane proteins, the role of acylation is not yet well understood (B).*

An illustrative example of a palmitoylated transmembrane protein is LRP6, a protein involved in Wnt/Wg signaling in mammals and flies. In the work of Abrami et al. [91] it was shown that palmitoylation is necessary to allow the protein to leave the endoplasmic reticulum (ER). The protein acquires a palmitate after translation and clearing the quality control in order to be able to reach the plasma membrane via the Golgi apparatus. The inhibition of palmitoylation led in experiments [91] to a retention of LRP6 in the ER. This phenotype was nevertheless rescued by dispatching several amino acid residues from the TMD. Thus, shortening of the non-modified protein restored the protein's ability to travel to the plasma membrane. Furthermore, a shortening of a protein that did undergo palmitoylation led again to a retention in the ER. This observation points to a possible role of hydrophobic mismatch in the quality control of the ER. It was proposed that palmitoylation promotes the tilting of the protein and thus reduces the hydrophobic mismatch between the TMD of the LRP6 protein and the surrounding bilayer.

As discussed in more detail in Section 1.5, hydrophobic mismatch is a central concept for understanding the behavior of transmembrane proteins in different membrane environments [15]. If the length of the transmembrane domain (TMD) does not match the thickness of the membrane's hydrophobic core, deformation of

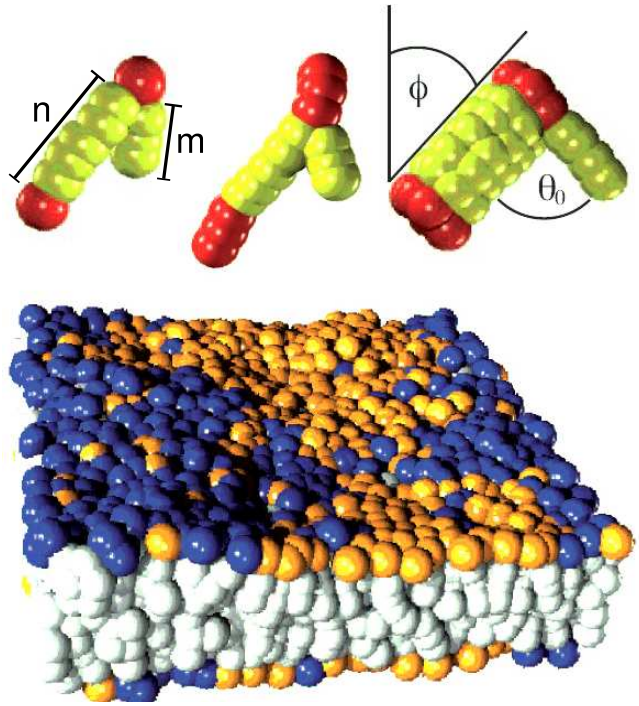

Figure 3.3: *Three models for an acylated transmembrane protein: HT_nH^A, $H_3T_nH_3^A$ and $(HT_nH)_7^A$, $(n = 5)$. Hydrophobic beads forming the TMD depicted in yellow, hydrophilic beads in red. The structure of $(HT_nH)_7^A$ is hexagonal resulting in a cylindrical shape, for this model we used an acyl chain of length $m = 4$. Lower picture: Inhomogeneous membrane - long lipid heads in blue, short lipid heads in orange, all tails in grey*

the lipids can lead to entropy-driven cluster formation [42]. While a negative mismatch (TMD too short) leads to a local compression of lipids, a positive mismatch (TMD too long) induces a local stretching of lipids. If the mismatch is too large to be compensated by lipid stretching, the protein may tilt relative to the bilayer normal [43]. Underlining its impact on biological function, hydrophobic mismatch has been shown experimentally to be an important driving force for protein sorting *in vivo* [50, 48].

Following up on these ideas, we aim here at elucidating the role of acylation on the positioning of transmembrane proteins in the membrane and their partitioning behavior.

3.2 Model

The membrane consists of simplified lipids (denoted as LT_3) modeled as linear chains of one hydrophilic (H) head and three hydrophobic tail (T) beads connected via Hookean springs and with a bending stiffness along the chain to increase the rigidity. For homogeneous, single-species bilayers all lipids were assigned the same

parameter values $k_{harm} = 100 k_B T / r_0^2$, $l_0 = 0.45 r_0$, $k_{bend} = 10 k_B T / r_0^2$ (see Chapter 2 for the details of the simulation procedure). For inhomogeneous bilayers, 50% of all lipids were assigned a relaxation distance $l_0 = 0.60 r_0$ for the Hookean spring. The resulting longer lipid species is denoted as Lt_3 with t standing for the hydrophobic beads of the longer lipid. The long lipids segregate spontaneously to form a membrane microdomain as illustrated in Fig. 3.3. The membrane is immersed in a water solvent (W). The repulsion parameters for the various bead types for the inhomogeneous membrane were:

$$a_{ij} = \frac{k_B T}{r_0} \begin{pmatrix} & W & H & T & t \\ W & 25 & 25 & 200 & 200 \\ H & 25 & 25 & 200 & 275 \\ T & 200 & 200 & 25 & 35 \\ t & 200 & 275 & 35 & 35 \end{pmatrix} \tag{3.1}$$

The simplest model for a transmembrane protein consisted of a linear HT_nH chain of beads. One hydrophilic head (H) at each end of the protein encloses a hydrophobic domain (T) with different lengths of the hydrophobic core ($n = 4, 5, 6, 7$). To one of the head beads a hydrophobic chain of length m was added (Fig. 3.3) representing the acyl chain ($m = 3$ unless stated otherwise). To inspect the more general case of a protein consisting not only of the transmembrane domain, but also of a hydrophilic cytosolic domain, we performed simulations with a model $H_3T_nH_3$ extended by a linear sequence of three additional hydrophilic beads at both ends of the transmembrane domain (Fig. 3.3). When considering this construct, the fatty acid chain was attached to the H bead adjacent to the hydrophobic chain. The acylated forms will be referred to as HT_nH^A and $H_3T_nH_3^A$, respectively. There was no bending potential imposed for a preferential angle between the acyl chain and the TMD, so that it was free to move relative to the TMD.

At the contact zone of the lipid phases in inhomogeneous membrane there is a local disturbance of lipid tilting resulting from the height difference between the two lipid domains. The protein model consisting only of a single chain is rather flexible and gets unnaturally bent especially in these bordering regions. Therefore, we also considered a more robust construct composed of a hexagonal arrangement of seven linear chains $(HT_nH)_7$. With an effective diameter of $2r_0$ corresponding to roughly 2 nm, this construct represents a protein with a stiff α-helical transmembrane domain. As before, the palmitate was a single chain of length $m = 4$ (unless stated otherwise) connected to one of the head beads on the

rim of the hydrophilic layer. Parameters for the connecting Hookean springs were again $k_{harm} = 100k_BT/r_0^2$, $l_0 = 0.45r_0$, $k_{bend} = 10k_BT/r_0^2$. Due to the increased TMD mass, we also imposed a preferred angle θ_0 between the fatty acid and the transmembrane domain with values $20° < \theta_0 < 90°$ to support the effect of the modification. Unless stated otherwise, the data presented below will refer to the acylated construct with $\theta_0 = 90°$ and $m = 4$.

The different lengths n of the proteins' transmembrane domain correspond to different degrees of hydrophobic mismatching. The protein model $n = 5$ has a length of 3.78 nm (see Section 2.10 for relation of DPD and SI units) and hence it fits best into the membrane core. This construct exhibits an almost vanishing mismatch. The shorter protein ($n = 4$) is 3.27 nm long and induces a compression of the surrounding membrane by ~ 0.50 nm. On the contrary, protein models $n = 6, 7$ with lengths 4.20 and 4.65 nm, respectively, are associated with a positive hydrophobic mismatch. The membrane thickness in the region surrounding the proteins is increased by ~ 0.80 nm for both $n = 6, 7$ [43]. This indicates that with a hydrophobic length exceeding $n = 6$ the bilayer cannot be stretched anymore to compensate for the mismatch. Instead of a further swelling of the bilayer encompassing the protein, a tilting of the protein's transmembrane segment with respect to the bilayer normal is energetically more favorable for models with $n > 6$.

The simulations were typically performed for 10^6 time steps after a barostat equilibration lasting 10^5 steps.

3.3 Results

Tilting of proteins First we examined whether acylation influences the tilting angle ϕ between the TMD and the bilayer normal (see Fig. 3.3). As already pointed out in Section 3.2, we used three different constructs to study the transmembrane proteins. All protein constructs were inserted in a membrane of LT_3 lipids. We studied the temporal variation of tilting angles between the bilayer normal and the protein axis with and without acylation. After an equilibration with barostat, ϕ was monitored for 10^6 time steps within a tensionless membrane patch of $\sim 10r_0 \times 10r_0$. Representative distributions of tilting angles $p(\phi)$ sampled over the whole simulation time are shown in Fig. 3.4. The shape and width of the distributions for non-acylated and acylated proteins is similar. The mean tilting angle $\langle\phi\rangle$ is nonetheless shifted toward larger values in the latter case.

Next we examined the dependence of the mean tilting angle on the hydrophobic length, acylation state and model type. Consistently with earlier results [40] on

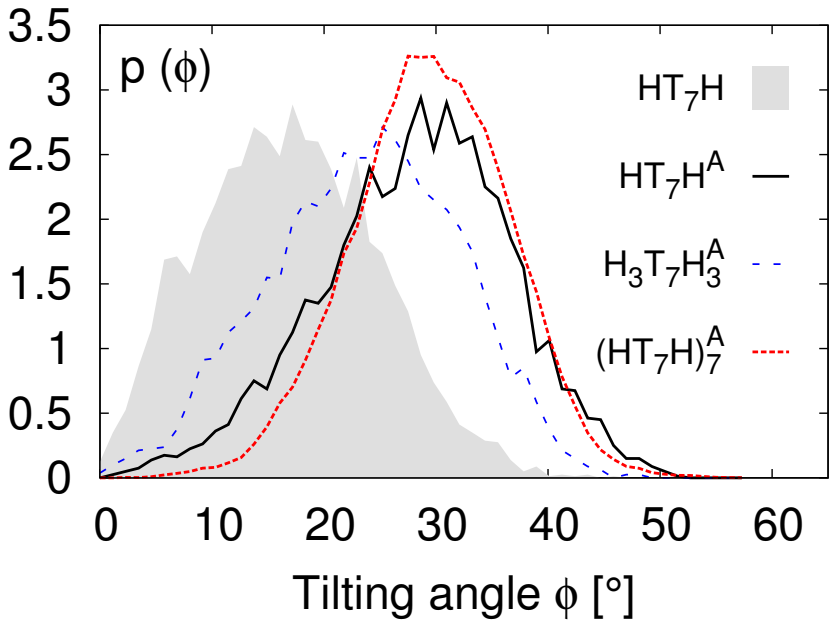

Figure 3.4: *Probability distributions of tilting angles for different model proteins with a hydrophobic core of $n = 7$, i.e. showing a considerable hydrophobic mismatch. All distributions have a similar width with a pronounced shift towards higher mean values for acylated constructs. An extensive hydrophilic domain ($H_3T_nH_3$) softens the effect, but it still remains significant.*

non-acylated proteins we found a small average tilting angle of $\phi \leq 10°$ for a vanishing (n=5) and negative ($n < 5$) mismatch (Fig. 3.5). The more robust structure $(HT_nH)_7$ perturbs more surrounding lipids when tilted, so that it is more stably anchored in the membrane. Here the tilting angle of the non-mismatched protein is even smaller. For a positive mismatch the tilting angle increases with the length of the hydrophobic domain of the inclusion (i.e. with the number of hydrophobic beads n).

When the fatty acid modification is attached to the protein, the average tilting angle is in general increased. This effect is particularly strong for proteins with a positive hydrophobic mismatch. Surprisingly, we observed an enhanced tilting also for the vanishing and negative mismatch, where the protein is even more buried into the membrane core upon acylation. The tilting angles of acylated and non-acylated proteins averaged over the whole simulation time are depicted in Fig. 3.5. In general, for acylated proteins we observe an enhancement of the dependence of tilting angle on the TMD length.

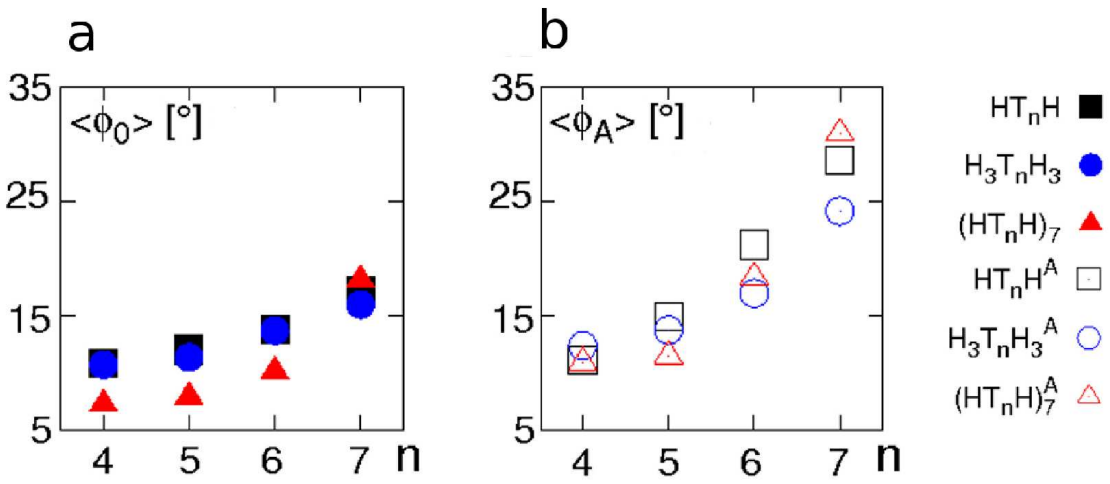

Figure 3.5: *Average tilting angles - non-modified (a) and acylated (b) proteins. The tilting angle increases with a positive hydrophobic mismatch, i.e. when the proteins TMD exceeds in length the membrane core (n=6,7). We observe a clear tendency of acylated proteins to be stronger tilted than the native versions.*

The stength of the effect of acylation depended on the construct used. The TMD of the basic model (HT_nH) consists of a linear chain and a single hydrophilic head group at either end of the TMD. This model has the advantage that it is rather loosely positioned in the membrane. Thus, the effects of acylation on the protein's situation are very pronounced. On the other hand, transmembrane proteins typically have larger hydrophilic domains exposed to the solvent. These additional domains could hinder the acylation-enhanced tilting by pulling the ends of the TMD towards the solvent. To address this point we added two extra hydrophilic beads at each end of the TMD chain ($H_3T_nH_3$). Indeed, the tilting was less pronounced yet still significant (Fig. 3.4,Fig. 3.5). Thus, the effect is robust even when considering larger soluble protein portions attached to the TMD and in further studies we used for simplicity only the TMD segment with a single layer of hydrophilic heads.

The most rigid hexagonal structure $(HT_nH)_7$ was implemented to avoid the undesirable flexibility of the linear chain models. This construct corresponds to a rigid α-helical transmembrane domain. To find optimal parameters for the model we also imposed a preferred tilting angle θ (see Fig. 3.3) between the transmembrane segment and the fatty acid. When varying θ between 20° and 90° an enhanced tilting is observed of similar character, but somewhat weaker for the smaller angles

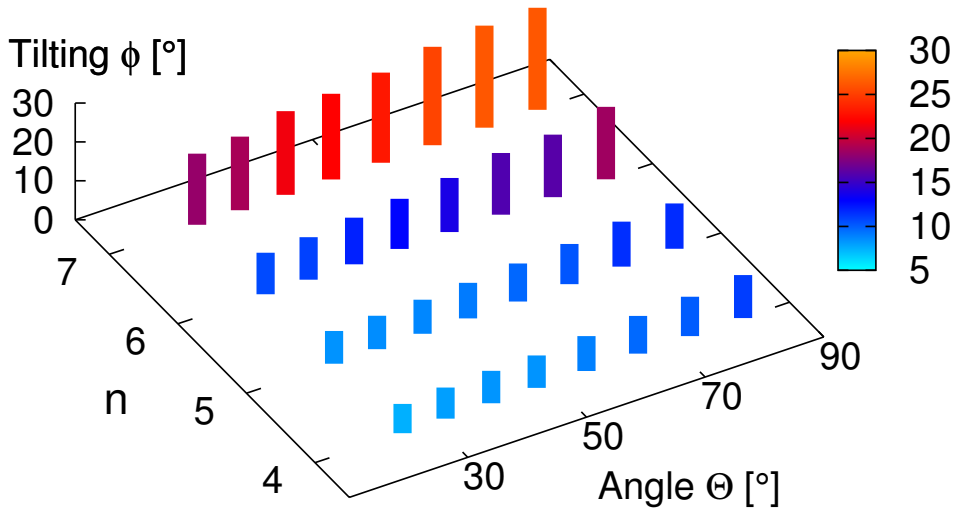

Figure 3.6: *Model $(HT_nH)_7$: Dependence of the tilting angle ϕ on protein length n and the preferred value of the angle θ between the fatty acid and the TMD segment which was fixed by an additional three-point potential. The tilting is increasing with a wider preferred angle θ.*

(Fig. 3.6).

When comparing the mean tilting angles of proteins with and without acylation, we can conclude that the described effect is significant for all studied protein lengths and types. This observation is illustrated by the ratio of average tilting angles with and without acylation $\langle\theta_A\rangle/\langle\theta_0\rangle$. The ratio is above unity for all the examined cases. The tilting efficiency of acylation quantified by $\langle\theta_A\rangle/\langle\theta_0\rangle$ is summarized in Fig. 3.7.

Effective hydrophobic mismatch is altered upon acylation The protein tilting is a mechanism to decrease the effective hydrophobic mismatch by burying a portion of the protein's TMD within the membrane core. By effective hydrophobic mismatch, Δh_E, we mean here the length of the TMD that exceeds an unperturbed membrane thickness when taking into account the protein tilting. Δh_E is a relevant quantity to assess the impact of acylation on the protein's orientation in the bilayer. As shown in Fig. 3.8, the acylated protein with $n = 7$ mimics the behavior of the shorter non-acylated inclusion of length $n = 6$. Also, there is a significant difference between the effective hydrophobic mismatch of acylated and non-acylated versions of the protein with a vanishing mismatch, $n = 5$. Here, the addition of acylation

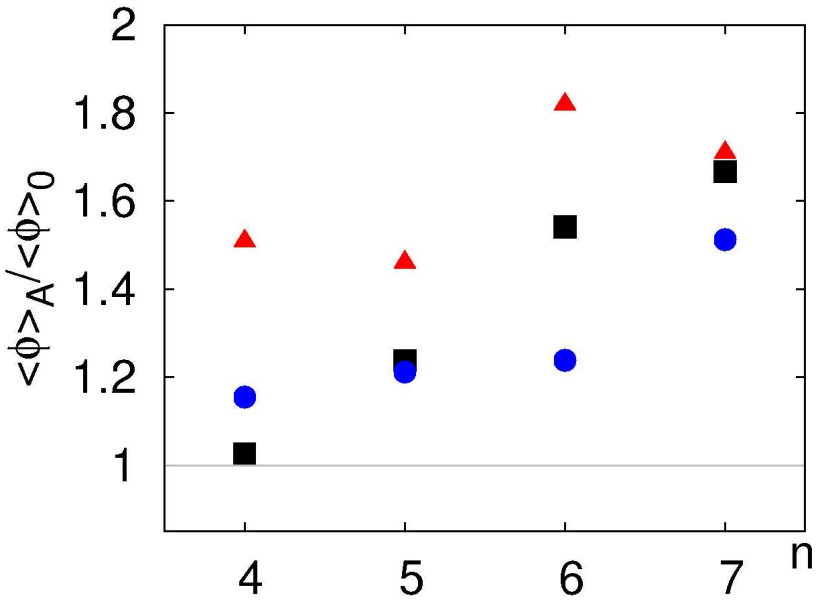

Figure 3.7: *Attachment of a fatty acid to the protein led to a pronounced enhancement of the tilting for all proteins with positive mismatch and even induced an increased tilting in case of negative mismatch, so that the ratio of average tilting angles* $\langle\theta_A\rangle/\langle\theta_0\rangle$ *is bigger than one for all the studied protein lengths and types. Black squares:* (HT_nH)*, blue circles* $(H_3T_nH_3)$*, red triangles* $(HT_nH)_7$

leads to a negative effective mismatch. These observations are in a good agreement with the experimental findings of Abrami et al. [91] which link the length of the TMD of the LRP6 protein and its acylation state to the protein's ability to escape the endoplasmic reticulum for plasma membrane.

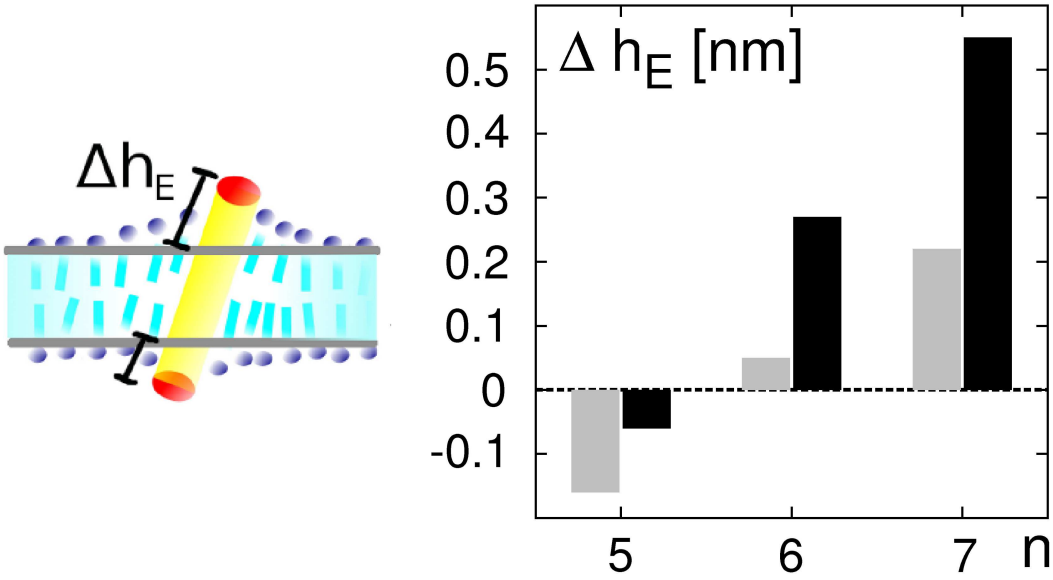

Figure 3.8: *Effective hydrophobic mismatch and the influence of acylation.* HT_nH *black,* HT_nH^A *grey.*

The length of the modifying acyl chain We next studied the influence of the length of the fatty acid chain, m, on the tilting angle (Fig. 3.3). We varied $m = 1, \ldots, 8$ and monitored the average tilting angle $\langle\phi\rangle$ of protein types HT_7H^A and $(HT_7H)_7^A$. As can be seen in Fig. 3.9, there exists an optimum length of the acyl chain which promotes the protein tilting with a maximal efficiency. For the single-chain model HT_7H^A we observe a sharp peak for the length $m = 3$. In case of the more robust protein $(HT_7H)_7^A$ the peak has a strong onset but is less pronounced and shifted to $m = 4$. In general, the most efficient length of the acyl chain $m \approx 3$ corresponds to the length of the hydrophobic tail of lipids forming the bilayer. We can conclude that the tilting is maximally affected when the acyl chain can roughly span one leaflet of the bilayer.

Impact of acylation on protein clustering We have seen that acylation strongly influences the effective hydrophobic mismatch of a transmembrane protein

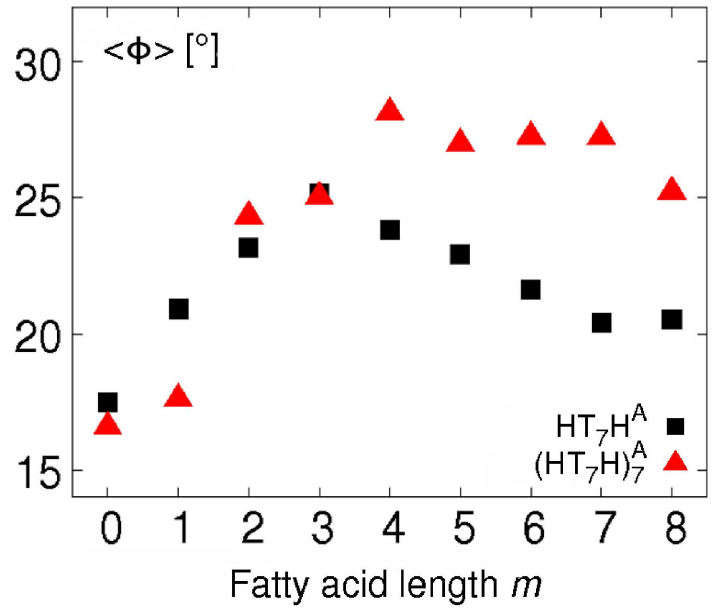

Figure 3.9: *Protein's tilting angle as a function of the length of the modifying fatty acid. The maximum tilting efficiency of acylation occurs with a fatty acid spanning roughly one layer of the membrane (the hydrophobic length of a lipid is* $n_{lipid} = 3$*)*

situated in a lipid bilayer. Taking into account the hydrophobic mismatch-driven clustering of transmembrane proteins, we asked how the protein oligomerization is affected by acylation. For this purpose we determined the radial distribution function $g(r)$

$$g(r) = k \frac{1}{\pi[(r+\Delta r)^2 - r^2]} \frac{2A}{N(N-1)} \tag{3.2}$$

where k is the number of pairs with a protein-protein distance in the interval of $r+\Delta r$, A is the area of the membrane patch and N is the total number of proteins in the patch. We obtain the number of pairs k directly from the measurements and this value is normalized by the size of the respective shell (second term) and by the overall density of inclusion pairs (third term). The radial distribution function $g(r)$ is a type of a pair correlation function commonly used to describe the structure of a fluid. It estimats the average density of particles at a coordinate r relative to any particle in the fluid.

We inserted nine proteins (HT_nH or $(HT_nH)_7$) in a tensionless membrane patch of size $\sim 30r_0 \times 30r_0$. The initial configuration of proteins was a regular pattern covering the whole area.

The clustering is indicated in $g(r)$ by a strong peak for small distances (see

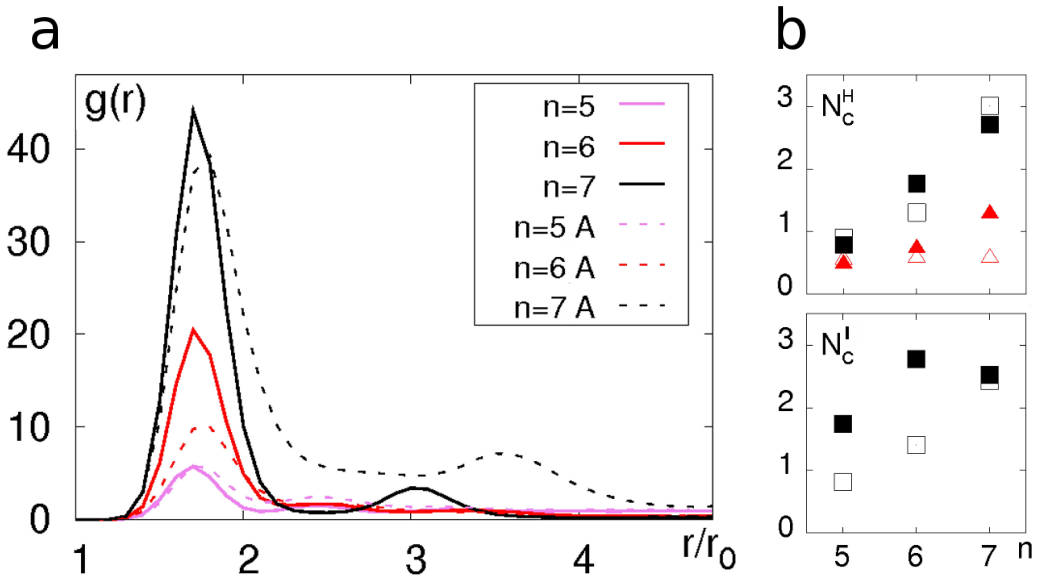

Figure 3.10: *Radial distribution function of proteins $(HT_nH)_7$ in a homogeneous membrane (a). Cluster sizes - average number of neighbors within a distance of $\approx 2.5r_0$ from a reference protein in a homogeneous (N_c^H) and inhomogeneous (N_c^I) membrane. In general, clustering upon acylation is diminished. Black squares: $(HT_nH)_7$, red triangles: (HT_nH), full symbols: non-acylated, open: acylated (b).*

a representative plot in Fig. 3.10a) which corresponds to a high probability of a small interprotein distance. Secondary peaks indicate the existence of some further prominent protein-protein distances, pointing to a higher order cluster. From $g(r)$ we also determined the number of neighboring proteins, N_c, with a protein-protein distance $\leq 2.5r_0$. For a vanishing hydrophobic mismatch ($n = 5$) cluster formation was hardly observed, i.e. $N_c < 1$ for all considered proteins. For $n > 5$ hydrophobic mismatch-induced cluster formation was well observed for $(HT_nH)_7$. Also HT_nH showed a significant yet less pronounced clustering in dependence on the TMD length (see Fig. 3.10b). As expected, the clustering of the less bulky protein model is weaker because the number of lipids affected by its presence in the membrane is smaller. Compared to the hexagonal model, the membrane deformation is less significant and thus less energy can be saved by clustering. Acylation in general abandoned cluster formation with the exception of $(HT_7H)_7$ that showed a slight increase in N_c.

In this context, it is worth noting that the oligomerization of proteins with a hydrophobic mismatch is driven by the deformations of the membrane and the entropy of lipid ordering. Upon acylation, the effective mismatch is decreased, but the acylation itself may present a substantial contribution to the membrane disturbances. The competition between these two aspects determines the overall behavior of the system. Hence, depending on the hydrophobic mismatch, acylation mainly reduces but can also support cluster formation.

In the presence of lipid microdomains To explore the possible role of acylation on the partitioning behavior of transmembrane proteins in inhomogeneous membranes, we implemented a model membrane that consisted of two lipid species that differed in length (cf. Section 3.2). These membranes show a spontaneous segregation of lipids [40] with a coexistence of two lipid phases of different thickness (Fig. 3.3). The membrane thickness in the two phases was measured to be $4r_0$ and $5.5r_0$, respectively. Since the simple HT_nH model protein proved to be unnaturally flexible and compressible when subject to forces at the domain borders, in the following we only use the $(HT_nH)_7$ and $(HT_nH)_7^A$ proteins.

Several studies have highlighted that a hydrophobic mismatch drives partitioning of a protein to the lipid phase with the least mismatch [43, 42, 50]. To quantify this observation, we measured the average fraction of short lipids among all lipids f_s surrounding a protein in a distance $r < 3r_0$. To check the validity of the averaging method we also measured the time dependence of $f_s(t)$ (Fig. 3.11, inset). Indeed, we observed that proteins with a short TMD did spend more time in the

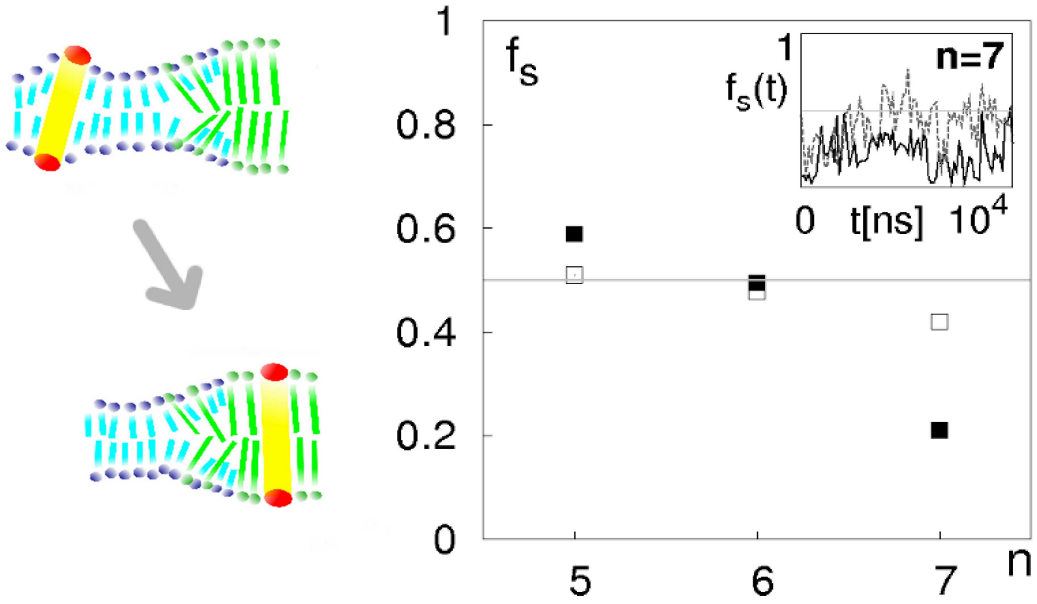

Figure 3.11: *Lipid environment of proteins - the fraction of short lipids among all lipids within a distance smaller than $3r_0$ from a protein of length n. Non-acylated proteins partition according to mismatch whereas acylation abolishes the preference for one lipid phase. Full symbols - non-acylated, open symbols - acylated. Inset: Time course of f_s for a non-acylated (full line) and acylated (dashed line) protein*

thinner domain, while long proteins preferred regions with longer lipids (Fig. 3.11). This mismatch-based partitioning was, however, abolished upon acylation, where f_s rather tended towards 50% indicating that acylation allows the protein to move with more freedom in the segregated membrane. The results suggest that acylation conceals the hydrophobic mismatch of the protein also in a more complicated membrane structure.

Similarly to the case of bilayers with a homogeneous thickness, acylation decreased the clustering tendency of mismatched proteins, i.e. the number of neighbors in a cluster N_c decreased (Fig. 3.10b). Already the setup with many acylated proteins embedded in a membrane with two phases allows for a variety of scenarios. It depends on the particular properties of the system whether and to which extent the clustering occurs and which one of the lipid phases is preferential. Although the data interpretation is here not straightforward, we observe rather an increase of protein's independence upon acylation. In the cell membrane, a much higher complexity of the environment and acylated protein types suggests a plethora of realizations. Still, the simple model presented here points to the possible underlying mechanisms involved in these processes.

3.4 Discussion and conclusion

Here, we have used coarse-grained membrane simulations to elucidate the role of acylation on transmembrane proteins. We have found that acylation significantly alters the tilting of transmembrane proteins in dependence on the TMD length. Moreover, the presence of a fatty acid modification was found to alter hydrophobic mismatch-induced clustering in homogeneous and inhomogeneous lipid bilayers. In nearly all the studied cases acylation prevented clustering. In addition, acylated transmembrane proteins showed a significantly different partitioning on phase-separated bilayers with regions of different thickness: While non-modified proteins always partitioned into the phase that matched best the length of their TMD, the addition of a fatty acid significantly increased the probability to also visit regions in which the TMD experienced a stronger hydrophobic mismatch. Due to the intrinsic coarse-graining of our model, we cannot distinguish between different types of acylation but the implications of our results for protein trafficking might be of special importance to palmitoylated proteins as the reversibility of palmitoylation allows for a cyclic change.

In our simulations, we have used three models for transmembrane proteins, HT_nH, $H_3T_nH_3$ and $(HT_nH)^7$, which varied in the rigidity and diameter of the TMD and in the extent of the hydrophilic portion. All models showed similar phenomena, with some minor changes in the actual numbers, hence underlining that the observed effects of acylation are fairly robust and not very specific to the chosen model. The higher flexibility of the single-chain constructs (HT_nH and $H_3T_nH_3$), however, may be inconsistent with the expected rigidity of natural α-helical TMDs, which rely very much on extensive hydrogen bonding. We therefore consider the $(HT_nH)^7$ construct to be a more realistic model.

The results and predictions of our simulations may be tested directly using artificial membranes (e.g., supported bilayers or giant unilamellar vesicles) and purified transmembrane peptides with a designed TMD length and acylation state. The predicted partitioning behavior of (acylated) proteins may be studied, for example, by simple time-lapse fluorescence microscopy on phase-separating ternary lipid mixtures. The inhibition of cluster formation due to hydrophobic mismatching may be studied on homogeneous membranes with fluorescence resonance energy transfer, which can test directly the oligomeric state of fluorescently labeled proteins. An alternative would be fluorescence (cross) correlation spectroscopy, which relies on the change in the (co-)diffusional mobility due to oligomerization.

Our findings support the notion that acylation, e.g. palmitoylation, indeed may be involved in the regulation of the transport behavior of transmembrane cargo proteins. Taking into account that the turnover kinetics of COPI and COPII vesicle machineries is modulated by clustering ([92, 93, 94]), we predict that acylation counteracts the sorting of transmembrane proteins into transport vesicles. This prediction may be tested by adding palmitoylation sites to simple transmembrane peptides with a well-characterized length of the TMD. The transport behavior of such tailored cargo proteins has been studied in detail (11), and therefore provides a suitable approach for testing our prediction. This prediction, however, assumes that ER membranes are fairly homogeneous in thickness, i.e., proteins do not partition diffusively into a domain with the least hydrophobic mismatch. Owing to the complexity of ER membranes, the existence of thinner and thicker domains is conceivable. In this case, acylation actually may promote ER export above a basal level by allowing proteins to explore the other domains more easily. Which of the two scenarios is applicable can only be decided by inspecting the particular protein construct. Coming back to the recent data on LRP6 (6), these, relate

the TMD length and acylation state to its transport behavior. Furthermore, the reported experimental data highlight an additional ER retention mechanism via ubiquitination of some, but not all of the studied LRP6 mutants. It is hence well anticipated that additional cellular factors will influence the transport of (acylated) transmembrane proteins, yet the effects described here are very likely a crucial ingredient that can tip the balance toward the desired trafficking behavior.

Chapter 4

Monotopic membrane proteins

In this chapter we use coarse-grained membrane simulations to study several aspects of the dynamics of monotopic membrane proteins, i.e. proteins permanently associated with the membrane surface by a hydrophobic anchor. First, we have studied how monotopic proteins with hydrophobic moieties of varying length and diameter perturb the host membrane locally. Second, we have examined the tendency of monotopic proteins to form oligomers due to non-specific membrane-mediated interactions. As a result, we observed that different types of oligomers form when PMPs are residing in the same and in opposite leaflets of a membrane. Finally, we discuss the relation between the local membrane perturbations and the cluster formation ability, and we also point out implications of our results on biological processes.

4.1 Introduction

Internal organization of biomembranes In recent years, our view on the organization of biomembranes has qualitatively changed. It is well accepted by now that membranes are not simple homogeneous two-dimensional fluids in which lipids and proteins are randomly dispersed. Rather, membranes are subdivided into (dynamic) islands composed of distinct lipids and proteins. In particular, the formulation of the 'raft hypothesis' by Simons and colleagues [95] has triggered numerous studies on the existence, composition, and dynamics of membrane microdomains. While in artificial bilayers the existence of lipid rafts, i.e. domains with a distinct lipid composition, is by now well established [96], the existence of protein-lipid domains/rafts *in vivo* is much less clear and still a matter of debate. It

is commonly appreciated, however, that the formation of (transient) higher-order structures on cellular membranes, e.g. during the formation of transport intermediates [97, 98] or in the context of signaling [99, 100], equips biomembranes with a distinct and dynamic substructure.

Membrane-mediated attraction between transmembrane proteins Work on membrane domains/rafts also pointed out the role of lipids as mediators of (attractive) interactions, which are complementary to specific binding events of proteins to and within membranes via cognate motifs emphasized by traditional biochemical approaches. Indeed, protein assembly due to membrane-mediated interactions was predicted as early as 1984 by Mouritsen and Bloom [42]. Subsequently, attractive forces between transmembrane proteins due to elastic distortions of the lipid bilayer have been investigated in more detail with continuum models [39, 101, 102]. Likewise, capillary forces [103], wetting effects [104], curvature [105, 106], and membrane fluctuations [107, 108, 109] have been implicated as a source for membrane-mediated attraction between transmembrane proteins. Theoretical and experimental work has highlighted that a mismatch between the hydrophobic thickness of a lipid bilayer and the length of the hydrophobic transmembrane domain of proteins can support oligomerization and protein sorting [48, 43, 50, 110, 111, 40]. Mismatch-driven assembly was also the subject of the previous chapter, where the role of acylation on oligomerization of transmembrane proteins with a hydrophobic mismatch was inspected.

Monotopic and peripheral membrane proteins A wide class of membrane proteins does not possess transmembrane domains but is only partially inserted into the lipid bilayer. Such proteins can associate with the membrane by means of ionic force, by a post-translational modification or by interactions with a more robust hydrophobic moiety. In the two first cases proteins can be washed away from the membrane without affecting the bilayer's stability. In many cases, the interaction with membranes can be tuned by switching between two conformational states of a protein, e.g. in case of the small GTPases Arf1 and Sar1. Here, an N-terminal amphitathic helix is exposed in the GTP-bound but not in the GDP-bound state[1]. Proteins bound to the membrane only temporarily or in cycles are usually referred to as **peripheral membrane proteins**. Integral proteins, on

[1]GTP - guanosine triphosphate - similarly to ATP this molecule has a role of energy source and activator of substrates in many cellular processes. It is essential to signal transduction. GDP - guanosine diphosphate - is the energetically poorer, hydrolysed form of GTP.

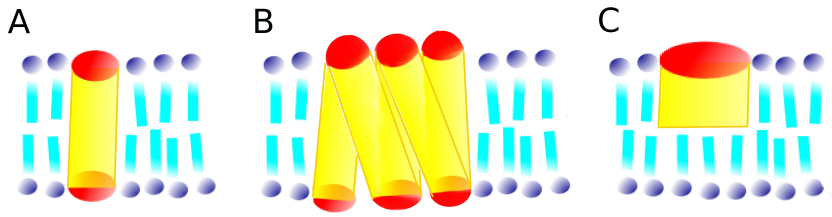

Figure 4.1: *Integral membrane proteins: (A) A single-pass and (B) a multiple-pass transmembrane protein (called in the classification by Blobel [112] as bitopic and polytopic, respectively). (C) Monotopic proteins interact with one membrane leaflet only.*

the contrary, are stably attached to the membrane and interact directly with its hydrophobic core. Besides transmembrane integral proteins, there are also proteins whose hydrophobic moiety does not span the whole membrane (see Fig. 4.1). This class is usually called **monotopic membrane proteins** [112]. In this chapter, the properties of monotopic proteins will be the subject of our interest.

So far, not many structures of monotopic proteins are available. The enzymes prostaglandin H2 synthase [113], fatty acid amide hydrolase [114], squalene cyclase [115], estrone sulfatase [116] and microsomal cytochrome P450 [117], however, have been described in detail [118]. All of these enzymes share some common features distinguishing them from integral transmembrane proteins, especially an arrangement that cannot be described as strictly $\alpha-$ or $\beta-$structures. Rather, they have globular shapes formed from a combination of motifs that run parallel with the membrane plane. One face of the protein is equipped with a hydrophobic plateau that is buried into one membrane leaflet only. In this membrane-resident domain also an active site entrance can be found. All of these enzymes function on both, lipophobic substrates and soluble homologs. Often they are composed as oligomers from several monotopic subunits.

The hydrophobic anchors of monotopic membrane proteins vary considerably in their spatial dimensions. Their length ranges between 3 and 30 Å and their surface area reaches up to 1600 $Å^2$. The insertion of peripheral and monotopic membrane proteins into lipid bilayers has already been studied in coarse-grained MD simulations for 11 protein species [119]. They were found to interact with the membrane only at the lipid-water interface in case of peripheral proteins and to reach deeply into the membrane if a more robust hydrophobic moiety was available. The proteins inserted deeply into the membrane core were shown to cause significant bilayer perturbations influencing for instance the bilayer thickness.

Monotopic or peripheral membrane proteins often serve crucial cellular functions, e.g. in the formation of coats around emerging vesicles [120, 97] and in signaling cascades [121]. In all these events, proteins on membrane surface need to build higher-order structures, sometimes even with partners that reside in opposite leaflets of the lipid bilayer. Given that membrane-mediated attraction has a considerable impact on transmembrane proteins, it is tempting to assume that also monotopic membrane proteins benefit from such a generic mechanism. We are not aware of theoretical studies on lipid-mediated interactions between monotopic membrane proteins. As it is also highly challenging to assess these phenomena experimentally, simulations lend themselves as a powerful alternative.

In the following, with the term "monotopic membrane proteins" we denote proteins that reside in one leaflets of the membrane via a rather robust hydrophobic anchor. The leaflet in which the protein is placed will be referred to as the "residential leaflet" in contrast to the "opposite leaflet" which may (at best) be in contact with the bottom of the protein.

4.2 Model

We modeled monotopic membrane proteins as cylindrical inclusions buried into one of the membrane layers. The model proteins (denoted as MP_n^k) were constructed as cylinders with a hexagonal cross section, consisting of one layer of hydrophilic beads and n layers of hydrophobic beads (Fig. 4.2). The hydrophilic layer of the protein is aligned with the headgroups of lipids, and the hydrophobic moiety is embedded in the membrane core. We used proteins with different radii k, where $(2k-1)$ is the number of beads along the hexagonal cross section of a protein. We have concentrated on proteins with membrane anchor length $n = 1 \ldots 5$. Lipids (denoted as L_m) were constructed as linear polymers consisting of one hydrophilic head and m hydrophobic tail beads. In all simulations, monotopic membrane proteins were inserted into pre-assembled lipid bilayers with a patch size of $(30\text{–}50r_0)^2$. Systems were equilibrated with a barostat until the membrane was in a tension-free state (2×10^5 time-steps). Afterwards, simulations of a duration of $1\text{–}2 \times 10^6$ time-steps Δt were performed during which the measurements of the systems' properties were recorded. A more detailed description of individual simulation settings and methods of data evaluation are described in the respective results sections.

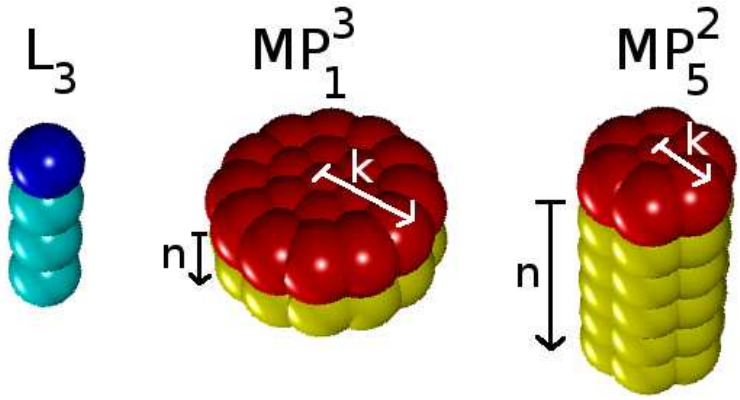

Figure 4.2: *Model system for monotopic membrane proteins. A model lipid consists of a linear chain of one hydrophilic head (blue) and three hydrophobic tails (cyan). Two representatives of monotopic proteins: a flat and wide protein MP_1^3 with radius $k = 3$ and hydrophobic length $n = 1$ and a far-reaching protein MP_5^2 with radius $k = 2$ and the length of membrane moiety $n = 5$. Protein heads are depicted in red, hydrophobic parts in yellow.*

4.3 Perturbation of lipid bilayers by monotopic membrane proteins

Unperturbed lipid bilayer As a starting point for a thorough study of the influence of a monotopic inclusion on the lipid organization in a membrane, it is useful to characterize a lipid bilayer consisting of L_3 lipids. The thickness of the bilayer was $h_0 = 3.84r_0$ when measuring the distance between the centers of lipid head beads in opposite leaflets. The thickness of one leaflet, i.e. the average distance between head and terminal tail bead within one leaflet, was $\lambda_0 = 1.63r_0$. Thus, the average distance between the terminal beads of lipids in the two layers was $\delta_0 = 0.58r_0$. Considering the effective radius r_0 of each bead a value $\delta < 2r_0$ indicates a slight interdigitation of the two monolayers with a maximal overlap of $\sim 1.4r_0$. The average tilting angle of individual lipids with respect to the bilayer normal was $\phi \approx 21°$ in agreement with earlier studies [43].

Characteristics of protein models First, we were interested in alterations of the lipid configuration and membrane shape as a result of the presence of a monotopic membrane protein in one layer. The measurements were performed with a single monotopic membrane protein with radius $k = 4$ and increasing hydrophobic length ($n = 1, 2, 3, 4, 5$). The resulting protein extension as measured

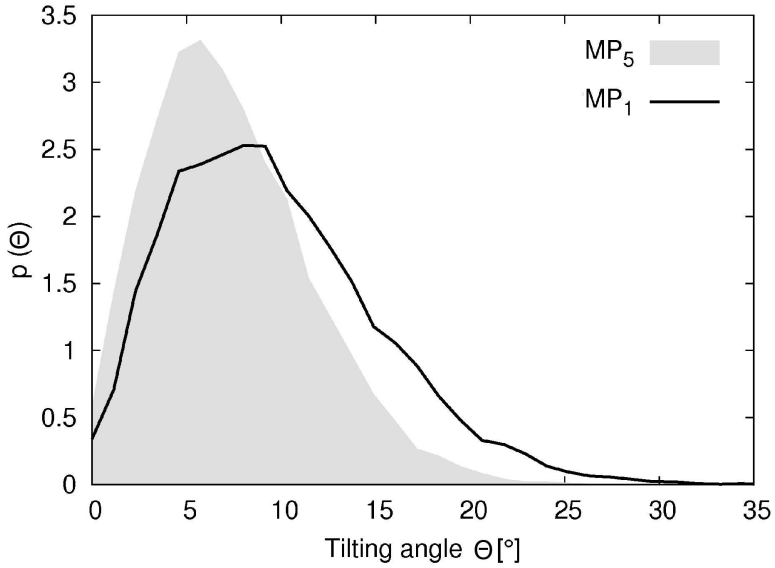

Figure 4.3: *Distribution of tilting angles of a protein MP_1^4 with length $n = 1$ (gray-shaded) is broader and has a higher mean tilting angle than proteins with longer hydrophobic moieties $n = 2 \ldots 5$ (represented here by MP_5^4).*

between the centers of protein hydrophilic beads and the terminal hydrophobic beads are listed in Table 4.1. A comparison with the thikness of one lipid layer, λ_0, suggests that the protein of length $n = 2$ reaches with its bottom roughly the midplane of the bilayer. To examine the positioning of a monotopic membrane protein in a bilayer, we determined its average tilting with respect to the bilayer normal. In general, the protein's average tilting angle was very modest with $\langle\theta\rangle < 6^\circ$ (see Table 4.1). Only the shortest protein MP_1^4 showed an enhanced tilting ($\langle\theta\rangle = 8.6^\circ$) and strong fluctuations around the mean. The latter is reflected in the distribution of tilting angles, $p(\theta)$, which was broader for MP_1^4 than in all the other cases (Fig. 4.3). This observation suggests that the flat protein with the shortest hydrophobic part is rather floating on the membrane surface while the longer proteins are more firmly anchored in the bilayer.

Membrane profile Next, we monitored the membrane's cross-section profile. Positions of lipid heads and terminal tail beads averaged over the simulation time are shown in Fig. 4.4. The plot displays the height profile of the two membrane monolayers and the placing of a monotopic membrane protein. In membrane regions close to the protein, marked perturbations are visible. To begin with, the membrane district opposite to the protein is deformed. When a protein is

longer than the thickness of its residential monolayer ($n = 3, 4, 5$), it intrudes the opposite monolayer and bends it outwards, i.e. away from the membrane midplane. In contrast, when the protein is shorter than a leaflet ($n = 1$), the opposing leaflet is bent inwards, i.e. towards the midplane. For protein length $n = 2$ ($1.4r_0$), which matches roughly the thickness of one monolayer ($1.63r_0$), we found almost no perturbation of the opposite leaflet. The maximum deflection in the height profile, Δz, i.e. the difference in z-coordinate at the protein rim and in the equilibrated membrane, is listed in Table 4.1. The absolute deflections from the midplane at the boundary of the PMP grew almost linearly with the length of the hydrophobic moiety. The residential monolayer of the protein was not found to be bent significantly for any of the studied cases.

Leaflet thickness As can be seen in Fig. 4.4, the thicknesses λ of the two leaflets is also affected by the presence of a monotopic protein. The leaflet in which the protein was embedded changed its thickness only marginally whatever protein was inserted (data not shown). The leaflet opposite to the MP^4_n, however, showed significant changes depending on the length of the hydrophobic moiety (Fig. 4.5a). In particular, for MP^4_4 and MP^4_5 a strong compression of the leaflet emerged while a length $n \leq 3$ of the hydrophobic moiety only had a negligible effect since the hydrophobic moiety was too short to penetrate strongly into the opposing leaflet.

Lipid tilting The findings for MP^4_4 and MP^4_5 are corroborated by the observation that lipids showed an enhanced tilting angle $\phi(r)$, i.e. they were more diverted from the bilayer normal, when being situated right opposite to these proteins (Fig. 4.5b, Table 4.1). In the leaflet opposite to long proteins ($n = 4, 5$), we observed a strong increase in tilting for lipids. The presence of shorter proteins induces less pronounced but still significant changes in lipid tilting. Here, the lipids aligned stronger with the bilayer normal, i.e. ϕ decreased. Lipids in the protein's residential leaflet were tilted stronger than average next to the shortest protein ($n = 1$) and the tilting decreased next to the single-leaflet spanning protein MP^4_2. In the proximity of longer proteins ($n = 3, 4, 5$) the lipid tilting in the residential leaflet was hindered even more giving a mean tilting angle of $-10°$ with respect to the equilibrium lipid tilting. The latter observation reveals that the nearest lipids align with a (typically only weakly tilted) long protein. Thus, in all cases the lipids' freedom is constrained which is entropically unfavorable.

It should be noted that lipid tilting and membrane leaflet thickness are interrelated quantities in our simulations. In general, when a leaflet is compressed, we

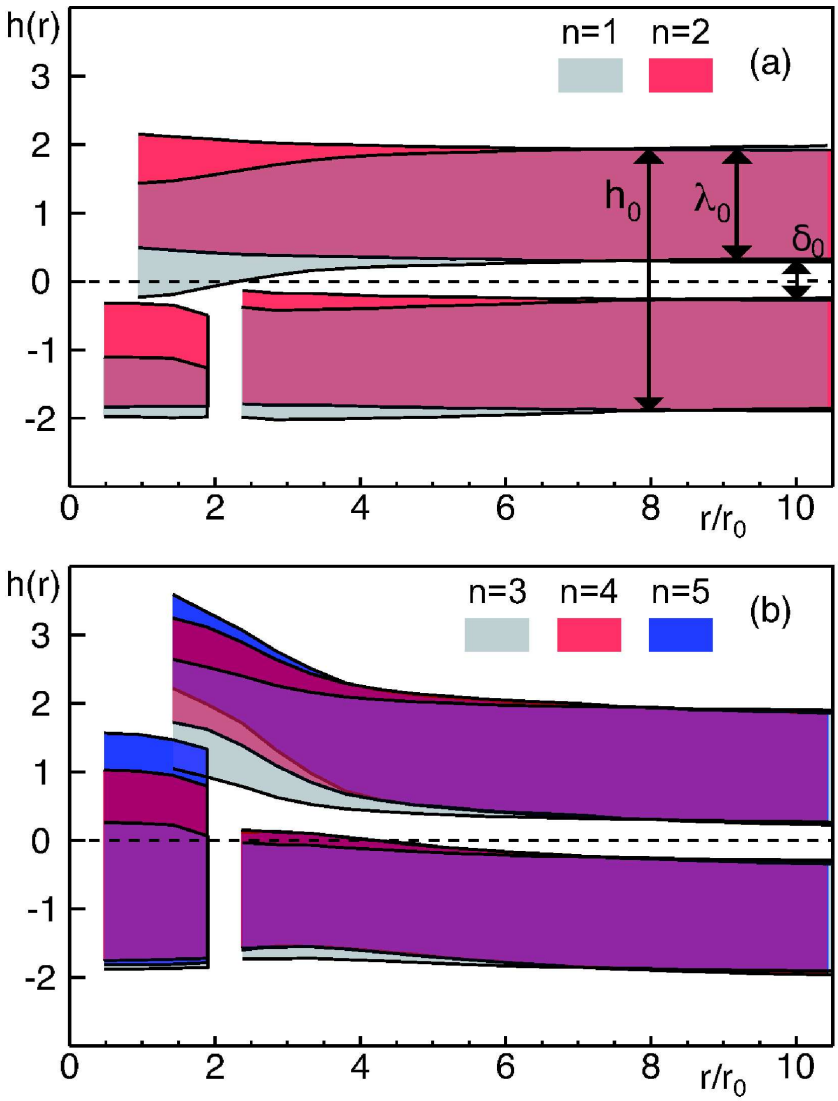

Figure 4.4: *Cross-section of the lipid bilayer as a function of the distance from the protein, r. Regions between the average positions of lipid head and terminal tail beads in the two leaflets are shown as colored stripes (overlap gives a color mixing). The unperturbed midplane is indicated as dashed line. A single MP was inserted in the lower leaflet (shape indicated in region $r < 2r_0$). Unperturbed membrane and leaflet thickness, h_0 and λ_0, are measured far away from the protein. (a) When inserting short proteins (i.e. MP^4_1 and MP^4_2) the upper leaflet bended towards the unperturbed midplane while the lower leaflet remained almost unperturbed. (b) For longer membrane anchors ($MP^4_{3,4,5}$), the upper leaflet bended away from the midplane due to the steric interference of the lipids with the opposing hydrophobic moiety of the protein. The lower leaflet bended only slightly inwards, hence resulting in a local thickening of the membrane. Also, the thickness of the upper leaflet, λ, was slightly reduced due to steric compression.*

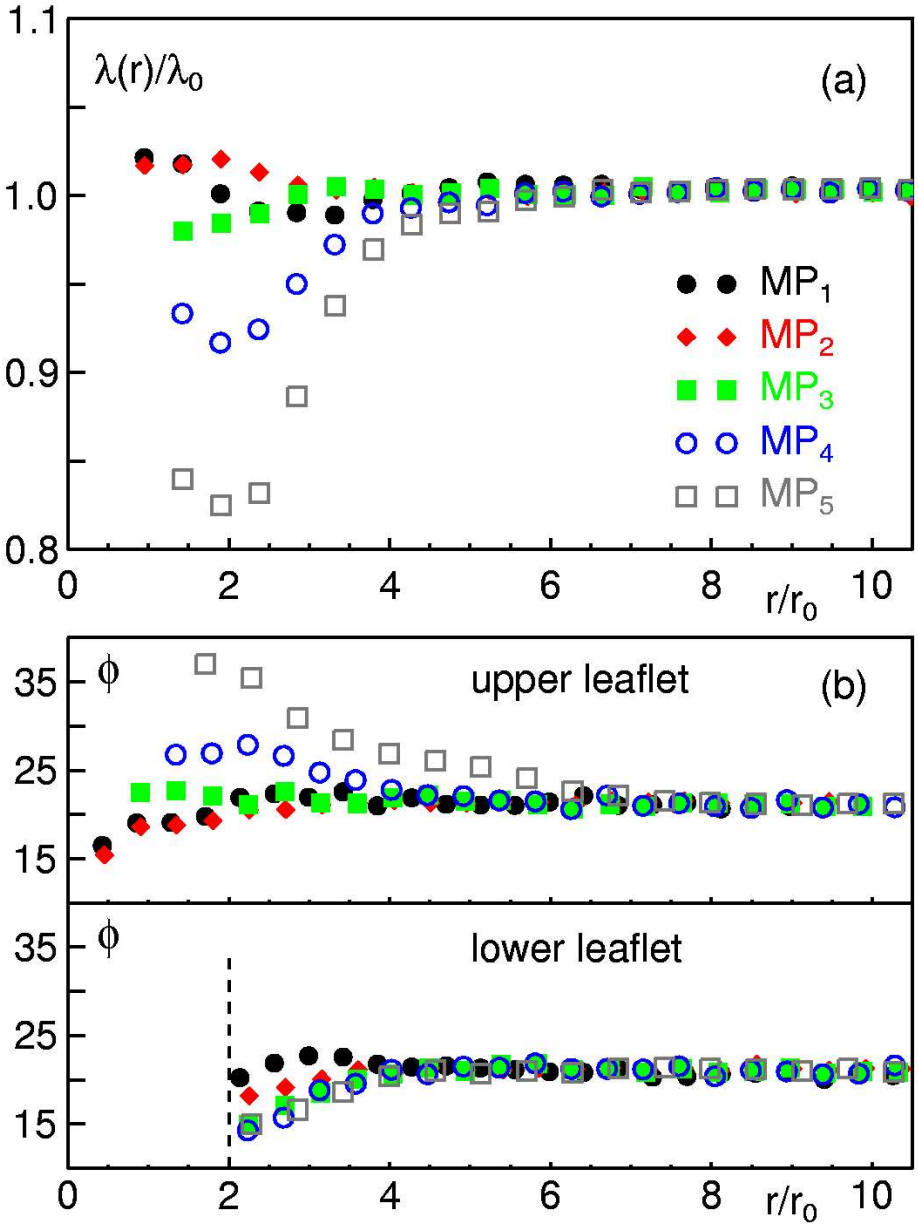

Figure 4.5: *Membrane perturbations when inserting a peripheral membrane protein: opposite leaflet thickness (a) and lipid tilting (b). When inserting a MP_n^4 construct, the thickness $\lambda(r)$ of the opposing leaflet is significantly altered near to the protein with respect to the unperturbed value λ_0. The compression of the leaflet increases when the length n of the hydrophobic moiety is increased. (a) The lipids' average tilting angle ϕ in the upper and lower leaflet is also affected in the vicinity of a PMP. Only far away from the protein a convergence towards the unperturbed value is observed. In agreement with the local compression of the upper leaflet, a stronger tilting of lipids is observed directly opposite to the protein. Legend as above. (b)*

observed an increase of lipid tilting, and when the leaflet expanded, we found a decrease of tilting. The reason for this lies in the relative stiffness of our model lipids, which conserve their length ($\approx 1.82 r_0$) and internal bending angles ($\approx 17°$) independently on the presence of the protein. It can be expected that in a less coarse representation an insertion of a hydrophobically mismatched protein or a monotopic protein would in addition lead to a straightening and prolongation of lipids.

To complete the above results, we furthermore analyzed the interdigitation of lipids in the two leaflets. We measured the average distance of the centers of the terminal lipid beads of the two leaflets. As expected, we found that the leaflets were closer to each other in membrane regions near to the shortest protein. Here the overlap of lipid terminal beads from the two layers is bigger than in unperturbed membranes. The distance between terminal beads was not affected for the optimally fitting protein MP_2^4, but it was considerably extended for the longer proteins (see $\Delta\delta$ in Table 4.1).

Table 4.1: ***Basic properties of the system.*** *The membrane deformation induced by the protein MP_n^4 can be described with the height profile change of each monolayer Δz, the monolayer thickness change $\Delta\lambda$, and the change in the distance between the two layers quantified by $\Delta\delta$ - all compared to a non-perturbed region distant from the protein. The values are shown only if a significant influence of the protein was detected.*

n	1	2	3	4	5
Proteins					
Prot. length $[r_0]$	0.8	1.4	2.1	2.8	3.3
Prot. tilting $\langle\theta\rangle$ [°]	8.60	5.72	5.72	6.30	5.72
Opposite monolayer					
Δz $[r_0]$	-0.5	0.3	0.8	1.5	1.8
$\Delta\lambda$ $[r_0]$	0	0	0	0.13	0.28
Lipid tilting ϕ [°]	0	0	0	6.5	15.5
Residential monolayer					
Lipid tilting ϕ [°]	1.6	-4	-10	-10	-10
Interdigitation					
$\Delta\delta$ $[r_0]$	-0.2	0	0.2	0.6	1.0

In summary, we observed that the presence of a monotopic inclusion has a major effect on the lipid conformation especially if the inclusion's length exceeded

the thickness of a leaflet. The residential leaflet is much less perturbed than the opposite one. The membrane deformations aim at to minimizing any vacant space around the protein and to prevent an exposure of hydrophobic regions to water.

4.4 Oligomerization of monotopic proteins within the residential leaflet

Dimer formation Given that monotopic membrane proteins perturb the lipid bilayer and reduce the lipids' degrees of freedom, one may expect a dynamic, entropy-driven clustering of proteins in analogy to observations made for transmembrane proteins [43]. As a first step we therefore inspected the dimerization behavior of two monotopic membrane proteins that reside in the same leaflet. Here, besides the length of the hydrophobic moiety, ($n = 1, 2, 3, 4, 5$), we also varied the radii of the proteins, ($k = 2, 3, 4$). For simplicity, the dimerization of a pair of identical proteins was examined.

To probe a potential dimerization, we used two different initial conditions: (i) proteins at random initial positions in the membrane , and (ii) proteins in a pre-dimerized configuration side-by-side (Fig. 4.6a). The first approach indicate whether dimer formation happened spontaneously. Setting (ii) was used to cross-check the stability of dimers in case that they would not find each other by diffusive search during the simulation. For the evaluation of a simulation run we recorded the temporal evolution of the interprotein distance, $d(t)$ (see Fig. 4.6b). This quantity was fluctuating strongly as long as the proteins were moving independently, but dropped to the mere center-to-center distance when they formed a dimer. Creating the probability distribution of distances, $p(d)$, allowed us to detect the occurrence of dimerization, which is highlighted by a peak in $p(d)$ for small distances. The distribution was broad and featureless if dimerization did not take place . Proteins were only assumed to be good dimerization partners when both approaches (i) and (ii) showed an unambiguous dimerization signature. To further quantify the stability of dimers, we also estimated the dimer lifetimes τ from $d(t)$ (Fig. 4.6c).

As a result, we found that monotopic membrane proteins residing in the same monolayer of a membrane formed dimers with varying lifetimes τ in dependence on their geometrical parameters. For the smallest radius ($k = 2$), most of the proteins exhibited only a very weak dimerization. Lifetimes $\tau \approx 10^4 \Delta t$ can be perceived rather as a prolonged random collision. Only for the longest protein, MP_5^2, we

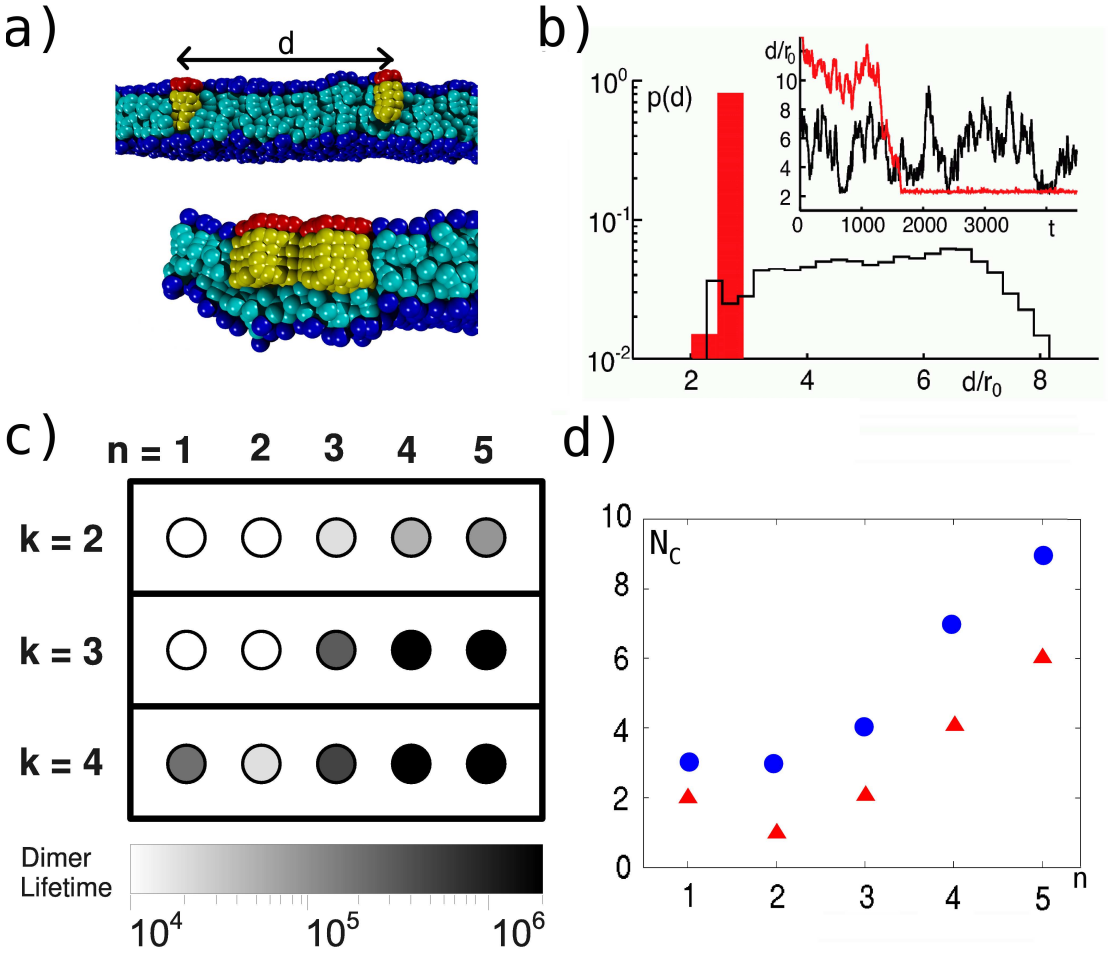

Figure 4.6: *Dimerization of proteins within one leaflet. (a) A snapshot of a membrane cross-section with two proteins inserted in the same membrane leaflet. The proteins are non-dimerized in the first and dimerized in the second picture. The distance d is measured between the centers of mass of the two proteins. (b) A representative probability distribution $p(d)$ of the distances between two proteins used for the evaluation of the dimerization events. A sharp peak at small distances d indicates a dimerization event, a broad distribution indicates an independent movement of the two proteins. The probability distributions are computed over the whole simulation time from a time-series of distances $d(t)$ as shown in the inset. (c) A phase diagram for the dimerization strength in dependence on the protein radius k and the hydrophobic length n. The lifetime (grey-scale) increases with the radius and the protein length. The weakest dimerization is observed for the protein fitting best into one membrane layer, $n = 2$. (d) Average size of clusters formed when 9 proteins are inserted into the same membrane leaflet, $k = 2$ (red triangles) and $k = 3$ (blue circles). The oligomerization is again the weakest for $n = 2$ and increases with k and n.*

found a significantly longer lifetime ($\tau \approx 10^5 \Delta t$). Nevertheless, when we increased the radius to $k = 3$, all proteins reaching into the opposite leaflet ($n = 3, 4, 5$) formed relatively stable dimers. The typical dimer lifetimes were in the range of $\tau \approx 2 \times 10^5 - 1.5 \times 10^6 \Delta t$. For the longest proteins, $\mathrm{MP}^3_{4,5}$, dimers were stable over the entire simulation ($\tau > 2 \times 10^6 \Delta t$). A further increase of the radius to $k = 4$ resulted in an even stronger dimerization: even the shortest proteins $\mathrm{MP}^4_{1,2}$ showed a significant dimerization. For MP^4_3 the lifetime increased to a value of $\tau \approx 5 \times 10^5 \Delta t$. For the longest proteins $\mathrm{MP}^4_{4,5}$ we again found dimers that were stable for the entire duration of the simulation ($\tau > 2 \times 10^6 \Delta t$). The actual lifetime of these dimers could not be determined due to computational restrictions. Yet, in analogy to observations for MPs with $n \leq 3$, we expect also for these proteins an increase of the lifetime when the radii are increased. In all cases, MP^k_2 which fitted best into a single leaflet and caused the least perturbations, showed almost no tendency to form dimers.

In summary, dimerization of MPs became stronger with increasing radii and increasing length of the hydrophobic moiety. Proteins which did not reach to the midplane of the bilayer ($n = 1$) floated independently on the surface and only showed dimerization when their radius was very large ($k = 4$). The weakest dimerization was found for MP^k_2 which matched best the thickness of one leaflet. These results are also in a good agreement with another recent related simulation study [122].

Larger clusters of monotopic membrane proteins within one membrane leaflet Starting from the existence of fairly stable dimers, we next investigated whether larger clusters emerge when many monotopic membrane proteins are embedded in the same leaflet. To this end, we inserted 9 proteins in the same leaflet at random initial configurations ($k = 2, 3$ and $n = 1, \ldots, 5$). The largest radius $k = 4$ was omitted here since the setup would have required a simulation box dimension beyond the avaliable computational power.

Consistently with the above results, we observed that monotopic membrane proteins formed oligomers with the size of the clusters depending on k and n (Fig. 4.6d). For the shortest protein with the smallest radius ($k = 2$), MP^2_1, we found rarely dimers. For the protein that fitted best into the leaflet, MP^2_2, we observed no oligomerization at all. With increasing length of the proteins, we found oligomers that increased in size. We observed dimers for $n = 3$, tetramers for $n = 4$ and clusters up to hexamers for $n = 5$. In case of a larger radius ($k = 3$) we found these oligomerization effects to be amplified, the clusters became larger. We

found now dimers for $MP^3_{1,2}$, trimers for MP^3_3, heptamers for MP^3_4 and nonamers for MP^3_5. These results underline our findings for the dimerization of monotopic membrane proteins and again clearly show that cluster formation increases with growing radii and with the hydrophobic mismatch between the proteins and their residential membrane leaflet.

4.5 Cross-leaflet interactions of monotopic proteins

In the previous section we had described the oligomerization of monotopic membrane proteins which do not span the whole membrane and still are able to assemble under certain conditions. This leads to an interesting question whether these proteins can also interact across the membrane. Such an interaction would be fruitful for various biological processes like signal transduction or coat formation.

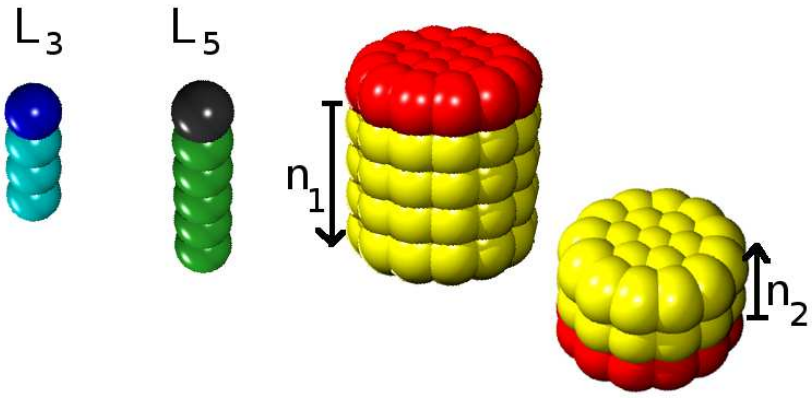

Figure 4.7: *Model of monotopic membrane proteins to be inserted in opposite leaflets. Short lipids L_3 have one head (blue) and three tail beads (cyan). Long lipids L_5 are composed of one head (gray) and five tail beads (green). The proteins (here $k = 3, n_1 = 4, n_2 = 2$) again have a cylindrical shape. The hydrophobic part (red) is exposed to water and hydrophobic moieties (yellow) are embedded in the membrane core.*

As before, model proteins were constructed as hexagonal structures of different lengths n_1 and n_2, and radii k with an overall cylindrical shape as illustrated in Fig. 4.7. Membrane lipids had a hydrophobic length 3 (L_3) and in one part of this study a lipid microdomain with lipids of a hydrophobic length 5 (L_5) was also used. We systematically varied the protein's radii ($k = 2 \ldots 4$) and the length of their hydrophobic moieties ($n_{1,2} = 1 \ldots 5$) in order to inspect the impact of the protein's geometry on their possible oligomerization.

Cross-leaflet dimers To elucidate if monotopic membrane proteins were able to interact across the two membrane leaflets, we inserted a single protein in each leaflet ($\mathrm{MP}^k_{n_1}$ and $\mathrm{MP}^k_{n_2}$) and examined the dynamical behavior of such a system. We used again two initial settings with (a) proteins at random initial positions and (b) proteins in a pre-dimerized configuration in order to assess the dimerization behavior of the proteins. We validated the data by measuring the center-of-mass distance of the two proteins in time and creating a probability distribution of inter-protein distances.

As a result, we observed cross-leaflet dimerization events that depended in their precise characteristics on the protein radius k and the combination of hydrophobic lengths n_1, n_2 (Fig. 4.8). For small radii ($k = 2$) proteins only formed stable dimers when the sum of hydrophobic anchor lengths was $n_1+n_2 = 5$. For this combination the dimerization was quite stable with lifetimes up to $3 \times 10^5 \Delta t$. Additionally, a combined hydrophobic length $n_1 + n_2 = 4$ lead to very short-living dimers with typical lifetimes $\tau = 2 \times 10^4 \Delta t$. When we increased the radii, the protein's ability to dimerize increased considerably. For radius $k = 3$ all combinations of membrane anchor lengths yielded dimers. Even in cases where we did not observe any dimers with the smaller radius, we now found a (rather weak) dimerization with a lifetime $\tau = 2 \times 10^4$–$5 \times 10^4 \Delta t$. In cases where a tendency of dimerization was detected already with the smaller radius, dimers now were much more stable and showed lifetimes up to $2 \times 10^6 \Delta t$. For even larger radii ($k = 4$), again an increase in dimerization strength was observed. Here the dimers were found to be very stable with lifetimes exceeding $\tau = 2 \times 10^6 \Delta t$ for all tested combinations of membrane anchor lengths.

The actual shape of the dimers depended on the length of the hydrophobic moieties of the two involved proteins . When the sum of the hydrophobic lengths of the two proteins was small enough ($n_1 + n_2 \leq 6$), the proteins were situated directly opposite to each other. In contrast, when the hydrophobic anchors of both proteins penetrated significantly the opposite leaflet ($n_1+n_2 > 6$), the dimerization partners were located side-by-side.

An effective transmembrane protein We have found that altering the radius of a monotopic membrane protein and/or the length of its hydrophobic moiety provides a means to induce cross-leaflet aggregation of initially independent proteins. Such a dimerization event may be regarded as the formation of an effective, metastable transmembrane protein from two monotopic membrane proteins located in opposing leaflets of a bilayer. Our observations further suggest that the

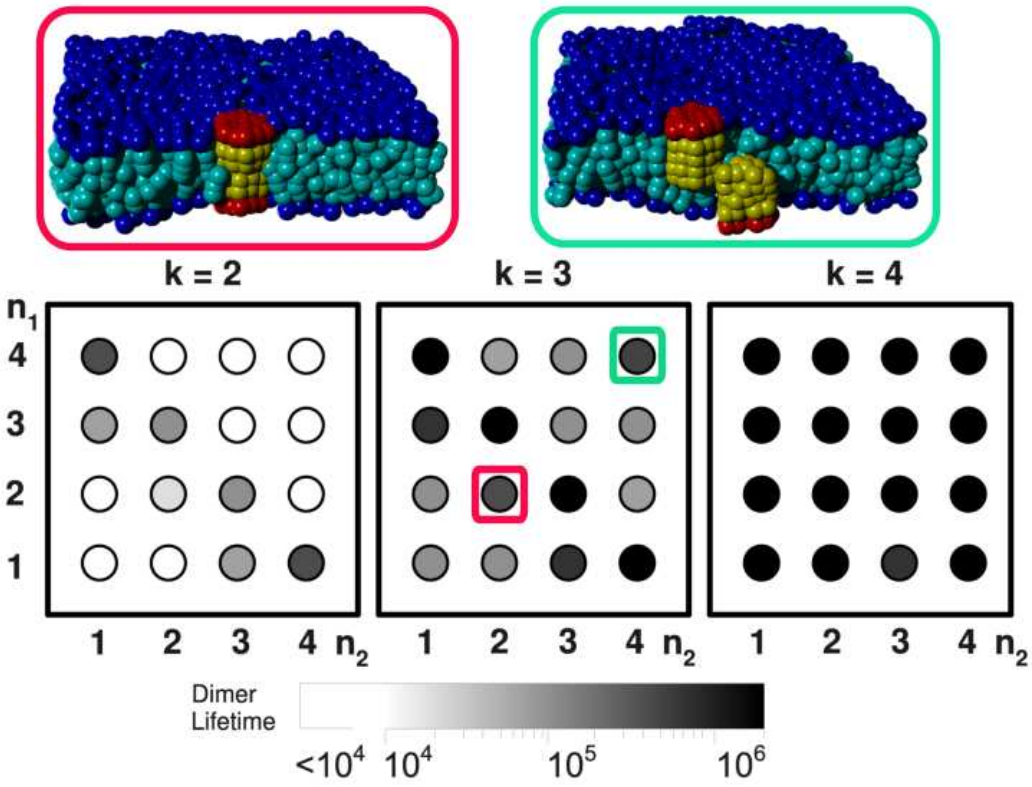

Figure 4.8: *Cross-leaflet dimers. The snapshots show a dimerization of two proteins tail-to-tail. An effective transmembrane domain is formed ($k = 3, n_1 = n_2 = 2$, highlighted in red) when the combined length of the proteins fits into the membrane core. The proteins oligomerize side-by-side if the combined length exceeds the membrane thickness ($k = 3, n_1 = n_2 = 4$, highlighted in green). The diagram shows the dimer lifetimes in dependence on radius and the lengths of the proteins. The dimerization increases strongly with the radius. Two proteins are good dimerization partners if their hydrophobic moieties exceed a membrane leaflet thickness, or if they are able to form a transmembrane domain without a strong mismatch with the membrane core.*

tendency of two proteins to form such a membrane-spanning dimer is strongest when the hydrophobic mismatch of the resulting transmembrane domain with the lipid bilayer is minimal. This is the case when such a combination of proteins where the sum of hydrophobic lengths is $n_1 + n_2 = 4, 5$ yielding a hydrophobic mismatch of the cross-leaflet dimer $\Delta = -0.2r_0$, resp. $\Delta = 0.5r_0$.

In agreement with this statement, we find that two proteins with $n_1 + n_2 = 4, 5$ form weak dimers already at the smallest radius ($k = 2$) and very stable dimers for larger radii. In contrast, proteins with a combined hydrophobic length $n_1 + n_2 = 2, 3$, i.e. with a negative total hydrophobic mismatch $\Delta = -1.4r_0$ and $\Delta = -0.8r_0$ show no dimerization for the smallest radius and only weak dimerization for a larger radius.

4.6 Establishing larger protein assemblies

To examine the interactions of a larger number of monotopic membrane proteins residing in different leaflets, we performed simulations with 5 proteins of radius $k = 2$ embedded in each membrane monolayer (Fig. 4.9). To examine larger radii $k = 3, 4$, we embedded only 3 proteins in each monolayer, in order to avoid finite size effects. Again, the lengths of the hydrophobic moieties n_1,n_2 of the proteins were varied systematically.

In the first instance we found again the formation of cross-leaflet dimers of monotopic membrane proteins which was described above. Subsequently, however, some of these dimers showed a tendency to form even larger assemblies when they were long-lived enough to meet each other due to diffusion. Concretely, we observed a formation of trimers of cross-leaflet dimers for a combination of proteins with lengths $n_1+n_2 = 1+4$. With increasing radii, also the lifetime of these trimers increased: $\tau = 1 \times 10^5 \Delta t$ for $k = 2$, $\tau = 5 \times 10^5 \Delta t$ for $k = 3$ and $\tau = 2 \times 10^6 \Delta t$ for $k = 4$. For a combination $n_1 + n_2 = 2 + 3$, we observed occasionally a formation of dimers of cross-leaflet dimers (i.e. tetramers) for the smallest radius $k = 2$, and again trimers of increasing stability in case of larger radii $k = 3, 4$. In the described constellations, the cross-leaflet dimers had a length of $4.3r_0$ (average distance of the head layer of the upper protein to the head layer of the lower protein). The effective transmembrane part of a cross-leaflet dimer therefore induces a small, assembly-driving hydrophobic mismatch ($\Delta = +0.5r_0$) with the unperturbed bilayer. We furthermore observed a dimerization/trimerization of dimers when the proteins had large radii ($k = 3, 4$) for the following combinations: $n_1 + n_2 = 1 + 1$ where the cross-leaflet dimer had a negative hydrophobic mismatch $\Delta = -1.4r_0$, for

$n_1 + n_2 = 1 + 2$ with $\Delta = -0.8r_0$, and for $n1 + n2 = 2 + 2$ with $\Delta = -0.2r_0$ mismatch. No higher oligomerization of dimers was seen for $n_1 + n_2 = 1 + 3$, where the dimer had only a very small mismatch $\Delta = -0.1r_0$.

We deduce from these findings that an absolute hydrophobic mismatch $\geq 0.2r_0$ of the effective transmembrane domain of a (meta)stable cross-leaflet dimer of two PMPs with the membrane yields an attractive, membrane-mediated interaction that can cause further oligomerization of the dimers. This outcome is in agreement with the notion that even a small hydrophobic mismatch can drive transient clustering [43]. The cross-leaflet dimers hence act in this respect similarly to actual transmembrane proteins.

The formation of a variant type of large clusters was observed when the PMPs in different leaflets were penetrating the opposing leaflet $n_{1,2} = 3, 4$. These clusters did not form via effective transmembrane entities as before but rather were a side-by-side assembly of proteins. The average number of proteins in the clusters was 3–6, and the clusters' lifetimes were $\tau > 2 \times 10^5$. Both, cluster size and stability increased again with an increasing hydrophobic length and radius of the involved proteins. The strongest clustering was observed for the largest radius ($k = 4$). Here, all proteins in the membrane assembled to just one large cluster that was stable for the entire simulation ($\tau = 2 \times 10^6 \Delta t$).

In addition to these two cluster forms, the length combination $n_1 = n_2 = 3$ yielded an intermediate phenotype where proteins in the two leaflets partially overlapped but did not form distinct cross-leaflet dimers. Here, the cluster stability was somewhat higher within the proteins' residential leaflets than across the leaflet. The lifetime of the cluster was long ($\tau = 1 \times 10^6 \Delta t$), but occasionally the two in-leaflet clusters separated.

Association of a monotopic membrane protein with a lipid microdomain
Finally, we intended to explore the behavior of monotopic membrane proteins in an asymmetric bilayer consisting of two lipid types, one species with a short tail length, L_3 (the standard lipid model used in our simulations), and a second species with a long tail length, L_5. The long species was residing only in one membrane leaflet and there it constituted $\sim 10\%$ of the lipid amount. Due to the imposed parameters long lipids formed a microdomain with a thickness of $\lambda_0 = 2.2r_0$ (average lipid head - lipid tail distance). To explore the potential association of a monotopic membrane protein with the lipid microdomain, we performed simulations with a single protein inserted in the opposite leaflet. We used proteins with radii $k = 2, 3$ and hydrophobic lengths $n = 1 \ldots 6$. To evaluate

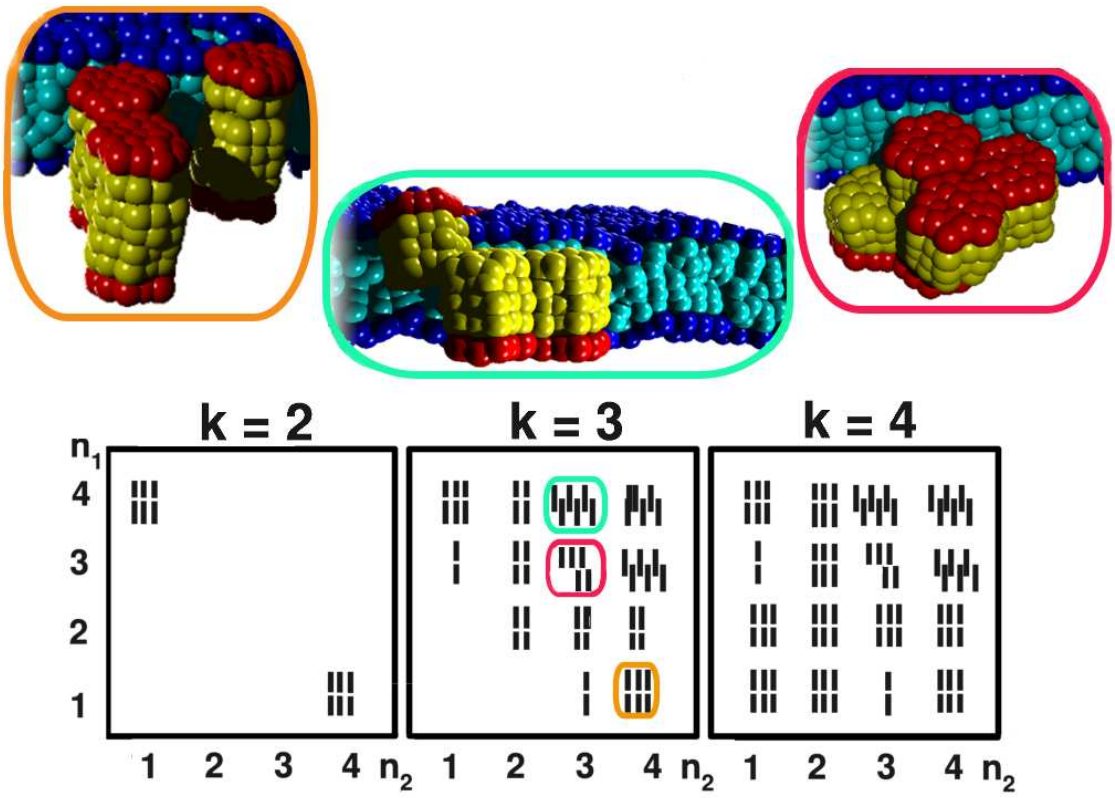

Figure 4.9: *Oligomers of monotopic proteins. The snapshots illustrate diverse resulting structures of protein clusters: a cluster of several effective transmembrane dimers (orange box, snapshot of $k = 3, n_1 = 1, n_2 = 4$), a cluster of proteins organized side-by-side in both leaflets (green box, snapshot of $k = 3, n_1 = 4, n_2 = 3$) and a mixed side-by-side cluster with a partial overlap (red box, snapshot of $k = 3, n_1 = 3, n_2 = 3$). These three structures are in a schematic way assigned to different combinations of hydrophobic moieties in the diagram describing the resulting cluster appearances in dependence on k and n_1, n_2.*

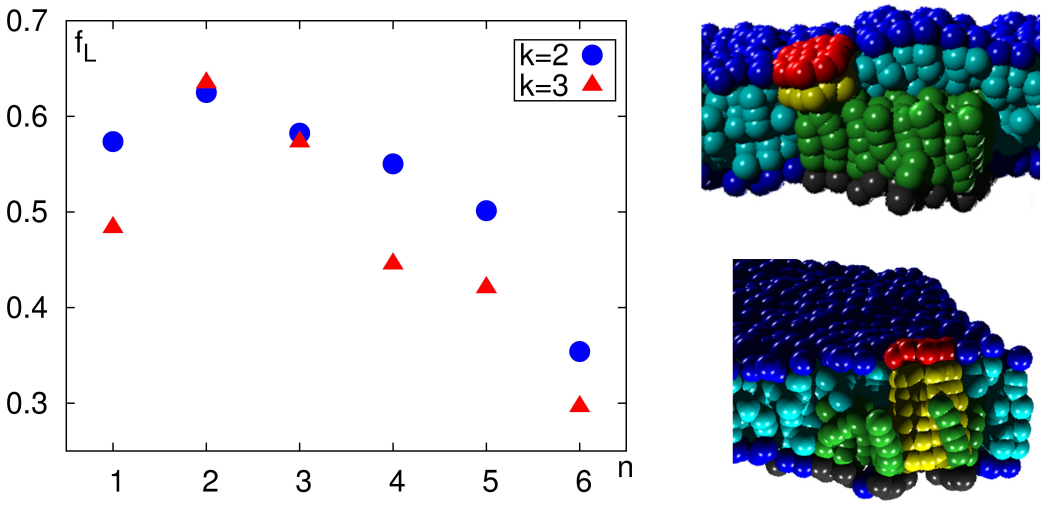

Figure 4.10: *Association of monotopic proteins with a lipid microdomain in the opposite leaflet. The plot shows the fraction of long lipids among all the lipids surrounding a protein within a distance $r < 2r_0$. Long lipids assemble beneath the protein if their hydrophobic moiety is rather short ($n = 1 \ldots 3$, first snapshot) and at the rim if the proteins are longer ($n = 4 \ldots 6$, second snapshot).*

the simulations, we quantified the lipid composition of the membrane within a distance of $2r_0$ around the protein. The ratio f_L of the number of long lipids to all lipids was averaged over the simulation time (see Fig. 4.10). We observed a significant affinity of proteins towards the long lipids, in particular for shorter hydrophobic lengths.

Thus, similarly to a monotopic protein, also a lipid microdomain can play a role in the cross-leaflet structure formation in membranes. Contrary to the pure protein assembly, however, a big radius of the inclusion does not always present an advantage for a strong collocalization with the lipid microdomain. In particular, proteins with a robust and long hydrophobic moiety rather avoided the long lipid environment. Snapshots (Fig. 4.10) of the simulations show that for proteins of short and medium length with $n = 1, 2, 3$ the long lipids assembled under the protein, while they rather surrounded it in the case of longer proteins with $n = 4, 5, 6$.

4.7 Discussion on the origin of membrane-mediated forces

In the following, we want to discuss the origin of the protein interactions described above. It is worthwhile stressing here that in the simulation no attractive forces have been imposed between the proteins, i.e. there are no specific interactions in the system which would make the proteins cluster. Their assembly hence takes place due to non-specific interactions that arise from the system. In other words, the physical properties of a monotopic membrane protein and its general interactions with other molecules make it a preferable state when proteins are arranged to clusters. Having observed the spontaneous oligomerization of proteins, one may wonder what is the driving force behind this structure formation. It is not too far fetched to draw the analogy to transmembrane proteins, for which the minimization of the bilayer perturbations is a driving force for structure formation [101, 43]. Unlike the case of transmembrane proteins, we are not aware of any continuum theory that one could apply easily to the problem studied here. Therefore, we will restrict ourselves to a phenomenological discussion of the problem and relate membrane perturbations, protein geometry and clustering only qualitatively.

Continuum mechanics predicts an increase in the free energy when membranes undergo bending and/or thickness compression [39, 101, 102]. A similar energetic penalty can be anticipated when instead of a bilayer two single leaflets are affected individually by bending and compression/expansion. Also, the observed change of lipid tilt angles close to a monotopic membrane protein suggests that there is an entropic contribution that supports clustering of MPs on the expense of decreasing the mixing entropy: Lipids that are tilted stronger or weaker near to a protein are confined in their configurations which results in an unfavourable decrease of their entropy contribution [43]. To liberate these lipids, i.e. to reduce the lipid-protein contact area, proteins need to cluster. As long as the gain in entropy from liberating the lipids overcompensates the decrease of the proteins' mixing entropy, cluster formation is supported in analogy to the formation of micelles by amphiphiles in water. In addition, altering the coupling between the membrane's leaflets, i.e. changing the distance between the monolayers, due to inserting a protein may amplify or weaken bilayer fluctuations. All of the aforementioned contributions are expected to vanish when the protein length matches the thickness of the leaflet (λ_0), i.e. the protein mimics the surrounding lipids. In contrast, with a growing absolute mismatch between the length of the protein's hydrophobic moiety and the leaflet thickness, the perturbations are expected to grow and clustering hence

can become a favorable means to relax the stress on the bilayer. Moreover, the membrane area in which lipids are perturbed by the presence of a protein increases with the MP's radius and hence a protein's tendency to cluster can be expected to increase with its radius.

Indeed, we observed in our simulations that the tendency to oligomerize was weakest for MP_2^k which matched best the unperturbed leaflet thickness λ_0. Increasing or decreasing the length n of the hydrophobic moiety resulted generally in stronger perturbations of the bilayer and a higher tendency to form oligomers. Also, in agreement with the above prediction, increasing the proteins' radii enhanced the oligomerization propensity. Being embedded in opposing leaflets, monotopic proteins also needed to respect another constraint, namely that the effective transmembrane length of a cross-leaflet oligomer matched roughly the unperturbed bilayer thickness. Interestingly, however, cross-leaflet clustering was also observed when the effective transmembrane domain of the resulting dimer did not match the bilayer thickness. Here, proteins assembled side by side. This configuration appears to be more favourable for the total system than suffering from the perturbations induced by two individual proteins. The observation that cross-leaflet dimers also frequently formed higher oligomers suggests that proteins aim at reducing their contact area with lipids to soften the energetic and entropic penalties due to deformations.

4.8 Relating the described clustering effects to biological problems

Our findings highlight a noteworthy aspect in the discussion about possible molecular interactions that take part in the structuring of biomembranes. When estimating the planar distribution of membrane constituents, typically specific interactions like hydrogen bonds and electrostatics between cognate residues are taken into account. Our study, however, demonstrates that fairly strong non-specific interactions can exist between peripheral membrane proteins simply due to local perturbations of the lipid bilayer: The mere presence of monotopic proteins in a membrane leaflet can lead to spontaneous oligomerization events and hence support the structuring of biomembranes. These membrane-mediated attractions potentially represent a significant contribution to the interactions of proteins. They may serve, for example, as a promoter of loose associations from which specific binding events become possible in the first place. Indeed, not only the encounter

rate of proteins is increased by membrane-mediated attractions but also the dwell time in the reaction zone close to each other is enhanced. Both effects support the probability that a specific reaction can take place. Thus, membrane-mediated oligomerization could be used as a preselection or sorting mechanism that facilitates signaling events, enzymatic reactions, or the formation of transport intermediates.

A well-known example of a cross-leaflet dimer is the channel protein gramicidin A, a dimer of two monomeric units each of which is located in one leaflet of the membrane. These two units locate opposite each other bottom-to-bottom and form a cross-leaflet dimer similar to the one we have studied in our simulations. In our model, the protein MP_2^2 with $n = k = 2$, would be an appropriate representative of a gramicidin monomer. Even though gramicidin dimer formation depends on specific interactions of the monomers, our results suggest that unspecific lipid-mediated interactions may play a pivotal role in the early assembly of the channel.

Our findings also imply a simple yet tunable means to transfer information across a membrane. Changing the shape of a monotopic protein, e.g. in the outer membrane leaflet, also perturbs the inner leaflet which may lead to an oligomerization with proteins in the inner leaflet. As signal propagation at the plasma membranes relies on cross-membrane information transfer, our data supports the hypothesis that transmembrane proteins are not mandatory for signaling cascades at the plasma membrane but that membrane-associated proteins alone are in principle sufficient. Typically, signal propagation is initiated by the binding of an extracellular ligand to a transmembrane receptor in the plasma membrane and a subsequent oligomerization of the receptor. This oligomerization event induces a (de)phosphorylation on the intracellular side of the membrane, hence triggering downstream parts of the pathway. Based on our simulations we put forward the hypothesis that binding of a ligand to a monotopic membrane protein in the plasma membrane's extracellular leaflet may increase the protein's radius and/or the length of its hydrophobic moiety, hence inducing a dimerization with another monotopic membrane protein in the intracellular leaflet. This dimer acts like an effective transmembrane protein and can hence trigger signaling by oligomerization in very much the same way as real transmembrane receptors do. Alternatively, a ligand may cross-link several monotopic membrane proteins in the extracellular leaflet which leads to an oligomerization of smaller monotopic proteins in the intracellular leaflet, thus producing a template for triggering downstream signal cascades. Clearly, the oligomerization effect described here is only a basic physicochemical core machinery that can drive signaling with monotopic membrane pro-

teins. Amino acid sequences and specific interactions may further fine-tune this phenomenon. Still, the cross-leaflet oligomerization of monotopic membrane proteins via membrane-mediated interactions yields to our knowledge for the first time an explanation of how signal transduction across the plasma membrane may happen without transmembrane proteins.

Concluding remarks In summary, we have shown that monotopic membrane proteins can (transiently) form higher order structures due to membrane-mediated interactions. The clustering ability can be tuned via the penetration depth of the protein's hydrophobic moiety and radius. Our general claims are supported by a number of (partially indirect) observations: GPI-anchored proteins in the outer leaflet of the plasma membrane, e.g. Thy-1 [123] and Ephrin-A [124], have been observed to transmit signals directly to peripheral membrane proteins in the intracellular leaflet, e.g. reggie/flotillin [121], without invoking transmembrane proteins. Also, the formation rate and lifetime of the gramicidin A channel has been shown to increase in membranes under tension [125], hence underlining the influence of the membrane's state on dimer kinetics. On the basis of these encouraging observations and the results shown here, we believe that dynamic structure formation of monotopic membrane proteins is a wide-spread yet often overlooked phenomenon. To further test our predictions experimentally we propose the following approach: Using mutagenesis of well-characterized MPs, e.g. in the context of signaling pathways, one my alter radius and hydrophobic length of proteins and exploit advanced fluorescence methods to directly probe the oligomerization state in vivo. As an alternative, well-characterized peptides (for which radius and hydrophobic length are known) may be studied on artificial membranes of well-defined compositions.

Chapter 5

Conclusion

5.1 Summary

Biological membranes play a central role in many vital process of the cell. Being more than a passive envelope of cells and organelles, membranes have many active functions, e.g. molecule translocation, signaling, or local formation of vesicles. In these processes the function of a lipid bilayer is supported by transmembrane and membrane-associated proteins. Besides the specific interactions among proteins, also more general membrane-mediated forces govern the collective behaviour of the system. A spontaneous oligomerization was shown to be triggerd by protein-derived deformations of membrane for transmembrane proteins with a hydrophobic mismatch. Here, the length of the protein's transmembrane domain does not match the lipid bilayer, hence giving rise to local stretching or compression of the bilayer. The aim of this project was to further study the role of the geometry of membrane inclusions in the structure formation on membranes via computer simulations.

We used a coarse-grained simulation technique, DPD, which is well suited for soft matter systems and allows one to explore large time and space scales. In DPD, several atoms are combined into effective beads that interact via conservative forces and are driven by a thermostat. The interactions have no hard core and are short-ranged, with the range r_0 defining the size of the beads. The repulsion parameter of the linear conservative force characterizes the interaction between three types of beads used: hydrophobic(T), hydrophilic(H) and water(W) beads. Larger entities like lipids and proteins were constructed by connecting individual beads i, j by a harmonic potential.

In the first part of the project, we explored the influence of protein acylation on transmembrane proteins. Protein acylation (e.g. palmitoylation) is a

post-translational modification that consists of attaching a fatty acid chain to a protein. Often, it serves to anchor soluble proteins in a membrane. Also many transmembrane proteins are subject to lipid modifications, although their association with the membrane is assured intrinsically by the transmembrane domain. Recent experimental studies indicated that the role of acylation of transmembrane proteins is linked to the regulation of their trafficking.

Using cylindrical inclusions of a hexagonal cross-section we modelled transmembrane domains of different lengths. A chain of hydrophobic beads was attached to the model as a representation of the modifying fatty acid chain. We found that acylation significantly enhances the tilting of transmembrane proteins with a clear dependence on the transmembrane domain length. Moreover, the presence of a fatty acid modification altered hydrophobic mismatch-induced clustering on homogenous and inhomogeneous lipid bilayers. In nearly all the studied cases, acylation prevented clustering. In addition, acylated transmembrane proteins showed a different partitioning on phase-separated bilayers with regions of different thickness: While non-modified proteins always partitioned into the phase that matched best the length of their transmembrane domain, the addition of a fatty acid significantly increased the probability to also visit regions in which the protein experiences a stronger hydrophobic mismatch.

Our findings support the notion that acylation can indeed be used as a means to regulate the transport behavior of transmembrane proteins. Using acylation, e.g. palmitoylation, cells may prevent the clustering of transmembrane proteins, thereby altering intracellular transport. Alternatively, cells may regulate the precise localization of transmembrane proteins on inhomogenous membranes, for instance in the endoplasmic reticulum. Besides specific protein-protein interactions, the effects described here may present the decisive ingredient that tips the balance towards the desired trafficking behavior of transmembrane proteins.

Using the same simulation approach, in the second part of the thesis we have studied the entropy-driven clustering of monotopic membrane proteins. As opposed to transmembrane proteins, monotopic proteins are associated with only one membrane leaflet. Proteins were modeled as hexagonal cylinders with one hydrophilic layer and several hydrophobic layers spanning approximately one leaflet of the bilayer.

We first found that monotopic membrane proteins perturbed their membrane environment locally. The perturbations were recognized in four parameters describing the state of the membrane: the bending of the two membrane monolayers,

their thicknesses, the tilting angle of lipids with respect to the membrane normal, and the coupling of the two monolayers. All of the parameters were found to change considerably in membrane regions surrounding the protein. The perturbations vanished within a distance of 4–6r_0 from the protein. The two leaflets were affected by the monotopic membrane protein to a different degree, with a much more pronounced deformations of the membrane layer opposite to the proteins as compared to the residential monolayer. These membrane deformations depended on the geometry of the proteins, i.e. the radius and the length of protein's hydrophobic moiety.

When inserting two proteins into a lipid bilayer, we frequently observed the formation of dimers with varying phenotypes. Here, not only radius and hydrophobic length of the proteins were the determining parameters but also whether proteins were situated in the same or in opposing leaflets. In general, the lifetime of all dimers was found to increase with increasing radii. Rim-to-rim dimers consisted of a pair of proteins sharing the same leaflet, or located in opposite leaflets and overreaching the membrane midplane. For this phenotype the dimer lifetime increased with its hydrophobic length. On the other hand, proteins located in opposite leaflets with hydrophobic domains that matched approximately one leaflet thickness, formed bottom-to-bottom dimers. In this case the dimerization was the stronger the better the length of the created transmembrane domain matched the membrane thickness. Nevertheless, a cross-leaflet clustering in many cases happened even when the resulting membrane-spanning dimer had a (rather weak) mismatch with the bilayer. Obviously the membrane perturbation induced by such a dimer is still smaller than the perturbations caused by two independent monomeric proteins. Inserting more than two proteins into the membrane resulted in the formation of higher-order clusters with variable shape and substructure. In particular, we observed the above mentioned cross-leaflet dimers with a hydrophobic mismatch to form higher oligomers. In this way, cross-leaflet dimers mimick the behaviour of transmembrane proteins. Finally, on inhomogeneous membranes we observed that monotopic proteins frequently associate with (thicker) lipid microdomains.

We propose that the described colocalization of monotopic proteins may present a fruitful generic mechanism involved in a plethora of processes in the cells. Especially the formation of cross-leaflet dimers and higher oligomers regulated by a simple tuning of the protein's geometry presents itself as a convenient tool for signal transduction across membranes. This observation suggests an alternative to the common view on signaling, in which transmembrane factors are essential.

5.2 Outlook

Non-cylindrical inclusions We have seen that membrane inclusions which induce membrane deformations and a derangement of lipids may spontaneously cluster. Starting from proteins with a hydrophobic mismatch, we broadened the view on these membrane-mediated interactions. We studied proteins with a mismatch decorated with a lipid modification and proteins which do not have a mismatch with the whole membrane core but rather with just one membrane leaflet. To complete the picture, we are now interested in transmembrane proteins which match exactly the membrane core but induce membrane deformations in a different way.

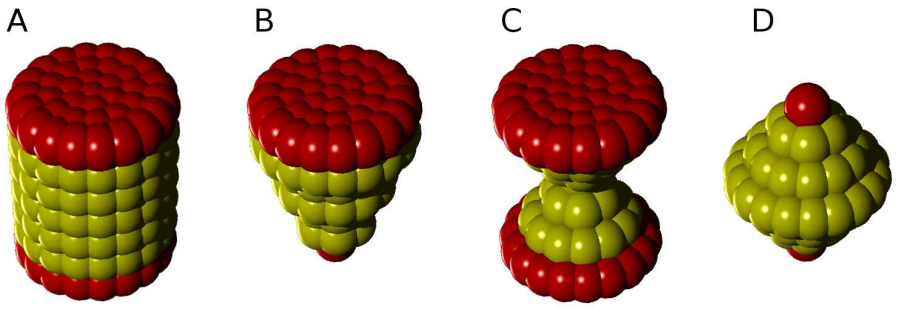

Figure 5.1: *Model proteins with no mismatch and different geometries: (A) cylinder, (B) cone, (C) hourglass, (D) barrel*

Currently, we are investigating geometry-induced, membrane-mediated interactions of non-cylindrical proteins. The models have a hexagonal structure resulting in a circular cross-section so that the rotational symmetry is still preserved. However, the radii of different layers of the protein beads differ, resulting in a cone, hourglass and barell-like shape (see Fig. 5.1). Such proteins (as opposed to cylindrical) have been predicted to induce significant changes of the bilayer pressure profile [51] and of the line tension [126]. Also, they may more realistically represent proteins with rather irregular and non-uniform shapes.

Preliminary results show a significant perturbation of the bilayer organization regarding the density profiles of the lipid bilayer surrounding the inclusions (Fig. 5.2). Here we averaged the density of head, tail (and water) beads in a region close to the protein ($r < 3r_0$). We observe a strong assymetry between the two leaflets in the vicinity of the cone and hourglass model. Insertion of a barrel-shaped inclusion into the membrane results in a decoupling of the two membrane leaflets, as indicated by a pronounced dip in the distribution of tail beads. For a

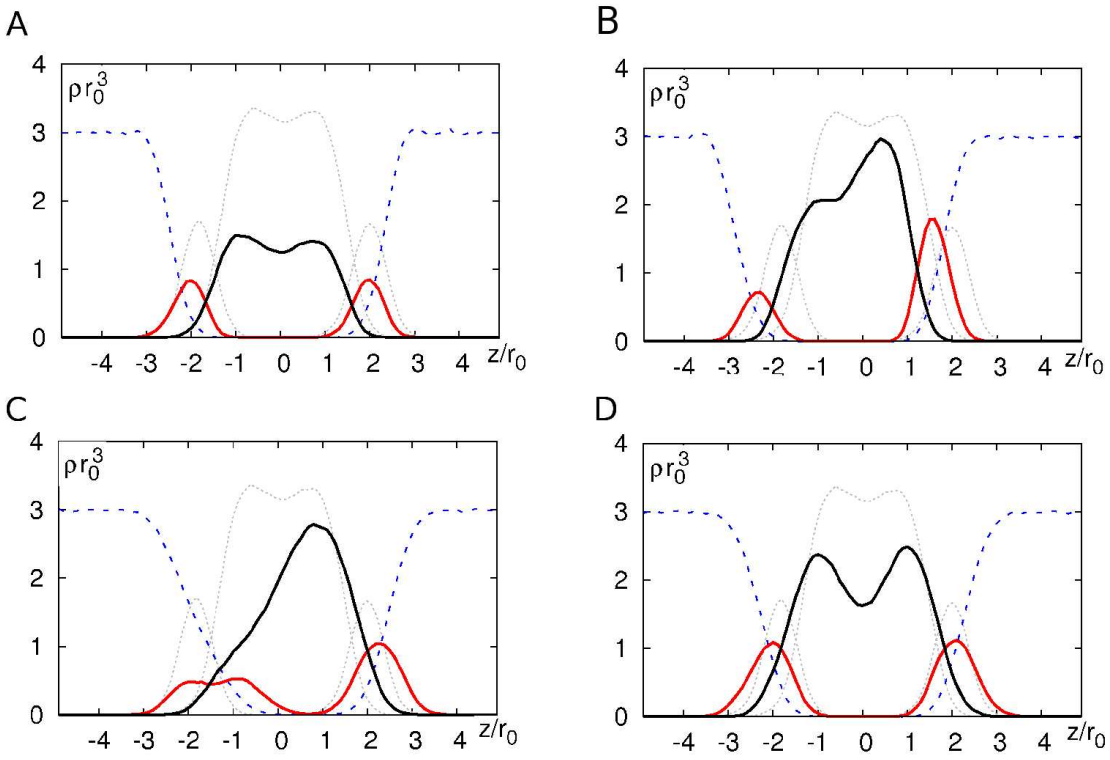

Figure 5.2: *Density profiles for different models: (A) cylinder, (B) cone, (C) hourglass, (D) barrel (grey-density profile in absence of any inclusion)*

more precise assessment of the impact of these inclusions on the bilayer, the construction of lateral pressure profiles will be more informative. When measuring the lipid tilting angles, we find that lipid in the vicinity of proteins do align with the inclusions. Two representative plots of lipid tilting can be found in Fig. 5.3. Whereas the lipid tilting derangement is symetrical in case of the barrel, the cone shaped protein induces more perturbations in the leaflet where the cone tip is located. We expect that the collective behaviour of the non-cylindrical proteins will again tend to minimize the overall membrane perturbation. The oligomerization behaviour of non-cylindrical inclusions is currently under investigation.

Parallelization of the code Although DPD as a coarse-grained technique offers a better time and length scale coverage than all-atom simulations, restrictions on the system size still present an obstruction for simulations of many interesting processes. Therefore, we have addressed mainly processes that take part "in two

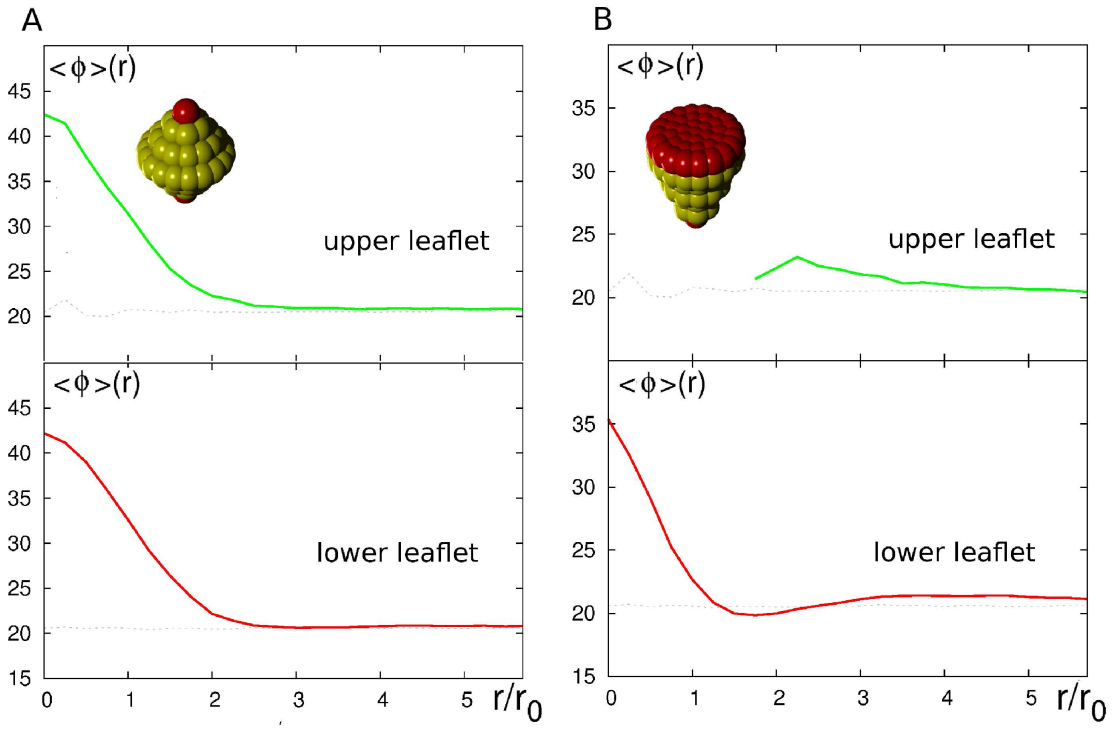

Figure 5.3: *Lipid tilting angles in the vicinity of inclusions: (A) barrel, (B) cone (green-upper leaflet, red - lower leaflet, grey-unperturbed lipid tilting)*

dimensions", in the membrane plane, with the dimension of the box perpendicular to membrane plane determined by the minimal value still avoiding finite size effects. Many events on membranes, however, are spatially more demanding as they occur "in three dimensions", e.g. on curved membranes or vesicles. At the same time, these processes usually take much longer. A parallel implementation of the DPD code to study such events would be a natural next step. For this purpouse, the use of graphic cards is considered. Concretelly, the CUDA programming environment provided by nVIDIA proved to be a suitable tool for many computationally demanding tasks in computational biology.

In particular, budding of vesicles and fusion (and formation) of lipid droplets would be possible applications for speeding up the code. Lipid droplets are small organelles composed of a single-layer membrane in which neutral lipids are packed. The biogenesis and maturation of these structures in cells is a subject of intensive research. Due to various complications, e.g. the small dimensions of the precursors of these organelles, light microscopy techniques did not yet succeed in giving a

generally accepted interpretation of their evolution. Using CUDA/nVIDIA as a tool for running large-scale DPD simulations may pave the way for deeper insight into these problems.

Bibliography

[1] B. Alberts, A. Johnson, J. Lewis, M. Raff, K. Roberts, and P. Walter. *Molecular Biology of the Cell.* Garland Science, New York, 2002.

[2] C. Tanford. *The hydrophobic effect: Formation of micelles and biological membranes.* New York: Wiley, 1973.

[3] A. Pockels. Surface tension. *Nature*, 43:437–439, 1891.

[4] I. Langmuir. The effect of dissolved salts on insoluble monolayers. *J. Am. Chem. Soc.*, 59:2400–2414, 1937.

[5] H. S. Frank and M. W. Evans. Free volume and entropy in condensed systems III. Entropy in binary liquid mixtures; Partial molal entropy in dilute solutions; Structure and thermodynamics in aqueous electrolytes. *J. Chem. Phys.*, 13:507, 1945.

[6] Kauzmann W. Some factors of the interpretation of the protein denaturation. *Adv. Prot. Chem*, 14:1, 1959.

[7] C. Tanford. Interfacial free energy and the hydrophobic effect. *PNAS*, 76, 1979.

[8] B. Lee. Solvent reorganization contribution to the transfer thermodynamics of small nonpolar molecules. *Biopolymers*, 31:993, 1991.

[9] G. Hummer, S. Garde, A. E. García, M. E. Paulaitis, and L. R. Pratt. Hydrophobic effects on a molecular scale. *J. Phys. Chem. B*, 102:10469, 1998.

[10] A. Pohorille and R. L. Pratt. Cavities in molecular liquids and the theory of hydrophobic solubilities. *J. Am. Chem. Soc.*, 112:5066, 1990.

[11] A. Ben Naim. Statistical mechanics of waterlike particles in two dimensions. I. Physical model and applications of the Percus-Yevick equation. *J. Chem. Phys.*, 54:3682, 1971.

[12] K. A. T. Silverstein, A. D. J. Haymet, and K. A. Dill. A simple model of water and the hydrophobic effect. *J. Am. Chem. Soc.*, 120:3166, 1998.

[13] N. T. Southall, K. A. Dill, and A. D. J. Haymet. A view of the hydrophobic effect. *J. Phys. Chem. B*, 106, 2002.

[14] R. Phillips, J. Kondev, and J. Theriot. *Physical Biology of the Cell.* Garland Science, Oxford, 2008.

[15] M. O. Jensen and O. G. Mouritsen. Lipids do influence protein function - the hydrophobic matching hypothesis revisited. *Biochim. Biophys. Acta*, 1666(1-2):205, 2004.

[16] K. Mitra, I. Ubarretxena-Belandia, T. Taguchi, G. Warren, and Engelman D. M. Modulation of the bilayer thickness of exocytic pathway membranes by membrane proteins rather than cholesterol. *PNAS*, 101:4083, 2004.

[17] A. D. Dupuy and D. M. Engelman. Protein area occupancy at the center of the red blood cell membrane. *PNAS*, 105(8):2848, 2008.

[18] A. Hildebrand, M. Pohl, and S. Bhakdi. Staphylococcus aureus alpha-toxin. Dual mechanism of binding to tarter cells. *JBC*, 266:17195, 1991.

[19] E. Gorter and F. Grendel. On bimolecular layers of lipoids on the chromocytes of the blood. *J. Exp. Med.*, 41:439, 1925.

[20] J. F. Danielli and H. Davson. A contribution to the theory of permeability of thin films. *J. Cell. Physiol.*, 5:495, 1935.

[21] W. Stoeckenius and M. D. Engelman. Current models for the structure of biological membranes. *J. Cell Biol.*, 42:613, 1969.

[22] Singer S. J. and G. L. Nicolson. The fluid mosaic model of cell membranes. *Science*, 175:720, 1972.

[23] E. Yechiel and M. Edidin. Micrometer scale domains in fibroblast plasma membranes. *J. Cell Biol.*, 105:755, 1987.

[24] M. Edidin. Lipids on the frontier: a century of cell-membrane bilayers. *Nature Reviews Molecular Cell Biology*, 4:414, 2003.

[25] D. M. Engelman. Membranes are more mosaic than fluid. *Nature*, 438:578, 2005.

[26] H. J. Galla, W. Hartmann, U. Theilen, and E. Sackmann. On two-dimensional passive random walk in lipid bilayers and fluid pathways in biomembranes. *J. Membr. Biol.*, 48:215, 1979.

[27] J. Korlach, P. Schwille, W. W. Webb, and G. W. Feigenson. Characterization of lipid bilayer phases by confocal microscopy and fluorescence correlation spectroscopy. *PNAS*, 96:8461, 1999.

[28] P. G. Saffmann and M. Delbruck. Brownian motion in biological membranes. *PNAS*, 72:1250, 1995.

[29] B. D. Hughes, B. A. Pailthorpe, and L. R. White. The translational and rotational drag on a cylinder moving in a membrane. *J. Fluid Mech.*, 110:349, 1981.

[30] M. Bretscher. Membrane structure: Some general principles. *Science*, 181(17):622, 1973.

[31] T. Pomorski and Menon A. K. Lipid flippases and their biological functions. *Cellular and Molecular Life Sciences*, 63(24), 2006.

[32] R. K. P. Zia, E. F. Redish, and S. R. McKay. Making sense of Legendre transform. *arXiv:0806.1147*, 2009.

[33] L. Euler. Recherches sur la courbure des surfaces. *Memoires de l'academie des sciences de Berlin*, 16, 1767.

[34] C. F. Gauss. *Disquisitiones generales circa superficies curvas.* Oct. 8, 1827.

[35] S. A. Safran. *Statistical thermodynamics of surfaces, interfaces and membranes.* Westview Press, Colorado, USA, 2003.

[36] W. Helfrich. Elastic properties of lipid bilayers - theory and possible experiments. *Z. Naturforsch.*, 28, 1973.

[37] O. Farago and P. Pincus. Statistical mechanics of bilayer membrane with a fixed projected area. *J. Chem. Phys.*, 120, 2004.

[38] E. Lindahl and O. Edholm. Mesoscopic undulations and thickness fluctuations in lipid bilayers from molecular dynamics simulations. *Biophys. J.*, 79:426, 2000.

[39] N. Dan, Pincus P., and Safran S. A. Membrane induced interactions between inclusions. *Langmuir*, 9:2768, 1993.

[40] U. Schmidt and M. Weiss. Hydrophobic mismatch-induced clustering as a primer for protein sorting in the secretory pathway. *Biophys. Chem.*, 151:34, 2010.

[41] S. Marčelja. Lipid-mediated protein interactions in membranes. *BBA*, 455:1, 1976.

[42] O. G. Mouritsen and M. Bloom. Mattress model of lipid-protein interactions in membranes. *Biophysical Journal*, 46:141, 1984.

[43] U. Schmidt, G. Guigas, and M. Weiss. Cluster formation of transmembrane proteins due to hydrophobic mismatching. *Phys. Rev. Lett.*, 101(12):128104, 2008.

[44] S. K. Kandasamy and R. G. Larson. Molecular dynamics simulations of model trans-membrane peptides in lipid bilayers: A systematic investigation of hydrophobic mismatch. *Biophys. Journal*, 90:2326, 2006.

[45] H. I. Petrache, D. M. Zuckerman, J. N. Sachs, J. A. Killian, R. E. Koeppe, and T. B. Woolf. Hydrophobic matching mechanism investigated by molecular dynamics simulations. *Langmuir*, 18:1340, 2002.

[46] J. A. Killian. Synthetic peptides as models for intrinsic membrane proteins. *FEBS Letters*, 555:134, 2003.

[47] T. A. Harroun, Heller W. T., Weiss T. M., L. Yang, and H. W. Huang. Experimental evidence for hydrophobic matching and membrane-mediated interactions in lipid bilayers containing gramicidin. *Biophys. J.*, 76:937, 1999.

[48] S. Munro. An investigation of the role of transmembrane domains in Golgi protein retention. *EMBO J.*, 14:4695–704, 1995.

[49] J. C. Rayner and H. R. B. Pelham. Transmembrane domain dependent sorting of proteins to the ER and plasma membrane in yeast. *EMBO Journal*, 16:1832, 1997.

[50] P. Ronchi, S. Colombo, M. Francolini, and N. Borgese. Transmembrane domain-dependent partitioning of membrane proteins within the endoplasmic reticulum. *J Cell Biol*, 181:105–18, 2008.

[51] R. S. Cantor. Lateral pressures in cell membranes: A mechanism for modulation of protein function. *J. Phys. Chem B*, 101:1723, 1997.

[52] J. Gullingsrud and K. Schulten. Lipid bilayer pressure profiles and mechanosensitive channel gating. *Biophys. Journal*, 86:3496, 2004.

[53] L. C. L. Lin and F. L. H. Brown. Simulating membrane dynamics in nonhomogeneous hydrodynamic environments. *J. Chem. Theory Comput.*, 2:472, 2006.

[54] B. L. de Groot and H. Grubmuller. Water permeation across biological membranes: mechanism and dynamics of aquaporin-1 and GlpF. *Science*, 294:5550, 2001.

[55] A. H. de Vries, A. E. Mark, and S. J. Marrink. Molecular dynamics simulation of the spontaneous formation of a small DPPC vesicle in water in atomistic detail. *J. Am. Chem. Soc.*, 126:4488, 2004.

[56] O. H. S. Ollila, H. J. Risselada, M. Louhivouri, E. Lindahl, I. Vattulainen, and S. J. Marrink. 3D pressure distribution in lipid membranes and membrane-protein complexes. *PRL*, 102:078101, 2009.

[57] J. C. Shillcock. Insight or illusion? Seeing inside cell with mesoscopic simulations. *HFSP Jour.*, 2(1), 2008.

[58] P. Hoogerbrugge and J. Koelman. Simulating microscopic hydrophobic phenomena with dissipative particle dynamics. *Europhys. Lett.*, 19:155, 1992.

[59] P. Español and P. Warren. Statistical mechanics of dissipative particle dynamics. *Europhys. Lett.*, 30:191, 1995.

[60] M. Laradji and P. B. Sunil Kumar. Dynamics of domain growth in self-assembled fluid vesicles. *PRL*, 93:198105, 2004.

[61] J. C. Shillcock and Lipowsky. Equilibrium structure and lateral stress distribution of amphiphilic bilayers from dissipative particle dynamics simulations. *J. Chem. Phys.*, 117:5048, 2002.

[62] P. Nikunen, M. Karttunen, and I. Vattulainen. How would you integrate the equations of motion in dissipative particle dynamics simulations? *Comput. Phys. Commun.*, 153:407–423, 2003.

[63] R. D. Groot. *Applications of Dissipative particle dynamics*, volume 640. Springer Berlin/Heidelberg, 2004.

[64] S. Nosé. A molecular-dynamics method for simulations in the canonical ensemble. *Molecular Physics*, 52:255, 1984.

[65] W. G. Hoover. Canonical dynamics - equilibrium phase-space distributions. *Phys. Rev. A*, 31:1695, 1985.

[66] H. J. C. Berendsen, J. P. M. Postma, W. F. van Gunsteren, A. Dinola, and J. R. Haak. Molecular dynamics with coupling to an external bath. *J. Chem. Phys.*, 81:3684, 1984.

[67] G. S. Grest and K. Kremer. Molecular-dynamics simulation for polymers in the presence of a heat bath. *Phys. Rev. A*, 33:3628, 1986.

[68] H. C. Andersen. Molecular dynamics simulations at constant pressure and/or temperature. *J. Chem. Phys.*, 72:2384, 1980.

[69] C. P. Lowe. An alternative approach to dissipative particle dynamics. *Europhys. Lett.*, 47:145, 1999.

[70] E. A. Koopman and C. P. Lowe. Advantages of a Lowe-Andersen thermostat in molecular dynamics simulations. *J. Chem. Phys.*, 124:204103, 2006.

[71] R. D. Groot. Applications of dissipative particle dynamics. *Lect. Notes Phys.*, 640:5, 2004.

[72] M. Venturoli and B. Smit. Simulating the self-assembly of model membranes. *Phys. Chem. Comm.*, 10, 1999.

[73] R. D. Groot and P. Warren. Dissipative particle dynamics: Bridging the gap between atomistic and mesoscopic simulations. *J. Chem. Phys.*, 107:4423, 1997.

[74] A. F. Jakobsen. Constant-pressure and constant-surface tension simulations in dissipative particle dynamics. *J. Chem. Phys.*, 122:124901, 2005.

[75] S. E. Feller, Y. Zhang, R. W. Pastor, and B. R. Brooks. Constant pressure in molecular dynamics: The langevin piston method. *J. Chem. Phys.*, 103:4613, 1995.

[76] S. J. Marrink and A. E. Mark. Effects of undulations on surface tension in simulated bilayers. *J. Phys. Chem. B*, 105:6122, 2001.

[77] R. D. Groot and K. L. Rabone. Mesoscopic simulation of cell membrane damage, morphology change and rupture by nonionic surfactants. *Biophys. J.*, 81:725, 2001.

[78] J. R. Lu, Z. X. Li, R. K. Thomas, E. J. Staples, I. Tucker, and J. Penfold. Neutron reflection from a layer of monododecyl hexaethylene glycol adsorbec at the air-liquid interface - the configuration of the ehylene-glycol chain. *J. Chem. Phys.*, 97:8012, 1993.

[79] G. Lantzsch, H. Binder, and H. Heerklotz. Surface area per molecule in lipid/C12En membranes as seen by fluorescence resonance energy transfer. *J. Fluoresc.*, 4(4), 1994.

[80] C. Rinehart. Introduction to molecular and cell biology (lecture syllabus). `<http://bioweb.wku.edu/courses/biol22000/2Bonds/images/FO2-18-PALMITATE.JPG>`, 2004.

[81] R. A. Clegg, editor. *Protein targeting protocols: Membrane targeting via protein Palmitoylation (by Veit, M. and Schmidt, F. G.)*, volume 88 of *Methods in Molecular biology*. Ed. Humana Press, Science, 1998.

[82] S. M. Mumby. Reversible palmitoylation of signaling proteins. *Curr. Op. Cell Biol.*, 9:148, 1997.

[83] P. B. Wedegaertner, D. H. Chu, P. T. Wilson, M. J. Levis, and H. R. Bourne. Palmitoylation is required for signaling functions and membrane attachment of Gq-alpha and Gs-alpha. *J. Biol. Chem.*, 268:25001, 1993.

[84] G. García-Cardeña, P. Oh, J. Liu, J. E. Schnitzer, and W. C. Sessa. Targeting of nitric oxide synthase to endothelial cell ceveolae via palmitoylation: Implications for nitric oxide signaling. *PNAS*, 93:6448, 1996.

[85] D. el Husseini A. and D. S. Bredt. Protein palmitoylation: a regulator of neuronal development and function. *Nat. Rev. Neurosci.*, 3(10):791–802, 2002.

[86] O. Rocks, A. Peyker, M. Kahms, P. J. Verveer, C. Koerner, M. Lumbierres, J. Kuhlmann, H. Waldmann, A. Wittinghofer, and P. I. Bastiaens. An acylation cycle regulates localization and activity of palmitoylated Ras isoforms. *Science*, 307:1746–52, 2005.

[87] J. B. McCabe and L. G. Berthiaume. N-terminal protein acylation confers localization to cholesterol, sphingolipid-enriched membranes but not to lipid rafts/caveolae. *Mol. Biol. Cell*, 12:3601, 2001.

[88] S. N. Zaman, Resek. M. E., and S. M. Robbins. Dual acylation and lipid raft association of Src-family protein tyrosine kinases are required for SDF-1/CXCL12-mediated chemotaxis in the Jurkat human T cell lymphoma cell line. *J. Leukocyte Biol.*, 84:1082, 2008.

[89] J. T. Dunphy and M. E. Linder. Signalling functions of protein palmitoylation. *BBA*, 1436:245, 1998.

[90] M. E. Linder and R. J. Deschenes. Palmitoylation: policing protein stability and traffic. *Nat. Rev. Mol. Cell Biol.*, 8(1):74, 2007.

[91] L. Abrami, B. Kunz, I. Iacovache, and F. G. van der Goot. Palmitoylation and ubiquitination regulate exit of the wnt signaling protein LRP6 from the endoplasmic reticulum. *Proc. Natl. Acad. Sci. USA*, 105(14):5384–9, 2008.

[92] J. Lanoix, J. Ouwendijk, A. Stark, E. Szafer, D. Cessel, K. Dejgaard, M. Weiss, and T. Nilsson. Sorting of Golgi resident proteins into different subpopulations of COPI vesicles: a role for ArfGAP1. *J. Cell Biol.*, 155:1199, 2001.

[93] M. Weiss and T. Nilsson. A kinetic proot-reading mechanism for protein sorting. *Traffic*, 4:65, 2003.

[94] R. Forster, M. Weiss, T. Zimmermann, E. G. Reynaud, F. Verissimo, D. J. Stephens, and Pepperkok. R. Secretory cargo regulates the turnover of COPII subunits at single ER exit sites. *Curr. Biol.*, 16:173, 2006.

[95] K. Simons and E. Ikonen. Functional rafts in cell membranes. *Nature*, 119:569–, 1997.

[96] S. L. Veatch and S. L. Keller. Seeing spots: complex phase behavior in simple membranes. *Biochim. Biophys. Acta*, 1746:172–85, 2005.

[97] R. Schekman and L. Orci. Coat proteins and vesicle budding. *Science*, 271:1526 – 1533, 1996.

[98] L. Pelkmans, T. Burli, M. Zerial, and A. Helenius. Caveolin-stabilized membrane domains as multifunctional transport and sorting devices in endocytic membrane traffic. *Cell*, 118:767–80, 2004.

[99] D. Scheel-Toellner, K. Wang, L. K. Assi, P. R. Webb, R. M. Craddock, M. Salmon, and J. M. Lord. Clustering of death receptors in lipid rafts initiates neutrophil spontaneous apoptosis. *Biochem. Soc. Trans.*, 32:679–81, 2004.

[100] E. G. Hofman, M. O. Ruonala, A. N. Bader, D. van den Heuvel, J. Voortman, R. C. Roovers, A. J. Verkleij, H. C. Gerritsen, and P. M. van Bergen En Henegouwen. Egf induces coalescence of different lipid rafts. *J. Cell Sci.*, 121:2519–28, 2008.

[101] N. Dan, A. Berman, Pincus P., and Safran S. A. Membrane induced interactions between inclusions. *Journal de physique II*, 4:1713, 1994.

[102] C. Nielsen, M. Goulian, and O.S. Andersen. Energetics of inclusion-induced bilayer deformations. *Biophys J.*, 74:1966–83, 1998.

[103] P. A. Kralchevsky and K. Nagayama. Capillary interactions between particles bound to interfaces, liquid films and biomembranes. *Adv. coll. interf. sci.*, 85:145, 2000.

[104] T. Gil, M. C. Sabra, J. H. Ipsen, and O. G. Mouritsen. Wetting and capillary condensation as means of protein organization in membranes. *Biophys. J.*, 73:1728âĂŞ1741, 1997.

[105] M. Goulian, R. Bruinsma, and P. Pincus. Long-range forces in heterogeneous fluid membranes. *Europhys. Let.*, 22:145, 1993.

[106] B. J. Reynwar, G. Illya, V. A. Harmandaris, M. M. Muller, K. Kremer, and M. Deserno. Aggregation and vesiculation of membrane proteins by curvature-mediated interactions. *Nature*, 447:461–4, 2007.

[107] K. M. Palmer, M. Goulian, and P. Pincus. Fluctuation-induced forces in stacked fluid membranes. *J. de Physique II*, 4:805, 1994.

[108] J. M. Park and T. C. Lubensky. Interactions between membrane inclusions on fluctuating membranes. *J. de physique I*, 6:1217, 1996.

[109] T. Sintes and A. Baumgaertner. Protein attraction in membranes induces by lipid fluctuations. *Biophys. J.*, 73:2251, 1997.

[110] G. H. Patterson, K. Hirschberg, R. S. Polishchuk, D. Gerlich, R. D. Phair, and J. Lippincott-Schwartz. Transport through the golgi apparatus by rapid partitioning within a two-phase membrane system. *Cell*, 133:1055–67, 2008.

[111] H. J. Sharpe, T. J. Stevens, and S. Munro. A comprehensive comparison of transmembrane domains reveals organelle-specific properties. *Cell*, 142:158–69, 2010.

[112] G. Blobel. Intracellular protein topogenesis. *PNAS*, 77:1496, 1980.

[113] D. Picot, P. J. Loll, and R. M. Garavito. The X-ray crystal structute of the membrane proteins prostaglandin H2 synthase-1. *Nature*, 367:243, 1994.

[114] M. H. Bracey, M. A. Hanson, K. R. Masuda, R. C. Stevens, and B. F. Cravatt. Structural adaptations in a membrane enzyme that terminates endocannabinoid signaling. *Science*, 298:1793, 2002.

[115] K. U. Wendt, K. Poralla, and G. E. Schulz. Structure and fucntion of squalene cyclase. *Science*, 277:1811, 1997.

[116] F. G. Hernandez-Guzman, T. Higashiyama, W. Pangborn, Y. Osawa, and D. Ghosh. Structure of human estrone sulfatase suggests functional roles of membrane association. *J. Biol. Chem.*, 94:L41, 2008.

[117] P. A. Williams, J. Cosme, V. Sridhar, E. F. Johnson, and D. E. McRee. Mammalian microsomal cytochrome P450 monooxygenase: structural adaptations for membrane binding and functional diversity. *Mol. Cell*, 5:121, 2000.

[118] M. H. Bracey, B. F. Cravatt, and R. C. Stevens. Structural commonalities among integral membrane enzymes. *FEBS Lett.*, 567:2–3, 2004.

[119] K. Balali-Mood, P. J. Bond, and M. S. P. Sansom. Interaction of monotopic membrane enzymes with a lipid bilayer: a coarse-grained MD simulation study. *Biochemistry*, 48:2135–45, 2009.

[120] C. Barlowe, L. Orci, T. Yeung, M. Hosobuchi, S. Hamamoto, N. Salama, M. F. Rexach, M. Ravazzola, M. Amherdt, and R. Schekman. COPII: a membrane coat formed by Sec proteins that drive vesicle budding from the endoplasmic reticulum. *Cell*, 77:895–907, 1994.

[121] M. F. Langhorst, A. Reuter, and C. A. Stuermer. Scaffolding microdomains and beyond: the function of reggie/flottilin proteins. *Cell Mol. Life Sci.*, 62:2228, 2005.

[122] S. Li, X. Zhang, and W. Wang. Cluster formation of anchored proteins induced by membrane-mediated attraction. *Biophys. J.*, 98:2554, 2010.

[123] S. M. Haeryfar and D. W. Hoskin. Thy-1: more than a mouse pan-T cell marker. *J. Immunol.*, 173:3581, 2004.

[124] A. Davy, N. W. Gale, E. W. Murray, R. A. Klinghoffer, P. Soriano, C. Feuerstein, and S. M. Robbins. Compartmentalized signaling by GPI-anchored ephrin-A5 requires the Fyn tyrosine kinase to regulate cellular adhesion. *Genes and development*, 13:3125, 1999.

[125] M. Goulian, O.N. Mesquita, D.K. Fygenson, C. Nielsen, O. S. Andersen, and A. Libchaber. Gramicidin channel kinetics under tension. *Biophys J.*, 74(1):328–37, 1998.

[126] N. Dan and S. A. Safran. Effect of lipid characteristics on the structure of transmembrane proteins. *Biophys. J.*, 75:1410, 1998.

Publications

D. Morozova and M. Weiss
On the role of acylation of transmembrane proteins.
Biophys. J. **8**(5), pp. 800-4 (2010)

D. Morozova*, G. Guigas*, and M. Weiss
Dynamic structure formation of peripheral membrane proteins.
submitted

*equal contribution

Acknowledgement

This work was done in the German Cancer Research Center, Heidelberg, during the years 2008-2010.

I gratefully acknowledge my first supervisor, Prof. Dr. Michael Hausmann, for his kind support and advice.

I am heartily thankful to our group-leader, Prof. Dr. Matthias Weiss, for the many encouraging and enriching discussions, for the deep insight he shared with us, and for his genuine interest in our progress. His enthusiasm and knowledge is for me a constant source of professional and personal inspiration.

I thank Gernot Guigas for collaboration on our common projects, for his helpful attitude, for correcting my German abstract, and, above all, for his friendship.

I am also obliged to my group colleagues, Nina Malchus, Maria Hanulova, Marcel Hellmann, and Jens Kuehnle, for valuable suggestions and corrections of this Thesis, and in particular for the joyful and friendly atmosphere in our group.

Last but not least, I thank my family for their lifelong care and love. My special thanks go to my husband, Sergej, for his patience and continuous support.